USING FIELD MEASURED PARAMETERS WITH THE SWAT HYDROLOGICAL MODEL TO QUANTIFY RUNOFF AT THE SUB–WATERSHED LEVEL

Yuestas David

A THESIS SUBMITTED TO
THE FACULTY OF GRADUATE STUDIES
IN PARTIAL FULFILLMENT OF THE REQUIREMENTS
FOR THE DEGREE OF
MASTER OF SCIENCE

GRADUATE PROGRAM IN GEOGRAPHY
YORK UNIVERSITY
TORONTO, ONTARIO

February 2014

Abstract

The SWAT hydrological model is a semi-distributed physically–based model. As a physically–based model, parameters are measurable in the field and can be implemented in the model. As rarely undertaken by SWAT modelers, this study aims to evaluate the potential of integrating field data (saturated hydraulic conductivity, bulk density, and canopy storage) into SWAT, based on the HRU semi-distributed discretization scheme and investigate its benefits for the Duffins Creek watershed in Southern Ontario, Canada. SWAT has the option of running simulations based on the empirically based Curve Number (CN) or the physically based Green & Ampt (GA) runoff method, both of which are evaluated with and without field data. The Tension Infiltrometer (TI) and Guelph Permeameter (GP) were used to measure the saturated hydraulic conductivity for the first and second (30 cm below the surface) soil layers respectively. Digital hemispherical photographs (DHP) and LAI-2000 were used to measure leaf area index to derive maximum canopy storage. Their agreement in common sites allowed for their use independently for short (LAI-2000) and tall/dense canopies (DHP). Field collected bulk density and saturated hydraulic conductivity depicted a range within each soil type that could not be represented by the single value per soil type that is used by default in the SWAT model. Without calibration or validation, adding field data improved performance of the GA method for both the calibration (2006-2008) and validation years (2010), but the CN method only improved for the validation year (2010). The CN calibrated or validated model did not benefit from field data, but the GA model significantly improved for the calibrated years while showing no improvement for the validated period. The effect of using field collected maximum canopy storage (CANMX) parameter or applying field collected values to similar HRUs outside of the subbasin it was collected in remains inconclusive.

Dedication

Dedicated to my loving family.

Acknowledgements

I wish to thank the following Toronto and Region Conservation Authority personnel for their kindness, support, expertise and data which made this collaborative effort possible: Glenn MacMillan, Dr. Rick Gerber, Margie Kenedy, Ryan Ness, Christy Graham, Matt Derro, Rita Lucero, Edlyn Wong and Rick Wilson. I'm thankful to Carey Gurden at Claremont Conservation for looking out for me during my field season and driving from miles away in the middle of the night each time I got locked in.

I also wish to thank Dr. Chen and his PhD student Rong Wang at U of T for lending digital hemispherical photography equipment and for taking the time to give me guidance with the instruments. I am also greatly indebted to the SWAT and SWAT-CUP online user community (especially to Dr. Karim Abbaspour) who have guided my understanding of the two applications and help me overcome many road blocks.

I wish to thank my family for their unwavering support, sacrifices and prayers; especially my father for showing me that the fruits of your labour can be very sweet. I am grateful for my colleagues and friends with whom I was able to vent my frustrations and share my joys especially Yikalo Araya, Alex Singh, Dr. Scott Tarof, and Nishani Senthilnathan.

I'm thankful for the Remmel Geoinformatics Lab for providing me space, printing, computing and other resources. I'm also indebted to the paramedics and medical staff at Rouge Valley Health System hospital for helping me through my peril of anaphylaxis to wasp sting during my field work.

Thank you Dr. Martin Bunch and Dr. Raju Das for reviewing my thesis and kindly stepping in as external examiner and chair for my thesis defence. Lastly, I'm indebted to my two supervisors who have been patient with me and instilled in me wisdom and knowledge far beyond my capacity. Dr. André Robert's motivation and support kept me going in times of doubt and I will continue to strive to meet Dr. Dr. Tarmo K. Remmel's standards of perfection, organization and efficiency.

This research is financially supported by York University, Natural Sciences and Engineering Research of Canada: Alexander Graham Bell Canada Graduate Scholarship, and Natural Sciences and Engineering Research of Canada Discovery Grant awards to Dr. Tarmo K. Remmel and Dr. André Robert.

Table of Contents

List of Tables

List of Figures

1. Introduction

1.1 Science of Water: Hydrology

Earth is called the “blue planet” in reference to the large proportion of its surface covered by water. The water on Earth plays a large role in the regulation of its climate. Atmospheric water vapour is the most abundant green house gas, responsible for 60-70% of the greenhouse effect (Hendriks 2010). Furthermore, the ocean conveyor belt circulation (also known as thermohaline circulation) supplies heat from the equatorial regions towards the poles regulating the temperature and ice formation in the polar regions (Hasumi 2002). Water also regulates temperature by absorbing or releasing energy when changing from one physical state to another. The process of evaporation of water absorbs energy from the surrounding area (the ultimate source being the sun), blown to another locale it will condense and precipitate releasing that energy. In addition to transport of energy, water also plays a role in the transport of matter: dissolved chemicals (including pollutants) and erosion and deposition of sediments (Dingman 2002). Among other uses, water is required for producing power, for cooling, and for irrigation. Most importantly it sustains life of plants, animals and humans as it is an integral part of all living cells. All but few living organisms require fresh water in particular. Although the abundance of water on Earth is obvious, the amount of freshwater is only a fraction (3%) of the global water volume, the majority of which is found as groundwater or locked up in glaciers (Ward and Robinson 2000). More importantly, our fresh water supply is distributed unevenly in both time and space (Ward and Robinson 2000). Modern hydrologists today concern themselves primarily with the management of this fresh water resource. The panel created by Dwight D. Eisenhower (the president of the United States in 1959) on Hydrology of the Federal Council for Science and Technology established hydrology as the study of Earth’s waters, their occurrence distribution, circulation, chemical and physical properties, and their interaction with the environment and living things (Linsley et al. 1982).

Early knowledge of water science, hydrology, was developed through the local engagement of managing and controlling it, as evident in the ancient Arabian wells, the Persian kanats, the Roman aqueducts, the water supply and drainage projects in the Indus Valley, and the Chinese canals, irrigation, and flood control systems (Chow 1964). Hydrology naturally emerged as an engineering discipline, mainly for the design and operation of hydraulic structures, and only recently (1960s) was realized as a scientific discipline (Ward and Robinson 2000). Since water is related to so many issues in nature and society, interdisciplinary research resonates strongly within the discipline for which the hydrological cycle serves as a central concept (Chow 1964).

1.2 Hydrological Cycle

Although the predecessor for the notion of a hydrological cycle (Figure 1) can be traced to Marcus Vitruvius in the first century, it was not until Perrault, Mariotte, and Halley who by modern scientific research showed evidence of the hydrological cycle in the seventeenth century (Viessman and

Lewis 1995). Perrault combined measurements of rainfall, runoff, and an estimation of the watershed area to conclude that rainfall quantity adequately explained river flow (Viessman and Lewis 1995). Mariotte recorded velocity of the river and used its cross sectional area to translate it in terms of discharge, while Halley calculated the rate of evapotranspiration of the Mediterranean Sea and found it sufficient to explain the outflow from the tributary rivers (Viessman and Lewis 1995). The cycle, driven by the energy from the sun, explains the dynamics of water as a renewable resource, which can be quite complex. A single water droplet can take various routes through the hydrosphere including air parcels in the atmosphere, as soil moisture between soil particles or as groundwater in the lithosphere (Viessman and Lewis 1995). The water from the oceans and other bodies of water is evaporated when heated by the sun. Water vapour in the atmosphere condenses into clouds and precipitates (i.e., rain, hail, snow), part of which may be intercepted by vegetation or structures. Thus, the cycle is also the means by which water quality is altered; from salt water to freshwater and vice versa. Intercepted water can drip down to the soil or evaporate back into the atmosphere. The water that reaches the soil surface either infiltrates the soil to replenish soil moisture and groundwater or fills depressions at the surface, the rest will runoff. Infiltrated water can evaporate, transpire through plants, be stored in deep aquifers, or travel laterally through the subsurface emptying into a channel. This interflow sustains the flow in channels between precipitation events and is known as baseflow. The surface runoff flows down slope reaching defined channels, usually much faster than the baseflow that originated from the same precipitation event. The flow continues downstream to the outlet and into the sea, from where it can be evaporated for the cycle to continue.

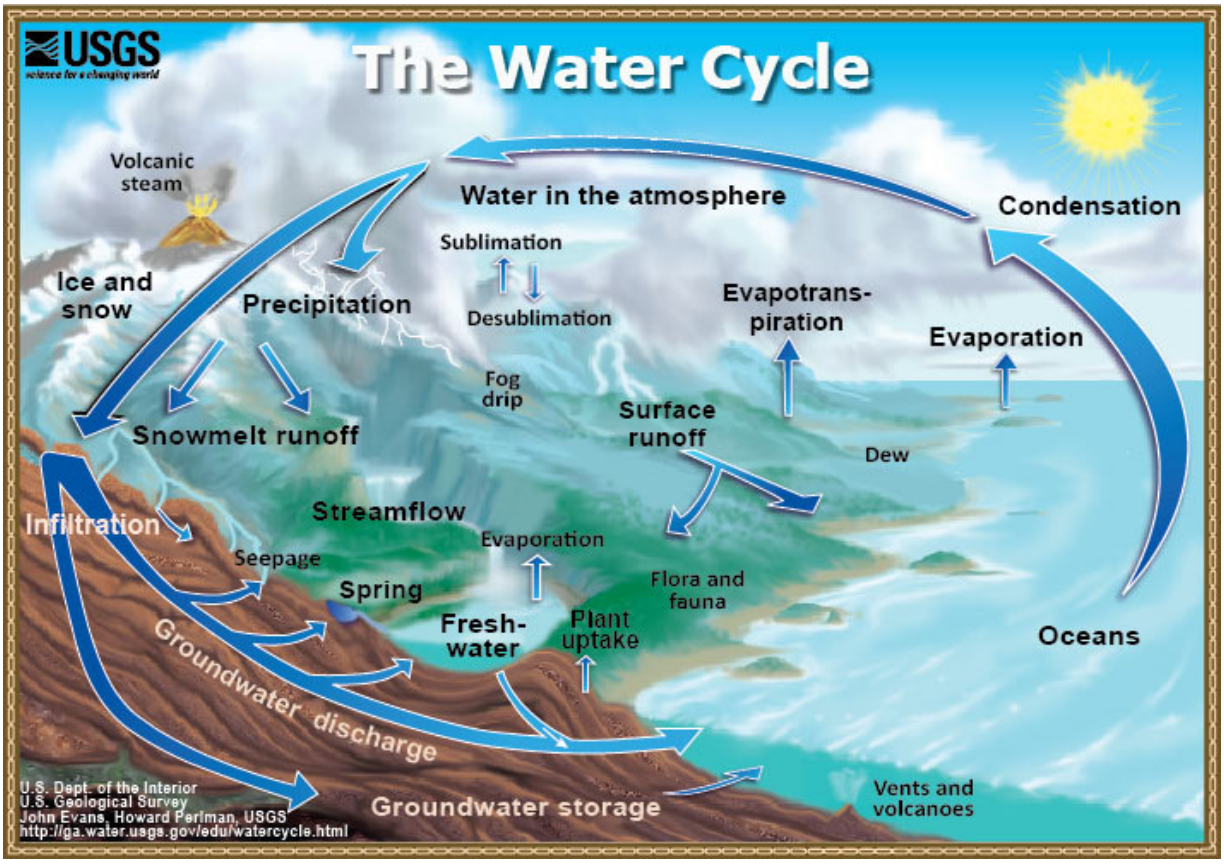

Figure 1. Hydrologic cycle as depicted by the U.S. Geological Survey. Source: U.S Geological Survey, 2014 (http://ga.water.usgs.gov/edu/watercycle.html).

1.3 Water Budget

The cycle holds true to the law of conservation of mass: mass is not created or destroyed but can change form and be rearranged in space, which allows for a water budget. A simplified water balance equation is as follows:

$$P - R - G - ET = \Delta S \tag{1}$$

where P is precipitation, R is surface runoff, $G$is groundwater runoff, ET evapotranspiration, and ΔS is the change in storage. Although not evident in this equation, a crucial process in the water budget is infiltration, which determines the proportion of precipitation partitioned as surface (R) and groundwater (G) runoff (Viessman and Lewis 1995). The water balance was a prerequisite to model continuous stream flow data, which became practical only after the discovery of methods to estimate evapotranspiration (Penman 1948; Thornthwaite 1948). The difficulty in applying this equation to real watershed often lies in the inability or inadequacies of measuring or estimating one or few of these terms.

Infiltration and evapotranspiration are identified as the two most important parameters controlling the water balance of a watershed (Sharma et al. 1980). Moreover, variability is considered to be of paramount importance in defining infiltration of an area (Achouri and Gifford 2013), but to represent its variability requires large amounts of data (Sharma et al. 1980). Similarly, long historical records for evapotranspiration to complement other hydro–meteorological data is not available at a sub–watershed scale and is often calculated as a residual of the water balance or as an areal average (Viessman and Lewis 1995). Since a watershed is defined as all the area that contributes surface runoff to a common most downstream outlet, it is traditionally the scale at which the hydrological budget is calculated for, but it can be estimated at finer and coarser scales.

1.4 Watershed Analysis

The management of many environmental issues can benefit from a watershed analysis framework. Montgomery et al. (1995) describe a disconnect between land management objectives and management practices. They believe that the watershed framework firstly offers a hierarchy of scales at which analysis and planning can be managed (Montgomery et al. 1995). It also facilitates accounting for spatial variability and linking physical watershed processes with biological communities and infrastructure (Montgomery et al. 1995). The watershed framework has been implemented for a number of different purposes including but not limited to strategizing the placement and quantifying the effect of Best Management Practice (BMP) (Hsieh et al. 2010), managing quantity (Pitt and Clark 2008), and quality of water resources (Sahrawat et al. 2010), predicting effects of climate change (Nunes et al. 2008), effects of agricultural practices (Zedler 2003), urbanization (Lee and Chung 2007), land use change (Cho et al. 2009), and water harvesting (Sharda and Ojasvi 2005). Calculating the potential streamflow from precipitation events is done on the basis of finding the residual of water loss through evapotranspiration (Blackie and Eeles 1985). Precipitation from high intensity storms falling on steep sloped impermeable ground will very quickly reach the stream channel in the form of surface runoff. In contrast, gently sloping watershed with permeable surface can accept and transfer precipitation to its subsurface system, eventually reaching the channel at a much later time (Blackie and Eeles 1985). Understanding the hydrology of the watershed is vital for many of the above applications, for which hydrological modeling has been instrumental.

1.5 Hydrological Models

Modeling in hydrology is an attempt to represent reality, with the understanding that it will never be a complete representation (Blackie and Eeles 1985). As a result, the intent is to sufficiently model the major processes, compare modeled data to measured data, and to refine the model accordingly (Blackie and Eeles 1985). Hydrological models also referred to as rainfall-runoff (R-R) models are used to both understand the hydrologic system and as a predictive tool to hypothesize changes in the hydrologic regime as a result of changes in the watershed (Arnold and Allen 1996). Inevitably, hydrological models

are simplifications of the real world system, yet they are valuable tools for researchers and decision makers (Moradkhani and Sorooshian 2008). Originally, motivation for hydrological modeling were engineering problems such as urban sewer design, land reclamation drainage systems design, and reservoir spillway design (Todini 1988). Thus, rainfall-runoff modeling was aimed at predicting the peak discharge rate and the time it took to reach the peak, predictions that were instrumental in designing hydraulic structures. It has now branched out to applications such as climate change, water supplies management, flooding prevention, and impacts caused by land management to list a few (Arnold et al. 1998). Construction of new hydraulic structures can be proposed as a result of the simulated hydrologic response; a number of different scenarios can be run quickly and non-destructively within the model as opposed to physically altering the environment (Viessman and Lewis 1995). Proposed construction designs and spatial placement within the watershed can be tested for influence on an area's hydrology (Viessman and Lewis 1995). Furthermore, much insight can be gained about the watershed during collection of data, parameterization of the model and output that can be spatially analyzed. From empirical formulas in the 19th century (known as the rational method), today, hydrological modeling has advanced to the integration of geographical information systems (GIS) capable of using time series input for real time analysis (Beven 2000). There are various means of differentiating hydrological models. They can be grouped by their theoretical conceptual basis (empirically/statistically, conceptually, and physically based), the discretization of the watershed (fully distributed, semi-distributed, and lumped), and temporal simulation properties (continuous vs. single event).

1.5.1 Watershed discretization: Lumped versus Distributed versus Semi-distributed Models

The conceptual model of the hydrological cycle can be viewed at different scales, but the most common spatial unit is that of the watershed or river basin (Davie 2008). From here on in, watershed and basin will be used interchangeably, and similarly sub–watershed and subbasin. Watershed can range in size from a few hectares to several million square kilometres akin to the Amazon basin (Blackie and Eeles 1985). A watershed outlines an area that drains surface water to a common single outlet (Davie 2008). Since water flows down slope, the boundary of a watershed can be determined by the topography of the area. It is important to note that these boundaries determined for surface water may not always hold true for groundwater (Davie 2008). However, carrying out the water balance equations merely at the watershed level will ignore the heterogeneity of the watershed. For example, the watershed may have different soil types that have different rates of infiltration, which cannot be represented if the water balance is calculated at the watershed level. Depending on the level of spatial heterogeneity to be accounted for in the model, various levels of discretization can be implemented (Arnold et al. 2010). Five different methods of discretization has been cited in the literature: 1) no discretization or lumped, 2) hydrologic response units (HRU), 3) catena approach, 4) topographic index approach, and 5) fully distributed approach (Arnold et al. 2010).

Lumped models are spatially–averaged models (Moradkhani and Sorooshian 2008). Although spatial averaging can occur at a number of scales and therefore is evident even within distributed models, here we regard lumped models as spatially averaged models at the watershed scale. In this case, the entire watershed is thought of as one unit in terms of output (Moradkhani and Sorooshian 2008). The hydrological processes do not have any spatial context upon which the model works. Lumped models can be based on physically based formulas, however, calibrating them requires long historical records (Abbott et al. 1986). Furthermore, calibration often requires extensive curve fitting between the inputs and the outputs, such that the physical basis becomes meaningless (Beven 1989). For instance, effects of land use change on model output cannot be analyzed with confidence and inversely the parameters in the models cannot be altered to represent changes in the watershed (Abbott et al. 1986). Lumped models can be traced back to the rational method which links precipitation to peak discharge by a runoff coefficient parameter (Todini 1988).

Further advances in computer power allowed for distributed models, which have the following benefits over the lumped models: 1) can evaluate the effects of spatially variable inputs and outputs including land-use change; 2) trace sediment and pollutant movement; and 3) model hydrological response at ungauged sites (Beven 1985). These benefits are in demand among practitioners in watershed planning and policy (Abbott et al. 1986). A fully distributed model involves a grid based discretization of the watershed where the water balance of the surface, lateral, and subsurface fluxes are calculated at each grid cell (Arnold et al. 2010). Each grid cell has a spatial location and is connected to surrounding cells. As a result, the distributed model has capabilities to analyze the hydrological response at multiple locations within the watershed as opposed to the single watershed outlet of lumped models (Freeze and Harlan 1969). Developed in the mid to late 1970s, the Système Hydrologique Européen (SHE) model was an ambitious physically based fully distributed model that describes the many processes involved in the movement of water (surface and subsurface) with differential or empirical equations (Bathurst and Cooley 1996). However, the large data and computation requirements prevent the use of fully distributed models on larger watershed (Arnold et al. 2010). Enlarging the grid cell size to increase computational efficiency can lump heterogeneous areas together (Arnold et al. 2010). The advanced nature of SHE and other distributed models requires the user to be well versed in hydrological principles and therefore is less likely to be used by water resource practitioners. Furthermore, distributed models need a higher number of parameters to be satisfied. Thus, collecting data for each parameter can have issues of expense and labour. Additionally, the need to satisfy a large number of parameters increases the likelihood of sensitive parameters that require higher precision in measurements. Bathurst (1986) claimed that instruments presently in use could not acquire this desired precision. Therefore, hydrological models often present a trade-off between complexity, ease of use, and uncertainty.

A semi–distributed model is the compromise between a lumped and a distributed model, having some of the characteristics of both. The watershed is discretized or partitioned further in a way to account for the spatial variability of basin parameters. However, within each partition the area is

considered homogeneous and thus assumes the characteristics of a lumped model. In essence, the semi-distributed model offers a compromise between computational efficiency and accounting for spatial variability. Both semi-distributed and distributed models offer insights about interior basin properties (channels, structures, interior locations) that cannot be attained from lumped models (Khakbaz et al. 2012). Commonly, the watersheds of a semi–distributed model is first partitioned into sub–watersheds or subbasins, delineated based on the land area providing surface water to a single reach of the stream network (Boyle et al. 2001). Subbasins are spatially connected to each other and as a result, upstream output of subbasins can affect downstream subbasins (Arnold et al. 2010). The rainfall–runoff response can be realized for each sub–watershed and the watershed as a whole at their respective outlets (Boyle et al. 2001). The subwatershed is partitioned further by various methods depending on the model.

The Hydrologic Response Unit (HRU) approach aims to lump together the hydrological processes of land areas with the same soil, slope, and land use combinations in each sub–watershed (Arnold et al. 2010). There can be more than one HRU within a subwatershed but because HRUs do not assume an actual spatial position within the subwatershed, they are not linked with each other but merely represent percentages of combinations (Arnold et al. 2010). Upslope HRU output do not affect downslope HRUs. Surface and subsurface water output from each HRU is totaled for the entire subwatershed and routed to its main reach. This approach is used in the Soil and Water Assessment Tool (SWAT) (Neitsch et al. 2011).

The Water Erosion Prediction Project (WEPP) watershed model (Flanagan et al. 2007), positions a representative hillslope within each sub–watershed. Known as the catena method, the hillslope offers more detailed routing of surface, lateral, and ground water and the impacts of upslope management on downslope areas can be realized (Arnold et al. 2010). However, this method accommodates only one single slope formation per subwatershed and some difficulties exist in extracting a hillslope formation that represents the area and its climate (Arnold et al. 2010). The Hydrological Simulation Program–Fortran (HSPF) model (Bicknell et al. 1997) simply differentiates between pervious and impervious areas within each subwatershed.

Rathjens and Oppelt (2012a) compared outputs from different discretization methods on the same watershed and hydrological model to see the effect the discretization method would have on the model response. Two different discretization methods were compared: the HRU and grid cell. The default user interface of the SWAT hydrological model was used for the HRU discretization while a combination of SWATgrid, TOPAZ and SWAT was used for grid cell based discretization (Rathjens and Oppelt 2012a). SWAT codes responsible for routing loadings through the watershed allows for grid cell, hillslope and subwatershed/hru discretization, but currently the GIS interface only supports the latter (Arnold et al. 2011). SWATgrid written in fortran90 and run on command line, processes inputs and outputs of SWAT for grid based discretization (Rathjens and Oppelt 2012a), while TOPAZ using topographic analysis determines grid cell drainage according to the deterministic eight-neighbour (D8) method (Fairfield and Leymarie 1991). Rathjens and Oppelt (2012a) showed that there was very little

difference between the flow out produced from both discretization methods (HRU vs. grid cell), scoring a correlation coefficient of 0.9977 when compared. Although comparable, the ability of a grid based watershed to model the management effects of upslope areas on downslope regions remains to be an advantage. Furthermore, field collected data will also be correctly spatially represented. However, simulation of grid based discretization takes an order of magnitude longer to run. Rathjens and Oppelt (2012b) reported that while the simulation time per year for subwatershed discretization took 30 seconds, the grid cell discretization took 12 hours.

1.5.2 Empirical/statistical versus Physically Based Models

Until the 1940s, stream flow response to rainfall was estimated based on statistical analysis of existing records (Blackie and Eeles 1985). Such analysis required long term records of rainfall and stream flow measurements, which were scarce and sometimes unreliable (Blackie and Eeles 1985). Available records were also used to derive empirical formula having a general structure of:

$$Q = A \times P \tag{2}$$

where Q is discharge, P is precipitation and A is a back calculated constant from collected data (Blackie and Eeles 1985). Empirical formula draw a correlation between the input and output without accounting for much of the underlying physical basis. These methods have been used as stand alone "models" (Todini 1988), but are also implicit within many complex models as equations to describe certain processes. With a more cohesive understanding of the parameters involved in the water balance, an attempt to represent processes through physical laws was made (Blackie and Eeles 1985). The categorization of these complex models are not well established, especially due to the many in-between model types that overlap. Following the strictly empirical models, the next order of conceptual complexity is defined in literature as lumped, lumped parameter, or conceptually based models. The division between these models and the highest order of conceptual complexity (physically based models) is at times blurred.

Lumped models simplify the hydrological response either by lumping/averaging the spatial variability and/or the representation of the physical processes (Blackie and Eeles 1985). Spatial averaging at various scales was discussed in the watershed discretization section. As an example of lumping physical processes, various forms of precipitation abstraction (infiltration, interception, storage) can be used as a single compounded term (Neitsch et al. 2011). In this case, the physical process of the three different abstractions cannot be distinguished but they are somewhat accounted for. As a result, lumped parameter models contain many assumptions and semi–empirical equations that aim to describe the physical processes as best as possible (Refsgaard 1996). Complex lumped models were made possible with the increased understanding in the movement of water through the catchment "stores" and the expansion of computer power (Jakeman and Hornberger 1993). It was not until the 1950s when a compound understanding of infiltration (Horton 1933; Philip 1954), storage and movement of water in the

soil (Richards et al. 1956), and hydraulics of groundwater flow was synthesized (Blackie and Eeles 1985). Computer assisted hydrological modeling began in the 1960s with the Standford Watershed Model (SWM) being the first successful computer model (Singh et al. 2006). In contrast to a simple curve fitting, SWM implemented processes of infiltration, the unit hydrograph, and recession functions to model daily rainfall-runoff response as opposed to estimating single extreme events (Crawford and Linsley 1966). Soon after, SWM was improved to model hourly stream flow response and included soil moisture accounting, flow routing techniques, and estimates of evapotranspiration (Crawford and Linsley 1966). The SWM model succeeded into the HSPF model, which was the first model to connect land surface contamination with in-stream chemical interactions (Singh et al. 2006). The continuous nature of HSPF required a watershed data management program (WDM) that could feed time series data into the model. This improved user interactivity came as a vast improvement to punched card inputs.

In the mid 1970s, existing models (lumped parameter models) could not tackle water management issues pertaining to the effects of land use change that came about from agricultural and forestry practices, waste disposal, and other issues tangent to water use (Abbott et al. 1986). The surfacing issues were the result of anthropogenic negative impacts on the hydrological cycle. European countries were faced with polluted surface and groundwater sources as a result of intensive farming practices (use of fertilizers/pesticide); contaminants from waste disposal sites were finding their way into water resources; the developing world was challenged by changes to high and low flow regimes and rapid soil erosion in response to large-scale deforestation; soil erosion was causing heavy siltation in reservoirs; and the cost of water pumping was increasing in conjunction with the rise in fossil-fuel costs (Abbott et al. 1986). The increasing cost of water resource development warranted a demand for an approach of hydrological modeling that could optimize project planning (Abbott et al. 1986). The development of such a model was faced with foreseen hurdles of resources (human expertise and computing power), and satisfying the potentially large amount of data to run the model (Abbott et al. 1986).

Physically based distributed models were developed to overcome these deficiencies (Abbott et al. 1986). A large amount of data and scientific understanding was available to be taken advantage of including digital elevation models (DEM), soil/land use maps, soil physics, and plant physiology that could be incorporated into the model to be better suited for project planning. Such a model needs to account for spatial variability (distributed or semi-distributed model). Models that can produce spatially variable output allows users to realize the output at various areas within the watershed (interior locations at the sub–watershed level or even finer scales) as opposed to just at the watershed outlet. Furthermore, a physically based and distributed model can also model the dynamics of point source pollution. That is if pollutants are added at a certain location, its dispersion can be modeled (Abbott et al. 1986). In addition, the physical basis of the model enables the hydrological response to react to changes in landscape or climate input. Beven (1989) realizes the need for physically based models but cautions against having unrealistic expectations regarding their ability to model hydrological processes. His critique directs

modelers against uncritical belief in the models and for pushing development forward with this in mind. Admittedly, full details of all hydrological processes are not incorporated and have not even yet been fully discovered. The physical basis is then a synthesis of empirical facts, theoretical knowledge and mathematics (Klemeš 1983). More importance is given to the dynamic interactions between the gross features (Gupta and Waymire 1983). However, the physical basis of the model is expected to be functional on catchments with little or no hydrometeorological record. This facet is highly favourable for modeling ungauged watersheds and for establishing a new measurement regime to be used as input within a short time span. With lumped parameter models, less interest will be shown to new measurement regimes since they would need to run for decades prior to serving as model inputs. Thus, there are few alternatives to physically based models when dealing with issues of catchment changes, ungauged catchments, spatial variability in catchment inputs and outputs, and point source contamination (pollutants and sediments) (Abbott et al. 1986).

However, it seems that the scale at which the watershed is discretized can lead physically based models into the same pitfalls as the lumped model. If the watershed is partitioned into 250 m x 250 m grids, the physical processes are essentially lumped for this area, without any framework that suggests its homogeneity (Beven 1989). Finer grid cells or the concept of HRUs can somewhat ease this concern. Other researchers found the utility of physically based model far superior to lumped models especially because of the ability to calibrate the model with physically based reasoning (Bathurst 1986). Nevertheless, Beven (1989) reminds model users that even the most complex physically distributed model (i.e., Systeme Hydrologique Europeen (SHE)) is a major simplification of a three-dimensional catchment with spatial and temporal heterogeneity. For instance, they assume that Darcy's law of hydraulic conductivity applies to both saturated and unsaturated flow (generally applies to saturated flow only) and that surface runoff occurs in a sheet flow manner with uniform depth and velocity (Freeze and Harlan 1969). Furthermore, the equations driving physically based models are based on small scale physics of homogeneous systems (Beven 1989).

1.6 Soil and Water Assessment Tool (SWAT)

The Soil and Water Assessment Tool (SWAT) is being continually developed as a solution to the dilemma of using a spatially distributed model while overcoming the common difficulties of the distributed model (Arnold et al. 1998). SWAT has readily available inputs for modeling large watersheds, it is computationally efficient (coded in Fortran), takes into account spatial variability of parameters and inputs, operates on a continuous daily time step, can support long periods of simulations to consider effects of management changes, and models both water quality and quantity (Arnold et al. 1998). Furthermore, because the model is based on equations of physical processes, it can model ungauged sites without calibrating the model with historical data (Arnold et al. 1998). Instead of dividing the watershed based on an orthogonal grid, SWAT divides its basin into subbasins using a digital elevation model (DEM). Subbasins are created using topography driven flow paths of precipitation (e.g., all of the ground area that

will contribute surface water to a stream segment will be considered within one subbasin). The subbasins are further divided into hydrological response units (HRU) which are unique overlay combinations of slope, soil, and land cover (Gassman et al. 2007). By having inputs for each HRU, the model produces a better representation of the spatial variability within the watershed.

The SWAT model can serve as a plug–in program integrated into a Geographical Information System (GIS) software. Presently it has been integrated as MWSWAT into a free GIS software known as Map Window, and as ArcSWAT within ArcMap. Hydrological modeling in this study is carried out with ArcSWAT for ease of map data preparation within ArcMap and its sophisticated map tools. ArcSWAT uses AML programming language for integration into ArcMap, visual basic for the graphic user interface and C++ for the internal database. However, the core SWAT program itself is programmed as multiple (one for each process) integrated programs written in Fortran. SWAT software and documentation can be downloaded free from the following website: http://swat.tamu.edu/ .

1.7 Spatial Variability and Field Sampling

While lumped models cannot express spatial variability, physically based models are by default distributed (Beven 1985). Distributed models allow for the representation of many spatially variable watershed parameters, among which the soil hydraulic conductivity has been found to be of particular importance (Freeze 1980). Hydraulic conductivity is the rate (volume per unit time per unit area) of water movement through the soil matrix given a unit potential–energy gradient (Dingman 2002). The rate is largely dictated by the cross sectional area of available pathways for water movement. Under unsaturated conditions, this is determined by both soil grain size and degree of saturation, while under saturated conditions it is grain size alone (Dingman 2002). Undoubtedly, infiltration and evapotranspiration are the most important processes that affect the movement of precipitated water through the watershed (Sharma et al. 1980), for which the spatial characterization of soil type and vegetation cover are required (Brath and Montanari 2000). By definition, parameters for physically based models can be measured in the field (Beven 1985). Taking into account that soil properties can vary considerably at the watershed scale and even at the field scale within a single soil type (Peck et al. 1977), many earlier studies complementing the advent of physically based models, studied the spatial variability of soil properties in a watershed. Through infiltration studies they found saturated hydraulic conductivity to be highly variable at the field scale (Russo et al. 1997), along a slope and across a slope (Gupta et al. 2006), and both horizontally and vertically (Carvallo et al. 1976). Collecting field data for model input was regarded to be very time consuming, and studies pushed to find alternatives such as using scaling factors with measured bulk parameters (Sharma et al. 1980) or transferring measured values from representative sites (Bathurst 1986). In recent years, there has been a disregard to represent soil property variability all together. Instead, it has been favourable to lump parameter values at coarser spatial scales (Brath and Montanari 2000). For example, studies opt to rely on readily available generalized soil surveys that assign one value to an entire soil type regardless of the position in the watershed (Zhu and Scott Mackay

2001). Unless the model is used solely for the prediction of flood flows where the runoff is produced through the Hortonian mechanism (infiltration capacity is depleted throughout the watershed in which case, variability of infiltration capacity does not matter) (Brath and Montanari 2000), neglecting spatial variability in simulating hydrologic response can include significant error (Brath and Montanari 2000)

Within the literature there was very little evidence of studies comparing the effectiveness of using field collected data with physically based models. In order to satisfy the need of the U.S. National Weather Service for improved hydrological model calibration procedures, Boyle et al. (2001) conducted a study comparing both semi-distributed and lumped models with and without spatially distributed model inputs and parameters. Their results show that spatial representation of model parameters such as soil properties (soil storage, lateral flow, and percolation) show little or no improvements unlike the significant improvements resulting from distributed precipitation input and soil moisture computations. However, the influence of spatially distributed soil properties were tested only by allowing values to vary during calibration and not through implementation of actual field data.

Within SWAT there are two methods for calculating runoff: the SCS Curve Number (CN) method and the Green & Ampt (GA) method. As the curve number method is merely an empirical formula to calculate runoff, it lumps interception by vegetation and soil infiltration into a single term, and does not account for their physical processes (Neitsch et al. 2011). On the contrary, a more physically based approach of calculating runoff is the Green & Ampt (GA) method for which hydraulic conductivity is listed as the most important parameter (Shin et al. 1998). Furthermore, GA method accounts for interception of precipitation by vegetation and subsequent evaporation based on measures of canopy cover (i.e., leaf area index (LAI)– one sided green leaf area per unit ground area). Our study aims to compare effects of spatially collected field data (soil hydraulic conductivity, bulk density, and LAI) on both the CN and GA rainfall-runoff methods within SWAT hydrological model.

1.8 Model Efficiency, Calibration/Validation and Uncertainty

Evaluation of hydrological models is based on the subjective or objective comparison of simulated to observed variables, which is most often the stream flow at the watershed outlet (Krause et al. 2005). Subjective analysis includes visual inspection of both the simulated and observed hydrographs assessing their dynamic (base flow, rising limb and falling limb) and systematic (over or under prediction) behavior (Krause et al. 2005). Objectively, an efficiency/objective criteria can be used as a mathematical measure of how well the observed and simulated values fit (Krause et al. 2005). The most frequently used statistic reported for hydrologic calibration and validation is the Nash-Sutcliffe model efficiency (NSE) coefficient (Eq.

(3)), where O_i is the observed flow discharge at time i , P_i is the predicted flow discharge at time i, and $\bar{O}$ is the average of observed discharge for length of the observed period (Krause et al. 2005). The root mean square error (RMSE) has also been cited to be of value among others, where O_i is the observed

flow discharge at time i , P_i is the predicted flow discharge at time i (Eq. (4)) (Abbaspour et al. 2004). The NSE ranges from -∞ to 1 and it is defined as one minus the sum of the absolute squared differences between the observed and predicted values normalized by the variance of the observed values (Nash and Sutcliffe 1970); RMSE ranges from 0 to infinity, 0 indicating a perfect fit. (Eq.

(3)).

$$E = 1 - \frac{\sum_{i=1}^{n}(O_i - P_i)^2}{\sum_{i=1}^{n}(O_i - \bar{O})^2} \quad (3)$$

$$RMSE = \sqrt{\frac{\sum_{i=1}^{n}(O_i - P_i)^2}{n}} \quad (4)$$

Although no absolute criteria has been established to judge model performance, Moriasi et al. (2007) has suggested that NSE values should exceed 0.5 at the monthly time step. The standard for daily and annual time step can be relaxed or tightened respectively. Generally, daily predictions have been noted to have the poorest results out of the three time steps with a few exceptions (e.g., Grizzetti et al. 2005). Poor results are generally attributed to lack of model calibration (Bosch et al. 2004), inadequacy in representing spatial variability of rainfall (Bouraoui et al. 2002), inaccurate measured streamflow data (Harmel et al. 2006), and insufficient calibration and validation periods (Muleta and Nicklow 2005).

Regardless of its popularity, Legates and McCabe (1999) advise against goodness–of–fit tests like the NSE for hydrologic or hydroclimatic model evaluations. Although it is deemed more suitable than the coefficient of determination (R^2), NSE and other correlation coefficients alike have been shown to be overly sensitive to extreme values (Legates and McCabe 1999). Thus, evaluating runoff predictions with NSE can cause over– and under–prediction of model performance during peak and low flows respectively (Krause et al. 2005). Willmott et al. (1985) show that the difference or error-based measures such as RMSE are better suited to evaluate hydrological model performance. Moreover, it can be appropriate to use both a measure of goodness-of-fit (e.g., NSE) and an absolute error measure (e.g., RMSE) for a more complete assessment of model performance (Legates and McCabe 1999). Furthermore, a bootstrap approach can be used for these indices to show reliability (Dahlke et al. 2009). In statistics, bootstrapping is an automated technique to take a number of smaller samples randomly within the larger original dataset and to compute the statistic (i.e., RMSE) for each sample individually. The distribution of the values will indicate the reliability of the statistic evaluation (Efron 1981).

In addition to gauging model performance, efficiency criteria like the NSE and RMSE statistics can be used for automatic model optimization or calibration. In such cases the index is referred to as the objective function, a measure to evaluate how well the simulation fits the observations (Beven 1985).

From lumped parameter to physically distributed models, calibration to some extent is carried out in an attempt to adjust model parameter values to produce streamflow outputs that better correlate with measured data. Until 1965, model fitting to observed data was done on a trial and error basis (Blackie and Eeles 1985). Subsequently, automatic parameter optimization was implemented which was carried out by inverse modeling, that is, using measured output data to back calculate hard to measure input parameter values (Abbaspour et al. 2004). This is often required for physically based models as the number of parameters are high, but not all of them can be measured in the field or given a value based on a priori knowledge. If left uncalibrated, parameters will assume model defaults or averaged values. A sensitivity analysis provides the basis for choosing the parameters to be used in the calibration procedure. It is used to rank the parameters to which the model is most sensitive to by evaluating the relative changes to the model output as a response to the relative changes in parameter values (Shen et al. 2009). Through calibration, the values of the chosen set of parameters are optimized to have modeled streamflow data correlate more closely to the measured gauged streamflow values. Automatic calibration methods operate their optimization procedure by aiming to maximize or minimize the objective function (i.e., minimize if RMSE, but maximize if it is NSE). To ensure successful calibration, the model is simulated for a new set of years for which the parameters have not been optimized for, and both measured and simulated outputs are compared again; this is referred to as validation. This validation gives practitioners the confidence that the model is sufficiently capable of representing the hydrological processes within the watershed.

It is important to note that due to the nature of calibration being inverse modeling, there lies the possibility of various parameter value sets and model structures producing similar objective function values (Beven and Freer 2001). This illustrates the problem of equifinality described by Beven (1993), that the same model result can be achieved in a number of different ways. The concept of equifinality cautions against the belief of a single "optimum parameter set" and suggests results of chosen parameter sets to be expressed with some degree of uncertainty (Beven 1993). Furthermore, there should be realization that using just the input–output of the model to calibrate cannot make up for the complexity of the model structure (Hornberger et al. 1985). Among other solutions, Hornberger et al. (1985) suggests that the number of parameters to be estimated should be reduced by specifying specific values for parameters (i.e., through field measurements) or eliminating them based on the hierarchy of a sensitivity analysis.

Calibrating a hydrological model is made difficult by intrinsic sources of uncertainties in model structure and input data (Singh et al. 2013). Uncertainties arise from model structure if sufficient watershed processes are not accounted for or if they are over simplified (Singh et al. 2013). Input data uncertainty can be attributed to errors in measurement (i.e., rainfall, temperature) or spatial interpolation (DEM) (Singh et al. 2013). In conventional uncertainty analysis (Bayesian approaches) only parameter and measurement errors are considered while errors related to model structure or input uncertainties are not accounted for, which can lead to unreasonable prediction uncertainty bounds (Yang et al. 2008). New

uncertainty analysis such as the Generalized Likelihood Uncertainty Estimation (GLUE) (Beven and Binley 1992) and Sequential Uncertainty Fitting (SUFI-2)(Abbaspour et al. 2007) have been developed to overcome these shortcomings. SUFI-2 is capable of running both an uncertainty analysis and optimization procedure (Abbaspour et al. 2007). Comparing a number of uncertainty analysis techniques including GLUE and SUFI-2, Yang et al. (2008) found SUFI-2 to produce good prediction uncertainty ranges with the smallest number of model runs when based on the Nash-Sutcliffe coefficient. This study aims to use the SUFI-2 uncertainty analysis for calibration while substituting certain parameters with their specific field collected values.

1.9 SWAT Applications

SWAT applications were driven by but not limited to the needs of various government agencies both in the U.S. and the European Union from the regional to the national scale (Gassman et al. 2007). Canadian applications have been limited partly due to the lack of data and the difficulty of integrating available Canadian data into the SWAT structure. Primarily, these applications have been about the effect on water resources (quantity/quality) induced by anthropogenic, climate change, and other factors. SWAT's first application was in simulating the impacts of hydrologic and/or pollutant losses from agricultural practices and municipal water use within 2,149 U.S. Geological Survey (USGS) watersheds (Gassman et al. 2007). The research was carried out within the Hydrologic Unit Model of the U.S. (HUMUS) modeling system (Arnold et al. 1999) to aid the U.S. Department of Agriculture (USDA) in analysis of the U.S. Resources Conservation Act Assessment of 1997 and to quantify the benefits of the conservation practices (Gassman et al. 2007). In Europe, SWAT has been included in a number of projects, testing for the model's ability to predict stream flow under various scenarios. Among others, projects include the Climate Hydrochemistry and Economics of Surface-water Systems (CHESS) in which the impacts of climate change was quantified for five different watersheds (CHESS 2001). SWAT was also among nine other models included in the EUROHARP project that tested the ability of models to predict nonpoint-source phosphorus and nitrogen losses to coastal waters and fresh water streams (Arnold and Fohrer 2005).

To summarize the world wide applications of SWAT, studies can be grouped into the following eight categories: calibration and/or sensitivity analysis, climate change impacts, GIS interface descriptions, hydrologic assessments, variations in configuration or data input effects, comparisons with other models/techniques, interfaces with other models, and pollutant assessments (Table 1).

Table 1. An Overview of SWAT studies reported in literature by application categories (source: Gassman et al. 2007).

Primary Application Category	Hydrologic Only	Hydrologic and Pollutant Loss	Pollutant Loss Only
Calibration and/or sensitivity analysis	15	20	2
Climate change impacts	22	8	–
GIS interface descriptions	3	3	2
Hydrologic assessments	42	–	–
Variation in configuration or data input effects	21	15	–
Comparisons with other models or techniques	5	7	1
Interfaces with other models	13	15	6
Pollutant assessments	–	57	6

1.9.1 Climate Change Impact Studies

SWAT can model climate change impacts on the watershed by accounting for increased atmospheric CO_2 within its plant development and transpiration processes, and by altering climatic inputs (i.e., changes to precipitation patterns) (Gassman et al. 2007). Studies conducted in both Texas (Muttiah and Wurbs 2002) and India (Gosain et al. 2006) simulated 20 year climate projections starting from 2040's, reporting increases in flood and drought severity. Majority of studies predict notable differences to baseline dominant weather patterns largely as a response to precipitation patterns suggested by global or regional climate models (Thomson et al. 2005, Stone et al. 2001, Jha et al. 2004). Takle et al. (2005) confirm that precipitation output from GCMs can be used to predict 20^{th} century annual streamflows for the upper Mississippi River basin and rank the association between GCM and SWAT highest among other models.

1.9.2 Variation in Configuration or Data Input Effects

Studies have reported on the effects of HRU/sub–watershed delineation on SWAT output (users have the option as to how fine or coarse the watershed delineation should be). There are one or more HRUs within a sub–watershed and more than one sub–watershed within an entire watershed. HRUs are the unique combinations of soil, slope, and land use/cover within the sub–watershed. There seems to be a consensus that streamflow predictions were insensitive to HRU/sub–watershed delineations (Manguerra and Engel 1998; Chen and Mackay 2004; Tripathi et al. 2006). However, limiting only one HRU per sub–watershed had poorer performance compared to having multiple (Haverkamp et al. 2002). Generally, streamflow estimates produced with higher resolution DEM, land cover/ use (LCLU) and soil

inputs show a better match with measured values (Bosch et al. 2004). Between the three, studies have identified DEM resolution to be of most importance for both flow and sediment outputs (Cotter et al. 2003; Di Luzio et al. 2005; Chaplot 2005). However, there seems to be a discrepancy between the importance of soil resolution as studies have showed cases of sensitivity (Chaplot 2005) and insensitivity (Di Luzio et al. 2005) to model outputs. Once parameters are calibrated for a certain watershed, transferring these calibrated ranges to another watershed resulted in a markedly reduction in model efficiency (Heuvelmans et al. 2004). A number of studies have realized the responsiveness of SWAT to land use change within a watershed (Gassman et al. 2007). Hernandez et al. (2000) has reported this responsiveness even within the sub–watershed scale (e.g., 8.2 km^2). Studies have shown that increasing density of precipitation gauges can improve streamflow estimates (Hernandez et al. 2000; Chaplot 2005) and that Next–Generation Radar (NEXRAD) (remotely sensed precipitation) inputs can be as good or better than dense rainfall gauges (Kalin and Hantush 2006).

1.9.3 Interfaces With Other Models

SWAT has been integrated into various other models to increase its functionality and research domains. SWATMOD is a an integration of SWAT within the MODFLOW groundwater model, which allowed for evaluation of management scenarios of groundwater withdrawal rates (Sophocleous et al. 1999). The same integration was used to show effects of irrigation on groundwater and streamflow levels in North Central Kansas (Sophocleous and Perkins 2000) and for modeling an entire watershed in Brittany, France (Conan et al. 2003). SWAT has also been linked to specialized physically based soil erosion models such as the Water Erosion Prediction Project (WEPP) (Renschler and Lee 2005). Through WEPP's geospatial interface (GeoWEPP), output from WEPP can serve as point sources in SWAT (Renschler and Lee 2005). Although long-term results from using SWAT alone and in conjunction with WEPP were similar, short term results presented noticeable differences (Renschler and Lee 2005). SWAT has also been paired with ecological models such as ELLA to predict the impact of land use change on both streamflow and species habitat (Weber et al. 2001). Even economic simulations have been undertaken with integration of SWAT into models such as the Agricultural Policy Extender (APEX) and a farm economic model to investigate both environmental and economic responses to manure management scenarios (Gassman et al. 2002).

1.9.4 Hydrologic Assessments

SWAT has been useful in many different applications but one that is foundational to all others is its ability to represent the hydrologic regime of the watershed. The CN runoff method is generally used over the Green & Ampt method (Gassman et al. 2007). Studies have reported equal or superior performance of CN method over the Green & Ampt (King et al. 1999; Kannan et al. 2007). Although SWAT's performance has been praised at the monthly and annual temporal scales in simulating both hydrologic and/or pollutant loads, in most cases, SWAT's performance at the daily scale has been less

than satisfactory and signify areas of weakness of the model (Gassman et al. 2007). This study investigates the possibility of improving the daily hydrologic output of SWAT by integrating spatially variable field data.

1.10 Goals and Objectives

Hydrological models are used to understand the hydrologic system of a watershed and to predict its future responses. This is best realized through physically based distributed models, which have the advantage of accounting for hydrological processes individually and the spatial heterogeneity of parameters. SWAT is a semi-distributed model and allows for changes in parameter values at the HRU level. Nevertheless, important parameters concerning process of infiltration and interception are usually only considered at the soil type or LCLU scale. That is, the heterogeneity within a soil type or LCLU class is neglected. To the author's knowledge at the onset of this study, very few have integrated field-collected data (other than hydro-climate data) into the SWAT hydrological model.

The first goal of this study is to investigate whether heterogeneity of parameters concerning infiltration (hydraulic conductivity and bulk density) and interception (leaf area index) can be accounted for at the HRU level through field sampling and be successively implemented into SWAT hydrological model. The objectives for this goal are as follows: 1) Setup the SWAT model for a Canadian watershed; 2) Test a field sampling technique based on HRU distribution that would compliment SWAT's parameterization structure; 3) Compare in–situ hydraulic conductivity and LAI from different instruments; 4) Compare field collected data with database values; and 5) Integrate field data into the SWAT model. Since SWAT allows parameters to vary at the HRU level and accommodates user input for the values, it is hypothesized that through the framework of the HRU concept field data could be seamlessly integrated into the model.

The second goal of this study is to evaluate whether field collected data and accounting for their heterogeneity at the HRU level will improve correlations between measured and modeled flow data at the daily timescale. The objectives for this goal are as follows: 6) Evaluate the Curve Number (CN) and Green & Ampt (GA) runoff model performances with and without field data; and 7) Determine the effect that field data has on default, calibrated, and validated models. It is hypothesized that the GA model will benefit greater from field data implementation as it is a physically based runoff method while the CN is not. Furthermore, the calibration and validation process is expected to benefit from field data as it will reduce the uncertainty for the parameters collected in the field. Without field collection, the values used may not reflect the landscape and therefore negatively impact the calibration process. Similarly, field collected values are expected to improve performance of uncalibrated default models

2. Methods

2.1 Study Site: The Duffins Watershed

2.1.1 Natural Landscape

The Duffins Creek watershed drains approximately 283 km^2 and is viewed as one of the healthiest among Lake Ontario's Northern shore watersheds (TRCA 2003). It lies in the eastern part of the Greater Toronto Area (GTA) watersheds under the jurisdiction of the Toronto and Region Conservation Authority (TRCA). The majority of the watershed is situated within the regional municipality of Durham Region, and the remainder within the York Region. The headwaters of Duffins Creek originate from the upland regions of Oak Ridges Moraine (ORM) traversing through 5 local municipalities of Whitchurch-Stouffville, Markham, Uxbridge, Pickering and Ajax, eventually emptying downstream into Lake Ontario (TRCA 2003). Duffins Creek watershed can be split into four different physiographic regions each with distinct slope gradients and soil types: the Oak Ridges Moraine, the Halton Till Plain, the Lake Iroquois Shoreline, and the Lake Iroquois Plain (TRCA 2002d). The upland landscape of ORM is covered with ponds and hills, a terrain primarily composed of sand and gravel (Chapman and Putnam 1984). The southern slope of the ORM contains drumlins (long thin hills formed from glacial debris) leading to the Halton Till Plain which contains gentle rolling hills and an array of soil types, some of which compliment agricultural practices (TRCA 2002b). A band of sandy soils exist further downstream along the Lake Iroquois shoreline which is remnant of the last glacial retreat. However, a lacustrine soil mixture of clay, silt and sand emerge closer to Lake Ontario along the Lake Iroquois plain (TRCA 2002b). The cold water streams in the upper portion of the watershed support rich aquatic life, large areas of forest, meadows, and wetlands (TRCA 2003). The middle of the watershed is rural with well defined valleys where agricultural practices dominate (TRCA 2003), although there has been a decline since the 1940s (TRCA 2002b). The southern portions of the watershed has become more urbanized and contains commercial corridors (TRCA 2003).

2.1.2 Climate

Duffins Creek watershed experiences similar ranges of weather conditions akin to the rest of Southern Ontario, including bitter winters and oppressive summer heat. It has a continental climate moderated by Lake Ontario (TRCA 2002c). Summer temperatures generally range from mid–upper 20s in the daytime to mid–low teens during nighttime. Winter temperatures can range from 0 to -30°C (TRCA 2002c). Within the watershed, daylong precipitation events are rare, instead shorter localized events are more common. Most of these storms are short duration and intense storm events that quickly run off into drains and streams (TRCA 2002c). On average, the annual total rainfall is approximately 700 mm, of which 15% is in the form of snow (TRCA 2002c). However, annual rainfall have significantly deviated from the average resulting in very wet and dry years (TRCA 2002c).

2.1.3 State of the Watershed

Among GTA watershed, Duffins Creek has been the most studied, partly due to monitoring campaigns to gather data in support of proposals for Pickering airport and Seaton land development. Although plans for the Pickering airport were cancelled, the Seaton community development project is believed to begin in 2014. Eight stream gauges had been put in place, but are in a threat of discontinuation due to a lack of funding (TRCA 2002d). In 2001, two new stream gauges have been placed in Claremont Conservation area where we have chosen to conduct our field sampling. Based on stream gauge records, the hydrologic response of Duffins Creek watershed still emulates that one of a natural watershed. Notably at the time of investigation (2002), peak flows occur once a year as opposed to urbanized watershed that have re-occurring peak flows throughout the year. Furthermore, the lag time for peak flows to be achieved is considerably longer than urbanized watersheds. During the rainfall event of 50–60 mm on 3 May 2000, Duffins Creek watershed took 13 hours to peak, while a similar watershed that was urbanized (Don River watershed) took only 4–5 hours with double the amount of flow (TRCA 2002d).

As one of the last watersheds along Lake Ontario's northern shore that functions well hydrologically, much attention must be paid to the water balance in formulating sustainable developments. The Durham region had increased in population by 40% between 1986–1996 to 460,000 and is projected to grow to 1 million by 2021 (TRCA 2002b). As significant portions of the watershed are publically owned (TRCA: 8%, Federal Government: 24%, Provincial Government: 10%), there is a great opportunity for leadership towards environmental consciousness. This requires not just placements of stream gauges but understanding how the watershed functions at finer spatial and temporal scales, particularly to project the effect development will have downstream during various precipitation events. Furthermore, while the water supply for the urban areas comes from Lake Ontario, the rural areas still depend on groundwater (TRCA 2002b). As urban sprawl continues northward, the water budget of the watershed needs to be understood for both the short and long term projections of population expansion.

2.2 Field Site: Claremont Conservation Area

Our study aims to see how field collected data can improve the modeling response at the sub–watershed scale. Among the various publically owned land, we were able to gain access to Claremont Conservation Area under permission of TRCA. We have chosen Claremont located at East side of the middle portion of the watershed to capture the hydrological response of a natural area of the watershed, that could eventually become urbanized. It was also chosen for having rain and stream gauges in proximity to our field sites, such that the alteration of model parameters according to field data can be realized at the stream gauge without any dampening effects of in between land. Claremont has an area of 1.61km^2 within which 44 sites were targeted for field collection based on HRU analysis (Figure 2). Within the watershed, there are four climate stations (two of which only record temperature), five precipitation gauges and 11 stream gauges (between TRCA and Water Survey of Canada). Despite the

abundance of monitoring, not all gauges have the same time span of recorded data, the time span for records from each gauge needs to be aligned for the model. Thus, we are limited by the gauge type (climate, precipitation, flow) with the smallest relative record, which in our case is the climate stations. The climate station limits us to years from 2005 to 2010. Precipitation gauges "Goodwood Pumping Station" and "Claremont Shop" were chosen as their data covers the greatest span between 2005-2010; all the years excluding winter precipitation and the full year of 2009. Only one flow gauge was used for this study ("East Duffins at Claremont") since the entire field site drains to this outlet.

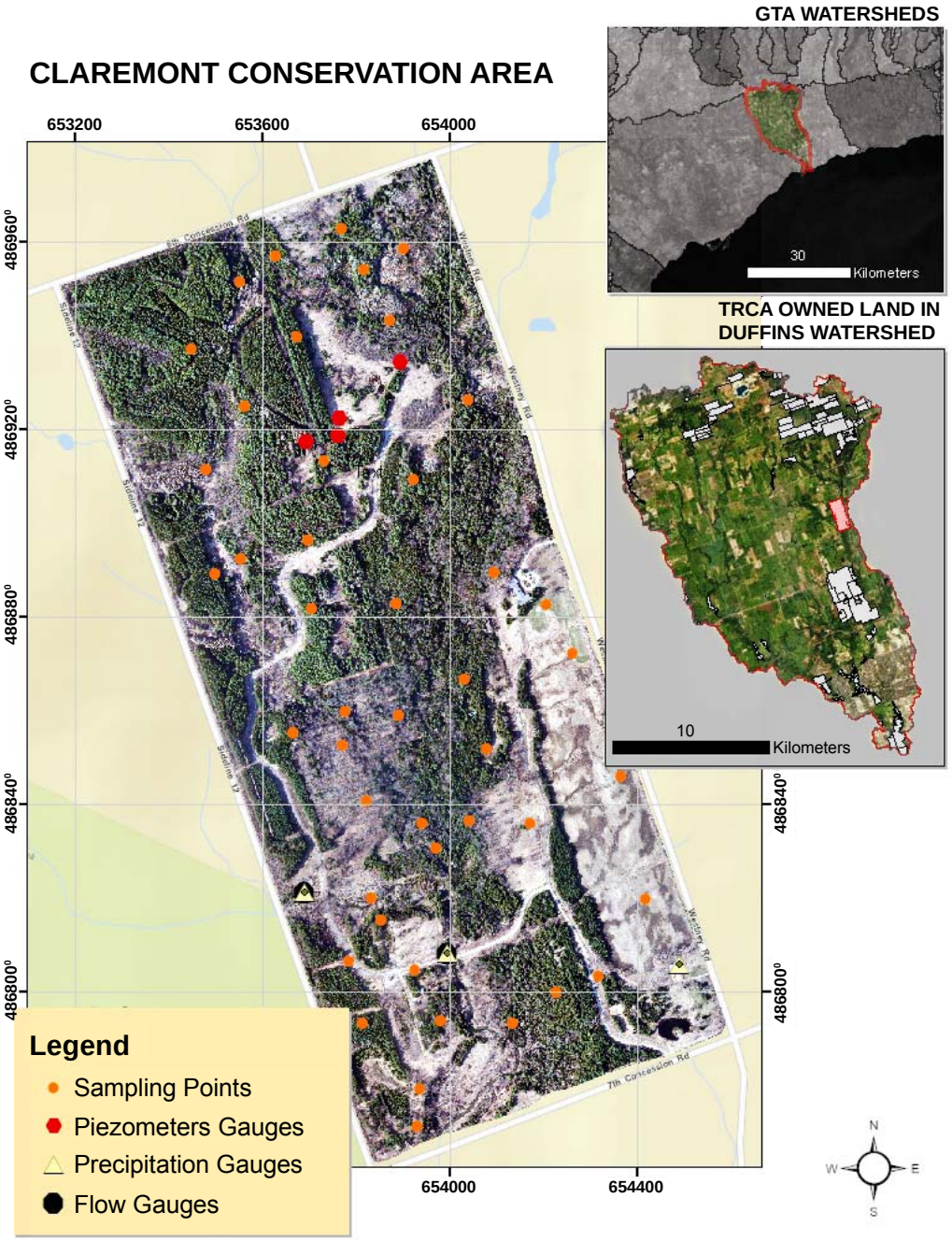

Figure 2. The study field site located in Claremont Conservation Area, Durham, ON, Canada.

2.3 SWAT Theory

The following has been summarized from Arnold et al. (1998) and from accompanying software documentation by Neitsch et al. (2011). Only the principle components that are directly influential for this study are reviewed below. In particular, water quality components (sedimentation, nutrients, pesticides and agricultural management) have been omitted as the focus of this study is the water balance. Water quantity, however, plays an integral role on water quality analysis.

2.3.1 Climate

All processes modeled by SWAT are driven by the climatic inputs of moisture and energy. SWAT requires inputs of precipitation (daily for CN method and hourly or daily for GA method depending on the preferred time interval for the output), maximum/minimum air temperature, solar radiation, and if the Penman–Monteith method is selected to model evapotranspiration, then wind speed and relative humidity as well. The inputs can be entered by the user from measured records or produced using a weather generator based on statistical analysis of climate normals and extremes. The weather generator is also used to fill in missing data in the measured data record.

2.3.1.1 Solar Radiation

The energy from the sun drives the hydrological processes (Viessman and Lewis 1995). The amount of solar radiation a location receives is based on the latitude; SWAT approximates 20% of this amount to be lost to the atmosphere. In this study the daily solar radiation is read in from the "Transport Canada" climate station retrieved by the TRCA. The dataset contains instantaneous measurements of solar radiation once every 15 minutes in units of kW/m^2 . We assume that solar radiation remains constant for the 15 minutes and multiple the instantaneous value by 900 (there are 900 seconds per 15 minutes). The value is divided by 1000 to convert kW/m^2 to MJ/m^2 and totaled to get a daily value required by SWAT. If the GA runoff method is used, hourly radiation is extracted from the daily sum by finding the fraction of solar radiation of that day received during that hour. Daily solar radiation is also used with mean daily temperature and moist soil albedo to calculate net radiation.

2.3.1.2 Temperature

The temperature input of daily maxima and minima influence a number of physical (e.g., infiltration), biological (e.g., plant production and organic decomposition), and chemical processes (e.g., mineralization). Daily average temperatures can be derived for processes by summing the maxima and minima and dividing it by 2. Daily maximum and minimum temperatures were retrieved from the TRCA for the Transport Canada and Goodwood Pumping Station climate stations. Hourly air temperatures can be derived through interpolation of an assumed sinusoidal function that stretches between the maximum and minimum temperatures.

Soil temperatures are calculated at the middle of each soil layer as a function of average annual air temperature, previous day's soil temperature, the current day's temperature at the surface and the depth in the soil profile. As the depth increases, the temperature for that day becomes closer to the average annual air temperature. This dampening effect is achieved through incorporation of bulk density (dry weight of soil per unit volume) and soil water. The soil temperature at the surface is calculated for bare soil using the measured solar radiation and albedo of the soil to which a weighting factor based on the amount of cover is added.

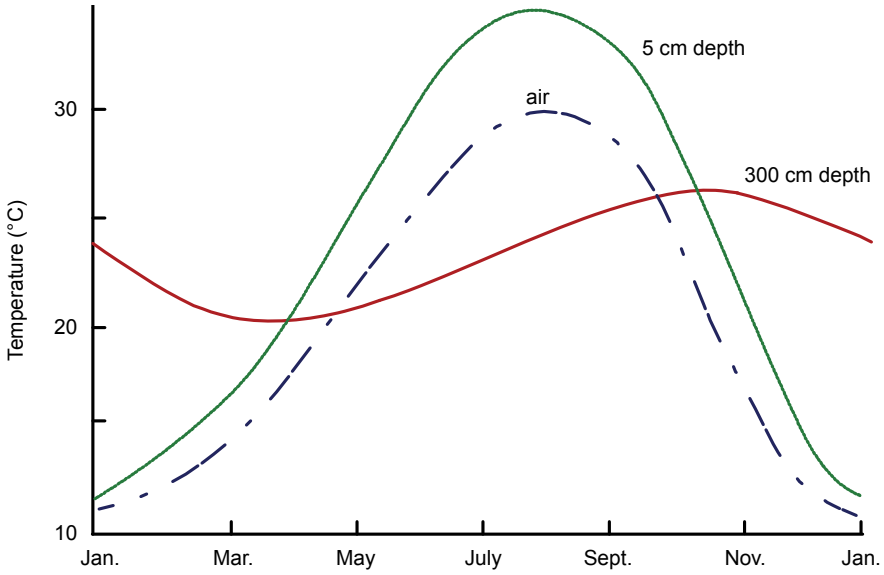

Figure 3. Four year average air and soil temperature at College Station, Texas showing the annual soil temperature cycle following a sinusoidal function having a decreasing amplitude with depth; Source: Neitsch et al. (2011).

2.3.1.3 Wind Speed

Daily average wind speed (m/s) is read into SWAT for this study. Records were retrieved by TRCA from the Transport Canada climate station. Values were 15 minute averages, which were averaged to a daily value. Wind speed is required by SWAT when the Penman-Monteith equation is used to estimate potential evapotranspiration.

2.3.1.4 Precipitation

Precipitation is identified as the primary parameter in hydrological models that influences the modeled streamflow (Chaplot et al. 2005; Shih et al. 2007). Therefore, it is critical that the distribution of

precipitation in space and time be adequately represented by the user entered data. Winter (1981) suspects that over a period of a year or longer, measured precipitation data can be expected to have a relative uncertainty of 10%. Furthermore, localized eddies are created at the mouth of the gauges as they obstruct the movement of wind, which decreases the catchment of smaller raindrops and snowflakes (Sieck et al. 2007). An estimated deficiency of 10% for rain and 30% for snow is reported by Larson and Peck (1974). Only two rain gauges within the watershed could be used in our study (Claremont Shop and Greenwood Pumping Station) due to the limited records of other gauges that corresponded with climate data year span. Precipitation data is applied to each sub–watershed from one of the two rain gauges that is closest to its centroid (Masih et al. 2011). Although precipitation records were available at 5 minute intervals, values were summed to daily and hourly totals for the CN and GA methods respectively. GA method can accommodate smaller time scales than hourly sums, but smaller times scale will require more values to be estimated by the weather generator for days with missing precipitation.

2.3.1.5 Relative Humidity

Estimating potential evapotranspiration using the Penman–Monteith or Priestly–Taylor equation requires measurements of relative humidity (Arnold et al. 2011). In addition, it is also used in calculations estimating the vapour pressure deficit on plant growth. Relative humidity is defined as the ratio between the actual and saturation vapour pressure of a volume of air:

$$R_h = \frac{e}{e^0} \tag{5}$$

where R_h is the relative humidity, e is the actual vapour pressure (kPa) and e^0 is the saturation vapour pressure (kPa) for a given day. Saturation vapour pressure is the maximum thermodynamically stable vapour pressure which Murray (1967) describe as a function of temperature:

$$e^0 = exp\left[\frac{16.78 \cdot \bar{T}_{av} - 116.9}{\bar{T}_{av} + 237.3}\right] \tag{6}$$

where e^0 is the saturation vapour pressure for the given day (kPa) and $\bar{T}_{av}$ is the average daily air temperature (°C). This study uses measured relative humidity values recorded at the Transport Canada climate station, retrieved by the TRCA. Equation (5) can be re-arranged and solved for e having values for R_h and e^0. The rate of evapotranspiration is proportional to the vapour pressure deficit, that is, the difference between e^0 and e.

2.3.1.6 Snow Cover

SWAT classifies precipitation as rain or freezing rain/snow based on mean daily air temperature and thresholds set by the user to define boundaries. The default threshold temperature of 1°C is used for

this study. Snowfall is regarded to be stored on the ground as a snow pack, but is reported as snow water equivalent (mm) – as depth over the entire HRU. The following mass balance equation describes the considered inputs and outputs of the snowpack:

$$SNO = SNO + R_{day} - E_{sub} - SNO_{mlt} \quad (7)$$

where SNO is the snow water equivalent of the snow pack on a given day (mm H_2O), R_{day} is the amount of precipitation as snow on a given day (if mean daily temperature < threshold temperature for snow), and E_{sub} and SNO_{mlt} are the amounts of sublimation and snowmelt respectively on a given day. Snowmelt is considered to be evenly distributed throughout the day and included in calculations of runoff and infiltration.

Snow cover is only briefly covered here as our study lacks winter precipitation input and therefore winter months were excluded during calibration and validation process. Interested readers are directed to Neitsch et al. (2011). SWAT models snowmelt as a function of the difference between the average snow pack temperature and the threshold temperature for snowmelt, and the snow melt factor (based on the day of the year).

2.3.2 Weather Generator

The weather generator in SWAT can be used to generate climate data (precipitation, max/min temperatures, solar radiation, relative humidity, and wind speed) if measured data is not available. However, it can also be used to substitute missing values for a specific time scale within a measured data set. A value of "-99" is placed for any missing climate data which signals the weather generator to substitute with a reasonable value. By default, SWAT uses the WXGEN weather generator (Sharpley and Williams 1990), which was developed for the U.S. and is used in this study. Alternatively, other generators can be used outside of SWAT, but may require reformatting of generated values prior to implementing them into SWAT. The estimation of climate variables by the generator is based on climate normals and extremes entered by the user (Table 2).

The statistics required by the weather generator needs to be calculated based on long historical data sets (20 years recommended). Three data sets were used to compile and compute the required statistics: archived Canadian Daily Climate Data (CDCD) dataset, climate normals, and 0.5 hr maximum rainfall rate. All three datasets were retrieved from Environment Canada, the first two can be freely accessed on their website and the last was purchased. Climate data was retrieved for district 561, region 135, zone 8, within which the majority of the Duffins watershed lies. Stations were selected based on the historical record span that would match our study period (Table 3). As the two stations selected from the CDCD were not present in Environment Canada's 0.5 hour maximum rainfall records, the records from the closest stations were incorporated with the CDCD stations (Table 3).

Table 2. Variables required by the weather generator to produce climate data based on historical record

Climate Variable	WGN Parameter Name	WGN Parameter Description	Format/Unit
Climate station details	STATION	Weather station name	
	WLATITUDE	Latitude of weather station	Degrees
	WLONGITUDE	Longitude of weather station	Degrees
	Xpr	X projected coordinate of weather station	
	Ypr	Y projected coordinate of weather station	
	WELEV	Elevation of weather station	Metres
Precipitation	PCPMM	Average daily precipitation for each month	mm/day
	PCPSTD	Standard deviation for daily precipitation in each month	mm/day
	PCPSKW	Skew coefficient for daily precipitation in each month	Numeric
	PR_W1	Probability of a wet day following a dry day in the month	Fraction
	PR_W2	Probability of a wet day following a wet day in the month	Fraction
	PCPD	Average number of days of precipitation in each month	Numeric
	RAINHHMX	Maximum 0.5 hour rainfall in entire period for each month	mm
	RAIN_YRS	Number years of maximum monthly 0.5 h rainfall data	Numeric
Temperature	TMPMX	Average maximum air temperature for each month	°C
	TMPMN	Average maximum air temperature for each month	°C
	TMPSTDMX	Standard deviation for maximum temperature in each month	°C
	TMPSTDMN	Standard deviation of minimum temperature in each month	°C
Solar radiation	SOLARAV	Average daily solar radiation in each month	MJ/m^2/day
Relative humidity	DEWPT	Average dew point temperature in each month	°C
Wind speed	WNDAV	Average wind speed in each month	m/s

Table 3. Weather stations with historical datasets retrieved from Canadian Daily Climate Data (CDCD) and Environment Canada (EC) to calculate climate statistics required by the weather generator. EC stations were used for 0.5 hr maximum rainfall records to compliment station climate normals downloaded from CDCD.

Station Name	Database	Latitude	Longitude	Elevation	First Year of Record	Last Year of Record	Year Count
Stouffville WPCP	CDCD	43.97	-79.25	267.0	1971	1993	22
Stouffville	EC	44.00	-79.27	312.4	1960	1975	14
Pickering Audley	CDCD	43.90	-79.05	110.0	1958	1985	27
Greenwood MTRCA	EC	43.90	-79.07	128.0	1960	1993	33

Although most of the precipitation statistics can be easily calculated with a spreadsheet program like Microsoft Excel, it is more difficult to calculate parameters such as PR_W1 and PR_W2 (Table 2). We used a freely available program " pcpSTAT" created by a SWAT user to calculate all the required precipitation statistics with the input of daily rainfall data. The program was freely accessible through the SWAT website (http://swat.tamu.edu/). Using pcpSTAT requires that there is full record of precipitation from January 1st to December 31st, such that missing values are denoted by a set numeric value (i.e., -99). Since precipitation records by default do not have an indication of which days have missing values (the day is just skipped over), a macro was created in Microsoft Access to find missing days from the record and to substitute a value of -99 for missing values. TMPMX and TMPMN were retrieved from climate normal data from Environment Canada's website. Values for TMPSTDMX and TMPSTDMN were achieved by summarizing CDCD data within Green Kenue ^{TM} software available through National Research Council Canada website. RAINHHMX and RAIN_YRS parameters were derived from purchased Environment Canada 0.5 h maximum rainfall data, while SOLARAV, DEWPT, and WINDAV were retrieved from climate normals published for various ecodistricts on the Environment Canada website. Based on the location of watershed, values for ecodistrict 561 was used. The statistics for each station is manually entered into the main SWAT Microsoft Access database in the "WGEN_user" table.

If all climate variables are lacking measured values, the weather generator first produces precipitation as it affects all other climate variables with the exception of wind speed. The daily total precipitation is computed and the distribution throughout the day is calculated if the GA method is chosen for runoff calculations. Firstly, a day must be determined to be wet or dry. Based on the previous day's

conditions, PR_W1 or PR_W2 is compared to a randomly generated number between 0.0 and 1.0. If for example the number is equal to or less than the probability held by PR_W1, it will be a wet day and vice versa. Once the day is determined to be wet, the amount of rainfall is calculated based on mean daily rainfall for the month (PCPMM), standard deviation of daily rainfall in that month (PCPSTD), skew coefficient (PCPSKW), and standard normal deviate (normally distributed random variable ranging from 0 to 1). The distribution of rainfall follows a double exponential function, one to describe rainfall until the peak rate is established, and the other to describe the subsequent decrease in rainfall. Solar radiation and temperature is calculated based on methods presented by Richardson (1981) using monthly averages and standard deviations (estimated as 1/4 the difference between maximum and mean values for solar radiation), but also adjusted for dry and wet days such that the wet day solar radiation average is less than those of dry days. Relative humidity is calculated based on four user inputs: TMPMX, TMPMN, DEWPT, and PCPD (Table 2). Daily wind speed is calculated as an exponential function of the average daily wind speed in that month (WNDAV) but is also influenced by a randomly generated number between 0.0 – 1.0.

2.3.3 Hydrology

In a vegetated area, precipitation initially is intercepted by canopy and proceeds to the soil surface. Precipitation either infiltrates into the soil profile, contributes to runoff , or a combination of the two. Runoff can induce short-term stream response, while infiltrated precipitation experiences a lag before evapotranspiration from the soil or contributing to subsurface water flow; eventually contributing to stream baseflow. The aforementioned routing is depicted in
Figure 4. The land phase of the hydrological cycle in SWAT is based on the following water balance:

$$SW_t = SW_0 + \sum_{i=1}^{t}\left(R_{day} - Q_{surf} - E_a - w_{seep} - Q_{gw}\right) \quad (8)$$

where SW_t and SW_0 are the final and initial soil water content (mm) respectively, R_{day} is the precipitation amount on the i^{th} day (mm), Q_{surf} is the surface runoff amount on day i (mm), E_a is the amount of evapotranspiration on day i (mm), w_{seep} is the percolation and bypass flow exiting the soil profile on day i (mm), and Q_{gw} is the amount of groundwater that reaches the stream on day i (mm).

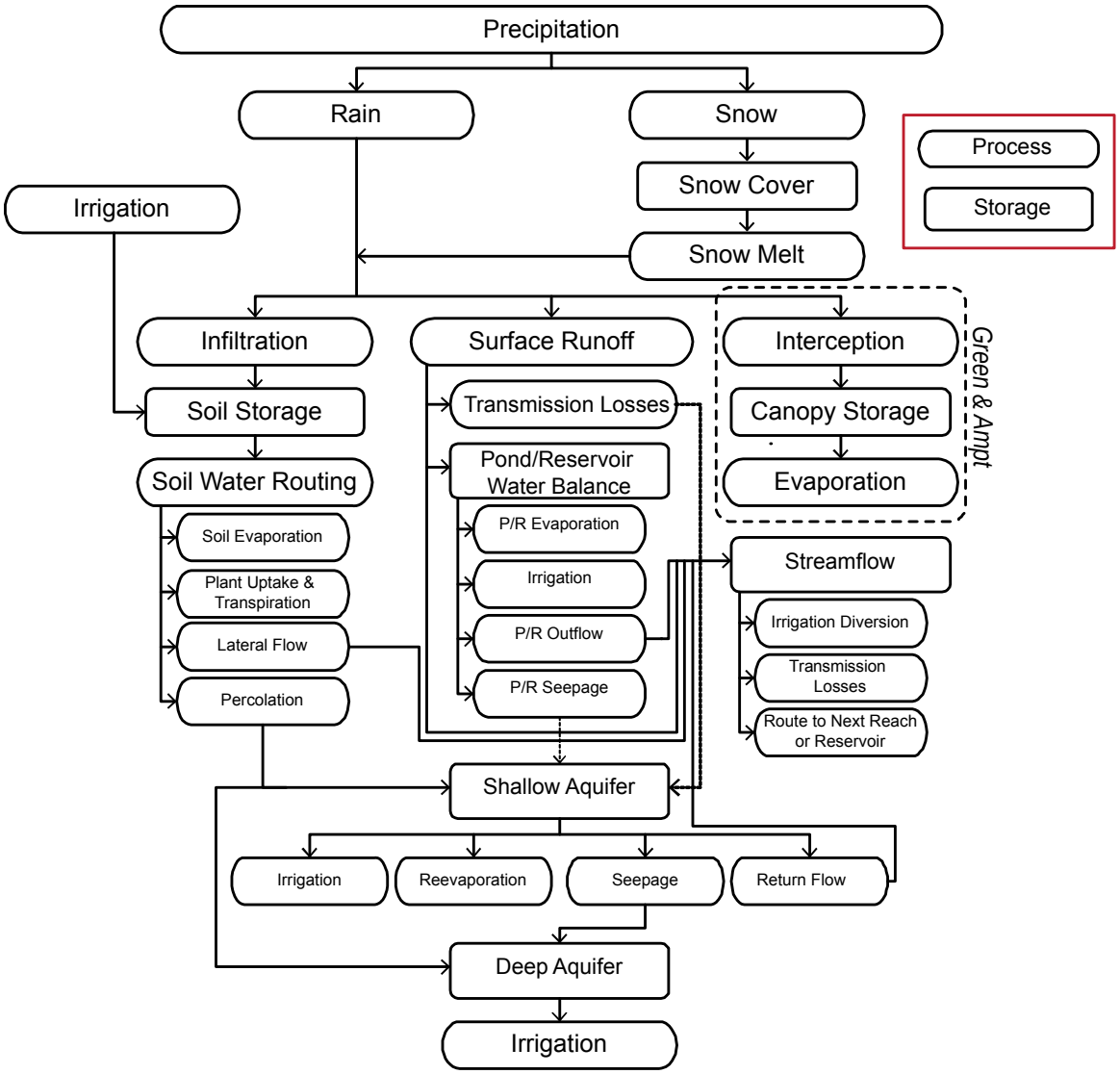

Figure 4. Schematic of possible water pathways in SWAT; After: Neitsch et al. (2011).

2.3.3.1 Surface Runoff

Surface runoff occurs when rate of precipitation exceeds rate of infiltration. As rate of infiltration decreases with continuous precipitation and/or an increase in rainfall intensity, the potential for runoff increases. Surface runoff flows downhill filling up any surface depressions along the way. SWAT contains two options for surface runoff calculations: Curve Number method (Soil Conservation Society 1972) and Green & Ampt method (Green and Ampt 1911). In our study both methods are used and resulting model performances are compared.

2.3.3.2 SCS Curve Number (CN) Method

The SCS curve number equation is as follows (Soil Conservation Society 1972):

$$Q_{surf} = \frac{(R_{day} - I_a)^2}{(R_{day} - I_a + S)} \quad (9)$$

where Q_{surf} is the runoff (mm), R_{day} is the daily rainfall depth (mm), I_a is the initial abstractions (mm) including infiltration prior to runoff , interception and surface storage, and S is the retention parameter that varies with changes to soil, land use, soil water content, management and slope. S can be defined as :

$$S = 25.4 \left(\frac{1000}{CN} - 10\right) \quad (10)$$

where CN is the daily curve number that correlates the amount of runoff to the amount of rainfall based on the LCLU (Figure 5).

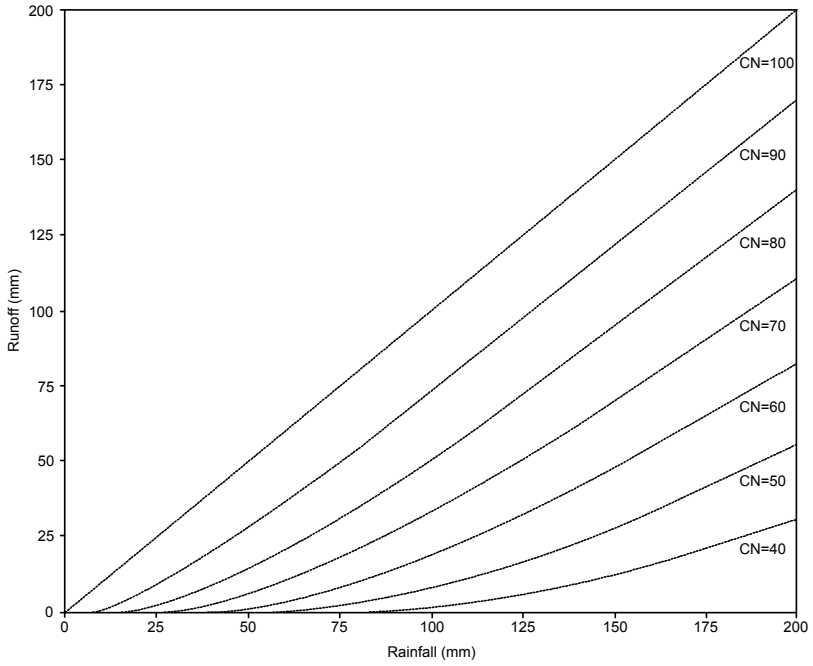

Figure 5. Relationship of runoff to rainfall in SCS curve number method; Source: Neitsch et al. (2011).

I_a has been approximated to $0.2S$ which can be substituted into equation (9) to get:

$$Q_{surf} = \frac{\left(R_{day} - 0.2S\right)^2}{\left(R_{day} + 0.8\,S\right)} \tag{11}$$

Therefore, runoff will occur if R_{day} exceeds I_a . Typically, the CN value in the above equation is estimated using tables provided by the (Natural Resources Conservation Service 1986) based on soil type, LCLU, and hydrologic condition. Higher CN values are used for soils with smaller storage capacities indicating a higher runoff potential and vice versa (Mishra and Singh 2004). Usually, the CN value is allowed to change between three different values based on the antecedent moisture condition (AMC): AMC I (dry), AMC II (average), AMC III (wet) (Mishra and Singh 2004). This simplification however can cause unreasonable jumps in the retention parameter S (Sahu et al. 2010). SWAT overcomes this simplification by coupling its continuous modeling of soil moisture to the retention parameter S as opposed to only having three different moisture conditions (AMC I – III) (Arnold et al. 1998). The following equation is used to modify S based on soil profile water content:

$$S = S_{max}\left(1 - \frac{SW}{[SW + exp(w_1 - w_2 \cdot SW)]}\right) \tag{12}$$

where S is the retention parameter (mm), S_{max} is the maximum possible retention parameter value (mm), SW is the water content of the entire soil profile not including the amount held at wilting point (mm), and w_1 and w_2 are shape coefficients. The shape coefficients w_1 and w_2 can be calculated from Eq. (13) and Eq. (14) respectively if the following assumptions are held:

1) The S value for AMC I corresponds to the wilting point of the soil profile
2) The S value for AMC III corresponds to the field capacity of the soil profile
3) When the soil profile is completely saturated, the CN value is 99

$$w_1 = ln\left[\frac{FC}{1 - S_3 \cdot {S_{max}}^{-1}} - FC\right] + w_2 \cdot FC \tag{13}$$

$$w_2 = \frac{\left(ln\left[\frac{FC}{1 - S_3 \cdot {S_{max}}^{-1}} - FC\right] - ln\left[\frac{SAT}{1 - 2.54 \cdot {S_{max}}^{-1}} - SAT\right]\right)}{(SAT - FC)} \tag{14}$$

where w_1 and w_2 are the first and second shape coefficient respectively, FC is the field capacity of the soil profile (mm), S_3 is the retention parameter for AMC III, S_{max} is the retention parameter for AMC I, SAT is the moisture content of the soil profile when completely saturated (mm), and 2.54 corresponds to the S value for a CN of 99. If the top layer of the soil is frozen, the retention parameter is modified as follows:

$$S_{frz} = S_{max} \cdot [1 - exp(-0.000862 \cdot S)] \quad (15)$$

where S_{frz} is the adjusted retention parameter for frozen conditions (mm), S_{max} is the potential daily maximum value of the retention parameter (mm), and S is the retention parameter for a soil water content described as calculated in Eq. (12). Rearranging Eq. (10) and substituting the daily moisture content adjusted retention parameter from Eq. (12) allows the curve number approach to be influenced by the soil water content of that day:

$$CN = \frac{25400}{(S + 254)} \quad (16)$$

where CN is the curve number and S is the retention parameter calculated for the soil moisture content on that day. It is important to note that initial CN values suggested by SWAT is based on LCLU and soil hydrologic group (describes surface runoff potential), which assumes that the surface has a slope of 5% (Neitsch et al. 2011). Williams (1995) proposes an equation to adjust CN based on average slope of the sub–watershed, but conversion must be done manually outside of SWAT. In order to compare our study results with the majority found in literature, we opt to accept the 5% slope assumption without adjustment.

2.3.3.3 Green & Ampt (GA) Infiltration Method

As an alternative to the empirical CN method of calculating runoff, SWAT has adopted the physically based Green & Ampt method modified by Mein and Larson (1973). The modified equation models infiltration prior to surface saturation and subsequent infiltration (Mein and Larson 1973). The integrated form solves for the cumulative infiltration at the end of the time step, and the residual of the precipitation not infiltrated becomes the runoff. Their method of calculating runoff has the following assumptions: 1) constant rainfall intensity, 2) homogenous soil, 3) uniform initial moisture content at zone of infiltration, and 4) soil above the wetting front is completely saturated (Mein and Larson 1973). The method is as follows:

$$f_{inf,t} = K_e \cdot \left(1 + \frac{\Psi_{wf} \cdot \Delta\theta_v}{F_{inf,t}}\right) \quad (17)$$

where f_{inf} is the instantaneous infiltration at time t (mm/hr), K_e is the effective hydraulic conductivity (mm/hr), Ψ_{wf} is the wetting front matric potential (mm), $\Delta\theta_v$ is the volumetric moisture content across the wetting front (mm/mm), and F_{inf} is the cumulative infiltration at time t (mm). When rainfall intensity is less than infiltration rate, all rainfall will infiltrate such that:

$$F_{inf} = F_{inf,t-1} + R_{\Delta t} \quad (18)$$

where F_{inf} is the cumulative infiltration for the given time step, $F_{inf,t-1}$ is the cumulative infiltration for the previous time step, and $R_{\Delta t}$ is the amount of rain falling during the time step (mm). Eq. (17) is integrated to find the total cumulative infiltration at the end of the time step as follows:

$$F_{inf,t} = F_{inf,t-1} + K_e \cdot \Delta t + \Psi_{wf} \cdot \Delta\theta_v \cdot ln\left[\frac{F_{inf,t} + \Psi_{wf} \cdot \Delta\theta_v}{F_{inf,t-1} + \Psi_{wf} \cdot \Delta\theta_v}\right] \quad (19)$$

Although K_e can be estimated as 1/2 the saturated hydraulic conductivity (Bouwer 1969), Nearing et al. (1996) present a calculation of K_e as a function of saturated hydraulic conductivity and CN. In this way, land cover impacts can be taken into account when K_e is calculated:

$$K_e = \frac{56.82 \cdot {K_{sat}}^{0.286}}{1 + 0.051 \cdot \exp(0.062 \cdot CN)} - 2 \quad (20)$$

where K_e and K_{sat} (Sol_K) are the effective and saturated hydraulic conductivity (mm/hr) respectively and CN is the curve number. The change in volumetric moisture content across the wetting front, $\Delta\theta_v$, is calculated at the beginning of each day as:

$$\Delta\theta_v = \left(1 - \frac{SW}{FC}\right) \cdot (0.95 \cdot \phi_{soil}) \quad (21)$$

where SW is the soil water content of the entire profile excluding the water held at wilting point (mm) and is calculated based on Eq.(8), FC is the soil profile at field capacity (mm), and ϕ_{soil} is the porosity of the soil (mm/mm). In this way both the CN and GA method of calculating runoff take the soil water content of the soil profile into account. The matric potential of the wetting front , Ψ_{wf} , is a function of percent sand m_s, percent clay m_c and porosity ϕ_{soil} (mm/mm) (Rawls and Brakensiek 1985):

$$\begin{aligned}\Psi_{wf} = 10 \cdot exp\big[&6.5309 - 7.32561 \cdot \phi_{soil} + 0.001583 \cdot {m_c}^2 + 3.809479 \cdot {\phi_{soil}}^2 \\ &+ 0.000344 \cdot m_s \cdot m_c - 0.049837 \cdot m_s \cdot \phi_{soil} + 0.001608 \cdot {m_s}^2 \cdot {\phi_{soil}}^2 \\ &+ 0.001602 \cdot {m_c}^2 \cdot {\phi_{soil}}^2 - 0.0000136 \cdot {m_s}^2 \cdot m_c - 0.003479 \cdot {m_c}^2 \cdot \phi_{soil} \\ &- 0.000799 \cdot {m_s}^2 \cdot \phi_{soil}\big]\end{aligned} \quad (22)$$

The porosity of the soil ϕ_{soil} can be calculated based on the moist bulk density ρ_b (mg/m^3):

$$\phi_{soil} = 1 - \left(\frac{\rho_b}{2.65}\right) \quad (23)$$

At each time step, following the calculation of precipitation that has infiltrated SWAT calculates runoff as the residual of the precipitation reaching the soil that has not infiltrated.

2.3.3.4 Time of Concentration

The time of concentration is calculated as the time it takes a drop of water falling on the point farthest away from the sub–watershed outlet to reach the outlet. It is a measure of the time it takes for the entire sub–watershed to be contributing water to the outlet. The time of concentration, t_{conc}, is a summation of the overland flow time (time to reach the channel), t_{ov}, and the channel flow time (travel time from the upstream to the downstream part of the channel), t_{ch} :

$$t_{conc} = t_{ov} + t_{ch} \tag{24}$$

The specifics of the calculation can be found in Neitsch et al. (2011), but it is briefly introduced here as it is used to determine rainfall intensity, an input for the GA method.

2.3.3.5 Rainfall Intensity

Rainfall intensity, i, is calculated in SWAT as the average rainfall rate, R_{tc}, during the time of concentration of the subbasin, t_{conc}:

$$i = \frac{R_{tc}}{t_{conc}} \tag{25}$$

Hershfield (1961) found rainfall during time of concentration to be proportional to the amount of rain during the 24 – hour period such that:

$$R_{tc} = a_{tc} \cdot R_{day} \tag{26}$$

where R_{tc} is the rainfall amount within the time of concentration (mm), a_{tc} is the proportionality of R_{tc} to the daily rainfall amount, and R_{day} is the total daily rainfall (mm). The proportion, a_{tc}, is calculated as a function of the time of concentration, t_{conc}, and the fraction of daily rainfall falling during the maximum half–hour rainfall, $a_{0.5}$.

$$a_{tc} = 1 - exp[2 \cdot t_{conc} \cdot ln(1 - a_{0.5})] \tag{27}$$

The daily maximum half hour rainfall data was purchased from Environment Canada, however, using the average maximum half hour rainfall of the month is also a possibility. The rainfall intensity calculated is taken to be constant when used in the GA method to calculate cumulative infiltration.

2.3.3.6 Surface Runoff Lag

SWAT incorporates a potential lag to the surface runoff released to the main channel on the same day it is generated. The lag functions as a storage feature, such that only a portion of the generated surface runoff reaches the channel, and the rest during days to follow. The proportion of runoff released to the main channel on a given day can be calculated as follows:

$$Q_{surf} = \left(Q'_{surf} + Q_{stor,i-1}\right) \cdot \left[1 - exp\left(\frac{-surlag}{t_{conc}}\right)\right] \quad (28)$$

where Q_{surf} is the daily amount of surface runoff discharged into the main channel from a given subbasin watershed (mm), Q'_{surf} is total amount of surface runoff generated in the subbasin on a given day (mm), $Q_{stor,i-1}$ is the lagged surface runoff amount from the previous day(mm), $surlag$ is the surface runoff lag coefficient, and t_{conc} as calculated in Eq.(24) is the time of concentration for the subbasin. The user can alter the surface runoff lag-coefficient; this study has chosen to leave it at the default value of four days. The proportion of surface runoff that will experience a lag is in part dependant on the size of the subbasin; larger subbasins will have a longer time of concentration, increasing the proportion that is lagged.

2.3.4 Evapotranspiration

Evapotranspiration as a collective term includes evaporation of intercepted water from the plant canopy, transpiration from plants, sublimation and evaporation from the soil. Evaporation usually exceeds runoff in most basins, approximately 62% of the precipitation input (Dingman 2002).

2.3.4.1 Canopy Storage

As mentioned, GA method requires that canopy interception be calculated separately as opposed to including it into a lumped "initial abstraction" term used in the CN method. Depending on the density of the plant cover, a significant portion of rainfall can be trapped by the canopy and evaporated without reaching the soil surface. The maximum amount of water than can be held this way varies daily as follows:

$$can_{day} = can_{mx} \cdot \frac{LAI}{LAI_{mx}} \quad (29)$$

where can_{day} is the daily maximum precipitation amount that can be trapped in the canopy (mm), can_{mx} is the maximum amount of precipitation that can be trapped by the canopy when it is fully developed (mm), LAI is the leaf are index of a plant on the given day of the year, and LAI_{mx} is maximum possible leaf area index of the plant. The canopy storage must be filled before precipitation is allowed to reach the soil; the amount that reaches the soil can be calculated as follows:

$$R_{day} = R'_{day} - \left(can_{day} - R_{INT(i)}\right) \quad (30)$$

where R'_{day} and R_{day} is the amount of precipitation before and after canopy interception (mm) respectively, and $R_{INT(i)}$ is the initial amount of free water held in the canopy on a given day (mm). In this study we use the measured LAI values for the selected HRUs to calculate can_{mx} and used it to parameterize the model using SWAT–CUP.

2.3.4.2 Potential Evapotranspiration

Penman (1956) defines potential evapotranspiration (PET) to be the rate of transpiration from a short green crop (i.e., grass), that is completely shading the ground, uniform in height and having an unlimited amount of soil water. There are a number of ways to estimate PET, three of which are accommodated in the SWAT model: Penman–Monteith (Monteith 1965; Allen 1986; Allen et al. 1989), Priestly–Taylor (Priestley and Taylor 1972), and the Hargreaves method (Hargreaves et al. 1985). The Penman–Monteith method requires climate inputs of solar radiation, air temperature, relative humidity and wind speed. The Priestly–Taylor method uses the same inputs excluding wind speed, and as a result it is limited to estimating potential evapotranspiration for areas with low advective conditions. The Hargreaves method solely uses air temperature to estimate potential evapotranspiration. As the various methods have not produced significantly different model outputs (Wang et al. 2006), we chose to use the Penman–Monteith method as the required datasets were available.

2.3.4.3 Actual Evapotranspiration

The actual amount of evapotranspiration must be deduced from the potential amount. Canopy intercepted water is evaporated first, followed by calculations of maximum potential transpiration and sublimation/soil evaporation based on a similar approach to Ritchie (1972). Subsequently, the actual amount of sublimation and/or evaporation is calculated. Once the canopy held water is evaporated, the remaining evaporative demand is partitioned between the vegetation and snow/soil. How much each soil layer contributes to the soil water evaporative demand can be controlled by the user entered value for the soil evaporation compensation coefficient $(esco)$. The value can range from 0-1. As the value decreases, more of the evaporative demand can be met from the lower soil levels. This parameter was used in calibration of the model (within SWAT–CUP) and allowed to vary between 0-1.

2.3.5 Soil Water

Among possible pathways of soil water (plant uptake, evaporation, aquifer recharge, lateral movement into channel), plant uptake removes the majority of water from the soil profile. The amount of water available to plants, also known as available water capacity (AWC) is the difference between the fraction of water present at field capacity (FC) and permanent wilting point (WP):

$$AWC = FC - WP \tag{31}$$

The field capacity is the volume of water held in the soil profile once all excess water has freely drained and the wilting point is the water content of the soil beyond which plants can no longer extract water, resulting in loss of turgidity and wilting (Ward and Robinson 2000). The permanent wilting point as a fraction of the total soil volume, WP_{ly}, can be estimated using the percent clay content, m_c (%), and the bulk density, ρ_b(Mg m^{-3}), of the soil layer.

$$WP_{ly} = 0.40 \cdot \frac{m_c \cdot \rho_b}{100} \tag{32}$$

The available water content as a fraction of the soil volume (AWC_{ly}) is inputted by the user, which along with WP_{ly}, can be used to solve for the field capacity as a fraction of the total soil volume as follows:

$$FC_{ly} = WP_{ly} + AWC_{ly} \tag{33}$$

Typically, water movement in soil can occur either when the layer is saturated or unsaturated. Redistribution refers to the movement of water through the soil profile due to differences in water content and it will cease once the soil moisture throughout the soil profile is uniform. Saturated flow is governed primarily by gravity, while unsaturated flow can be driven by gradients between adjacent areas of lower or higher water content. SWAT eliminates the complexity of unsaturated lateral movement by evenly distributing the water content horizontally. Saturated flow occurs when water content exceeds the field capacity, allowing excess water to percolate or flow laterally. Percolation occurs when there is unsaturated soil layer below a saturated one, the rate of which is unique to each soil layer and is determined using the saturated hydraulic conductivity. Moreover, saturated hydraulic conductivity also plays an important role in quantifying net lateral flow discharge at the outlet, and also the lag associated with it.

2.3.6 Groundwater

Groundwater is found in the saturated zone under greater than atmospheric pressure. Groundwater storage receives input by infiltration/percolation and sometimes by seepage from surface water bodies. Groundwater flows out of storage as discharge into rivers/lakes or through upward capillary movement. SWAT considers groundwater storage in two forms: shallow unconfined aquifer and deep confined aquifer (Arnold et al. 1993). Water in the shallow aquifer participates in the input/output mechanisms described above. However, water that enters the deep aquifer is assumed to be discharged outside of the study basin and thus is considered lost from the system. To model the delay in aquifer

recharge from percolation, SWAT uses an exponential decay weighting function proposed by Venetis (1969):

$$w_{rchrg,i} = \left(1 - exp\left[\frac{-1}{\delta_{gw}}\right]\right) \cdot w_{seep} + exp\left[\frac{-1}{\delta_{gw}}\right] \cdot w_{rchrg,i-1} \quad (34)$$

where $w_{rchrg,i}$ is the recharge amount entering the aquifers on day i, $\delta_{gw}$is the delay time associated with the overlying geologic formations (days), w_{seep} is the total water amount exiting the bottom of the soil profile on day i, and $w_{rchrg,i-1}$ is the amount of recharge that entered the aquifers on day $i-1$. The delay time for aquifer recharge (δ_{gw}), cannot be directly measured, but can be estimated by substituting different values and comparing simulated output to the measured data. In this study, δ_{gw} (GW_DELAY) is one of the parameters chosen to be calibrated within SWAT–CUP.

Groundwater is allowed to enter the reach as baseflow only if the user specified shallow aquifer storage threshold (GWQMN) is exceeded. This is one of the parameters used in the SUFI-2 calibration algorithm within SWAT-CUP. The steady–state groundwater flow from storage to baseflow is calculated as a function of saturated hydraulic conductivity, the distance from subbasin divide to the main channel, and the water table height. The baseflow recession constant (ALPHA_BF) is used to calculate the decay of baseflow contribution to the channel from the recharge event. The constant ranges from 0.0 to 1.0, with values between 0.9 and 1.0 representing a very rapid response. The baseflow filter program (downloaded from the SWAT website) is used to determine the recession constant based on measured streamflow data. A value of 0.75 was attained and used for the basin. Groundwater can also move up into the unsaturated zone where it can participate in evapotranspiration. This process labeled as "revap" occurs only if the user entered shallow aquifer storage threshold (REVAPMN) is exceeded. A value for REVAPMN is also attained by using it as one of the parameters in the calibration process. The maximum possible amount of revap is calculated by multiplying the revap coefficient (GW_REVAP) by the potential evapotranspiration.

2.4 GIS Data Layers

SWAT requires three data layers to produce hydrologic response units (HRUs), the basis of SWAT's semi-distributed modeling approach: Digital Elevation Model (DEM), land use/cover (LCLU), and soil layers. The coordinate system used for all GIS data layers is NAD83.

2.4.1 Digital Elevation Model Layer

The DEM for the watershed was acquired from the TRCA, and has a spatial resolution of 10 m. It was originally published by the Ministry of Natural Resources in 2006. The DEM data is an interpolation of five main datasets: contour line, OB-DTM, Spot Height, Water Poly Segment, and Water Virtual Flow. This DEM product stretches province wide and is often used for surface water modeling with horizontal precision of +/- 10 m and vertical precision of +/- 5 m. The DEM is used in SWAT to define streams

based on elevation, from which boundaries of subbasins and subsequently the basin is drawn. The fine spatial resolution and precision ensures that even smaller streams can be traced. The DEM is also used to calculate a slope layer which is used as one of three layers to derive unique combinations of HRUs. Slope in SWAT is calculated as percent slope (m), a format commonly used in U.S. :

$$m = 100 \cdot \frac{rise}{run} \tag{35}$$

2.4.2 Land Cover/ Land Use Layer (LCLU)

The LCLU layer identifies both land uses (e.g., transportation, agriculture) and land covers (e.g., deciduous forest, bare soil). The dataset was retrieved from the TRCA but was compiled by YPDT (Regional Municipalities of York, Peel, Durham, and the City of Toronto)–CAMC(Conservation Authorities Moraine Coalition) using four different sources: Southern Ontario Land Resource Information System (SOLRIS), Landcover GTA 2002 (LC–GTA), Provincial Land Cover 2000 (PLC2000), and AVHRR Land Cover Data (AVHRR_ONT). All datasets are resampled to a resolution of 20 m. SOLARIS and AVHRR were originally vector datasets that were translated to a grid using 20 m sampling, however AVHRR was only used to fill in missing information in other datasets. PLC2000 was sampled from a 25 m grid and LC_GTA from a 15 m grid using Grass–GIS. The Reclassify tool (Spatial Analyst Tools) in ArcGIS was used to reclassify YPDT–CAMC`s classifications into categories used by SWAT (Table 4).

Table 4. Reclassified YPDT–CAMC LCLU classes into SWAT LCLU code

Original Description	Cell Count	Area (ha)	SWAT Reclassified Description	SWAT Reclassified Code
Open Shoreline	19	0.76	Water	WATR
Forest	15058	602.32	Forest-Mixed	FRST
Forest - Coniferous	54679	2187.16	Forest-Evergreen	FRSE
Forest - Mixed	70672	2826.88	Forest-Mixed	FRST
Forest - Deciduous	128899	5155.96	Forest-Deciduous	FRSD
Plantations - Tree Cultiv	35562	1422.48	Forest-Evergreen	FRSE
Hedge Rows	25673	1026.92	Forest-Deciduous	FRSD
Transportation	125989	5039.56	Transportation	UTRN
Extraction	27224	1088.96	Southwestern US (Arid) Range	SWRN
Urban Area Pervious	37000	1480.00	Pasture	PAST
Urban Area Impervious	142881	5715.24	Residential-High Density	URHD
Swamp	74880	2995.20	Wetlands-Forested	WETF
Fen	28	1.12	Wetlands-Forested	WETF
Marsh	5777	231.08	Wetlands-Forested	WETF
Water - Open	15355	614.20	Water	WATR
Urban Or Urban Green Space	13678	547.12	Pasture	PAST
Water - Deep Clear	4	0.16	Water	WATR
Water - Shallow Sediment	102	4.08	Water	WATR
Wetland - Open	576	23.04	Wetlands-Non-Forested	WETN
Wetland - Treed	4073	162.92	Wetlands-Forested	WETF
Water - Urban	66	2.64	Water	WATR
Urban	19361	774.44	Pasture	PAST
Agriculture - Pasture Or Abandoned Fields	391756	15670.24	Pasture	PAST
Agriculture - Cropland	254946	10197.84	Agricultural Land-Row Crops	AGRR

Several instances of each LCLU category were visually inspected using a mosaic of orthophotos taken in 2007 and 2008 for the York and Durham regions respectively, with a resolution of 20 cm. The photos were published by First Base Solutions Inc. and retrieved through York University`s Map Library. Most reclassifications are self–explanatory. "Urban pervious" areas were noted to be mostly golf courses and or small parks within residential areas which was reclassified into the most appropriate category of "Pasture". Instances of the "Urban" category were found to be short grass areas along roads and as a result reclassified also as "Pasture". "Urban Areas Impervious" was noted to be "High Density Residential" areas (subdivision housing). "Plantation–Tree Cultiv" was classified as "Evergreen Forest" since this was the tree cultivation type witnessed within the study subbasin. "Hedge Rows" were observed to be deciduous in nature based on orthophoto image, sometimes trees, sometimes bushes, and at times a combination of both. Areas labelled as "Extraction" were bare ground or construction sites, which was reclassified as "Southwestern US (Arid) Range". A look–up table is created and loaded during

the HRU synthesis process to match the LCLU layer into categories that SWAT recognizes. Similarly, a separate look–up table is created for the soil layer. Details to create the look–up tables are given in Winchell et al. (2013).

2.4.3 Soil Layer

The soil layer was downloaded from The National Soil Database (NSDB) which can be accessed through the Canadian Soil Information Service (CanSIS) website. From the NSDB, version 3 of the Detailed Soil Surveys at a scale of 1:50,000 or (25 m spatial resolution) was retrieved for Ontario. The GIS layer was imported into ArcGIS and clipped with a 1 km buffered border added to the delineated study watershed. The use of the soil layer within SWAT is twofold: i) used as one of the three layers to identify unique combinations of HRU ii) the majority of the hydrological calculations at the land stage depend on the parameters associated with the soil type. SWAT has an internal database for soils found in the U.S. such that inputting soil codes that represent the soil type will relate it to its attributes (e.g., hydraulic conductivity for different layers, bulk density, AWC). However, Canadian soils are not recognized and as a result, these soils and their attributes had to be added manually to the "usersoil" table found in the main SWAT database (located in the "Databases" folder of the current SWAT project). In total 23 new soils were added and 18 attributes were satisfied for each type; values for certain attributes have to be satisfied for each layer (Table 5).

Muck and Marsh soil types did not contain information regarding percentage of sand, silt and clay for the first layer, and therefore were substituted with the percentages of the second layer. The water category did not have a soil hydrologic group specified (HYDGRP) and was given the value "A" (low runoff potential); it is unlikely that water falling on bodies of water will runoff quickly as they serve the purpose of water storage. Saturated hydraulic conductivity was converted from cm/hr to mm/hr by multiplying the value by 10. Similarly, soil depths were converted from cm to mm. Available water capacity (SOL_AWC) of the soil layer was calculated using Eq. (31). The soil layers table downloaded from NSDB (Figure 6) identifies water retention at various pressures of kilopascals (kP). Two in particular, 33 kP (KP33) and 1500 kP (kP1500) are water retained at field capacity and permanent wilting point respectively in percentages of total soil volume. The tables from NSDB had recorded these values as percentages, which were converted to decimal fractions for SWAT input. Both soil albedo and Universal Soil Loss Equation (USLE) soil erodibility factor could not be calculated with reasonable accuracy given the available data. Since these parameters do not play a large role in our modeling response, they were given the average value of all the other U.S. soils in the database. Values for the majority of the attributes were derived from the soil attribute tables provided with the downloaded soil layer from NSDB; the model structure provided on the Detailed Soil Surveys (version 3) page has to be followed to connect attributes to the right soil type (Figure 6).

Table 5. Soil attributes required by SWAT for each soil type and their definitions. Attributes from SOL_Z1 to USLE_K1 need to be satisfied for each layer; the layer that the value represents is denoted by the number following the attribute name.

Soil Attribute	Definition
SNAM	Soil name
NLAYERS	Number of layers in the soil
HYDGRP	Soil hydrologic group
SOL_ZMX	Maximum rooting depth of soil profile
ANION_EXCL	Fraction of porosity (void space) from which anions are excluded
SOL_CRK	(Optional) Crack volume potential of soil
TEXTURE	(Optional) Texture of soil layer
SOL_Z1	Depth from soil surface to bottom of layer
SOL_BD1	Moist bulk density
SOL_AWC1	Available water capacity of the soil layer
SOL_K1	Saturated hydraulic conductivity
SOL_CBN1	Organic carbon content
CLAY1	Clay content
SILT1	Silt content
SAND1	Sand content
ROCK1	Rock fragment content
SOL_ALB1	Moist soil albedo
USLE_K1	USLE equation soil erodibility (K) factor

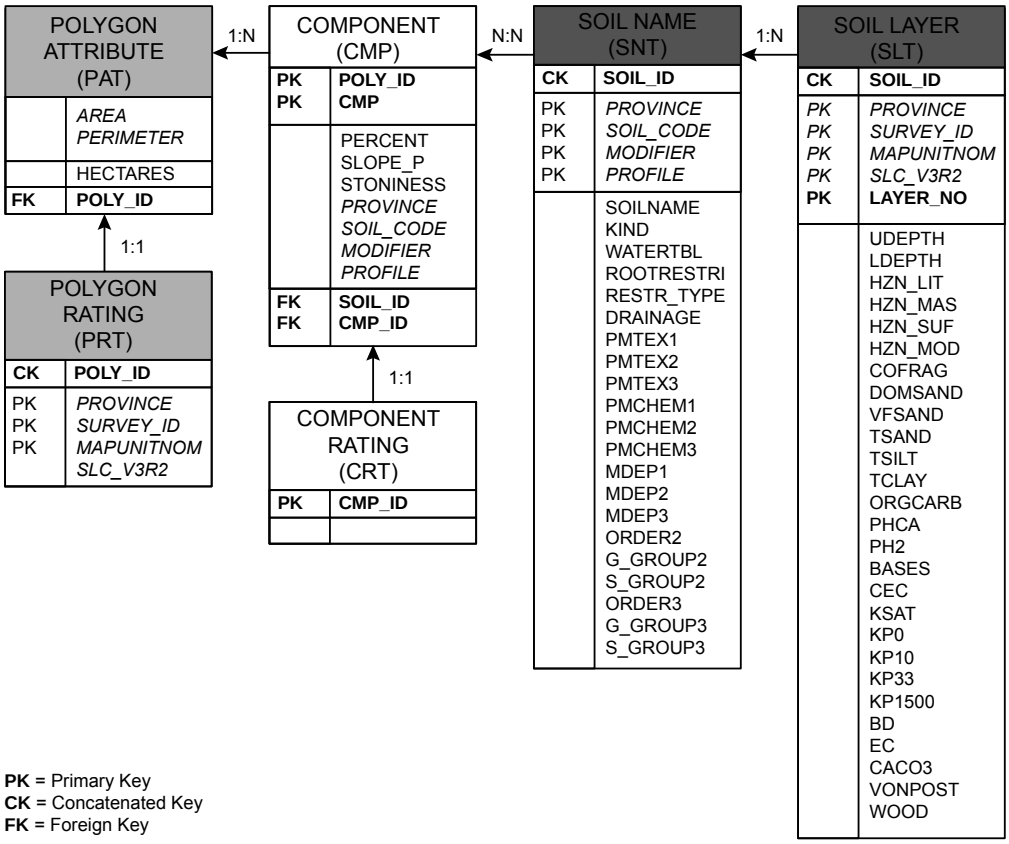

Figure 6. Model structure for the Detailed Survey Data from CanSIS; Source: CanSIS Detailed Soil Survey: http://sis.agr.gc.ca/cansis/nsdb/dss/v3/model.html

Notice that each soil type regardless of where it occurs will only have one value for each attribute. However, it is certain that attributes such as hydraulic conductivity and bulk density can vary spatially even within the same soil type. Using geostatistical techniques, Achouri and Gifford (2013) found infiltration measurements to be randomly distributed even within a 2 m grid spacing.

2.5 Field Sampling

Our study aims to test if accounting for spatial variation of model parameters can improve model performance. As mentioned above, many of the parameters associated with the hydrology are related to the soil type or the land use/cover. Although this accounts for some spatial variation, the variability within a soil type or land use/cover is not represented. For example, compaction can alter the bulk density and hydraulic conductivity which can be a localized phenomena within the same soil type. SWAT has the capability to represent such variability at the HRU level (unique combination of soil, LULC, and slope). Bulk density, hydraulic conductivity and LAI are three measurable parameters that play a significant role in the hydrologic balance of an area and are chosen to be measured in this study. To establish the locations they are to be measured at, HRUs within the study site were selected based on uniqueness and

spatial spread using ArcGIS. Point locations were added based on referencing selected HRUs and orthophotos to ensure accessibility. Point locations for sampling were imported into a handheld GPS (Garmin GPSmap 60CSx; horizontal accuracy <10 m) which helps direct the researcher to the sampling area.

2.5.1 Bulk Density

Soil cores were collected using soil corer manufactured by the Oakfield Apparatus Company (model B). Cores are collected from the soil surface to a depth of 30 cm and from 30 – 60 cm. Cores are separated by soil horizon based on visual inspection of colour changes and placed into separate ziplock bags (Figure 7). The depth at which horizons start and finish are measured using a tape measure. Bulk density is calculated as the mass of oven dried soil divided by its volume (Osunbitan et al. 2005). Soil samples are oven dried for 48 hours at 105°C after which they are measured for dry weight using an electronic scale (I 1200 Compact Professional Balance). Since the soil corer is not a typical cylinder, the standard equation to find the volume of cylinder could not be used. We noted all the different lengths of soil horizons and poured fine sand into the corer to represent the soil cores for each noted length. The sand is poured back out into a graduated cylinder to estimate the volume of the soil core.

Figure 7. Soil core separated into soil layers by visual inspection.

2.5.2 Infiltration/ Hydraulic Conductivity

From the onset of precipitation, the rate of infiltration will decline with time until a steady state rate is reached. The initial infiltration rate will depend on the initial soil moisture content prior to onset of

precipitation and the final rate will be equivalent to the saturated hydraulic conductivity (Viessman and Lewis 1995). Therefore, there is a relationship between the steady state rate of infiltration and the saturated hydraulic conductivity.

Infiltration rates are difficult to assess due to spatial and temporal variability (Sharma et al. 1980). Nevertheless, knowledge of this processes is vital for hydrological modeling as it controls the routing of water within watersheds (Sharma et al. 1980). The infiltration rates of soils are largely impacted by the hydraulic conductivity of soils (Grayson et al. 1992) and thus is paramount in solving water management problems such as drainage, irrigation, rainfall-runoff response, pollutant transport and erosion. Hydraulic conductivity affects the velocity or the rate at which a liquid can flow through a porous media (i.e., infiltrate) which is described in Darcy's law as:

$$v = -K\left(\frac{\delta h}{\delta l}\right) \tag{36}$$

where v is the macroscopic velocity of groundwater ($m \cdot d^{-1}$), $\delta h/\ \delta l$ is the hydraulic gradient, which include the hydraulic head (h) and the distance along the direction of flow (l), and K is the hydraulic conductivity (Eq.(36)). K takes into account both the properties of the fluid and the media (Smith et al. 2002). Hydraulic head is the height of a water column above a given datum (generally taken as the mean sea level) and describes the energy of the water per unit weight (Kasenow 1997). The total head is the summation of the pressure head which increases with depth below the soil surface and the elevation head which decreases with depth (Kasenow 1997). Since the pressure gradient is negative in the direction of flow (water flows from an area of high pressure to an area of low pressure), a negative sign is required to ensure positive velocities. Depending on the moisture content of the soil, K can either represent the saturated hydraulic conductivity (K_s) or the unsaturated hydraulic conductivity (Smith et al. 2002). If the rate of infiltration is approaching zero at the surface, precipitation reaching the surface will be routed as runoff. Alternatively, if the rate of infiltration is quite high, runoff is reduced accordingly. Infiltrated water can be further subdivided into components such as percolation, lateral flow, groundwater recharge, return flow, and deep aquifer recharge (Arnold et al. 1998). Infiltrated water is important as it can be both the source of base flow in rivers, streams and creeks (sustaining flow during dry periods), in addition to being the main water supply in certain locales. Furthermore, knowledge of infiltration rates allows engineers to assess and control storm water runoff. As a result, quantifying the hydraulic conductivity of the soil and thereby the infiltration rate is of great importance to hydrological modeling and water management. In addition, it is important to account for the spatial variability of hydraulic conductivities that may arise as a result of spatial heterogeneities within a locale (e.g., different soil types and land cover).

The Guelph Permeameter (Figure 8) and Tension Infiltrometer (Figure 9) are two instruments used to measure infiltration/hydraulic conductivity of soils. Studies comparing various methods to

measure infiltration have found the Tension Infiltrometer (TI) and Guelph Permeameter (GP) to have various advantages over other methods. Joel and Messing (2001) compared a drip infiltrometer with the TI to find that TI has the ability to model rainfall at different intensities similarly to the drip infiltrometer but without disturbing the soil pores; TI had similar values as the high intensity drip infiltrometer test when set to a pressure head of -20 mm and similar values as a low intensity drip infiltrometer test when set to a pressure head of -50 mm. Furthermore, the TI requires substantially less water for each run making it practical for field studies. The Guelph Permeameter (GP) simultaneously measures the three most important parameters that governs the flow of liquids within the vadose zone: field-saturated hydraulic conductivity (K_{fs}), sorptivity (S) and the hydraulic conductivity–pressure head relationship [K(Φ)] (Reynolds and Elrick 1986). While K_{fs} controls how fast liquid will go through the soil medium, sorptivity is the capacity of the soil to absorb the wetting liquid (Philip 1969). As the hydraulic head decreases (becomes more negative), the hydraulic conductivity (K) also decreases as an exponential function (K_{fs}) (Gardner 1958). All three of the terms are solved for by finding the steady state fall rate of the water in the GP as it infiltrates into the soil (Reynolds and Elrick 1986). Since TI measures infiltration rate at the soil surface and GP below the surface (30cm below), the calculated hydraulic conductivities can be used for the first and second soil layers respectively.

2.5.2.1 Guelph Permeameter

The Guelph Permeameter (GP) is set up in proximity (not more than 2 m away) to the TI and because it uses a larger volume of water, it is always set up slightly downhill from the TI. This prevents water outflow from the GP from saturating the TI measurement area. The soil auger is attached to the auger handle assembly to bore a hole with a diameter of 6 cm and a depth of 30 cm. Once the soil is excavated, the sizing auger is used to flatten the bottom of the hole. The well prep brush is pushed into and out of the hole 2 times to reduce the effects of smearing caused by the augers. Tripod legs are attached to the tripod base and placed over the bore hole. The tripod bushing is placed on the support tube. The air tube in the reservoir tube and the support tube are connected and the support tube is attached to the reservoir tube. The notch on the reservoir valve is kept at the 12 o'clock position so that infiltration will begin using both reservoirs. If infiltration is considerably slow, it is switched to the 6 o'clock position which only uses water from the inner reservoir tube (magnifies water level drop). The air tube is pushed in completely (acts as a plug to prevent water leaking through the air inlet tip when filling) and water is filled to the top through the fill port and closed with the fill plug. The filled permeameter is placed into the tripod assembly and lowered into the bore hole. In this study, the GP is used to measure infiltration at two different heads: 5 cm and 10 cm (Kodešová et al. 2010). The 5 cm head is set first by sing a tape measure to pull the air inlet tube 5 cm high. The drop in water level was recorded every 2 minutes until the steady state rate of fall (used to calculate saturated hydraulic conductivity) has been reached (when the rate of fall does not change over 3 consecutive time intervals). Once the 5 cm head is

completed, the 10 cm head is set by pulling the air inlet tube 5 cm higher to a total of 10 cm. Water level drop is recorded once again every 2 minutes until the steady state rate fall is reached or stopped prematurely if the water runs out too quickly to record. To calculate the soil saturated hydraulic conductivity, the accompanying "Guelph Permeameter Ksat Quick Calculator" excel spreadsheet is used (http://www.soilmoisture.com/operating.html). In this study the double head method is carried out, requiring inputs of the reservoir used (inner or combined), the head heights (5 and 10 cm), the borehole radius (6 cm), the soil structure category (1-4; explained in the spreadsheet), and the two steady state rates of water level change.

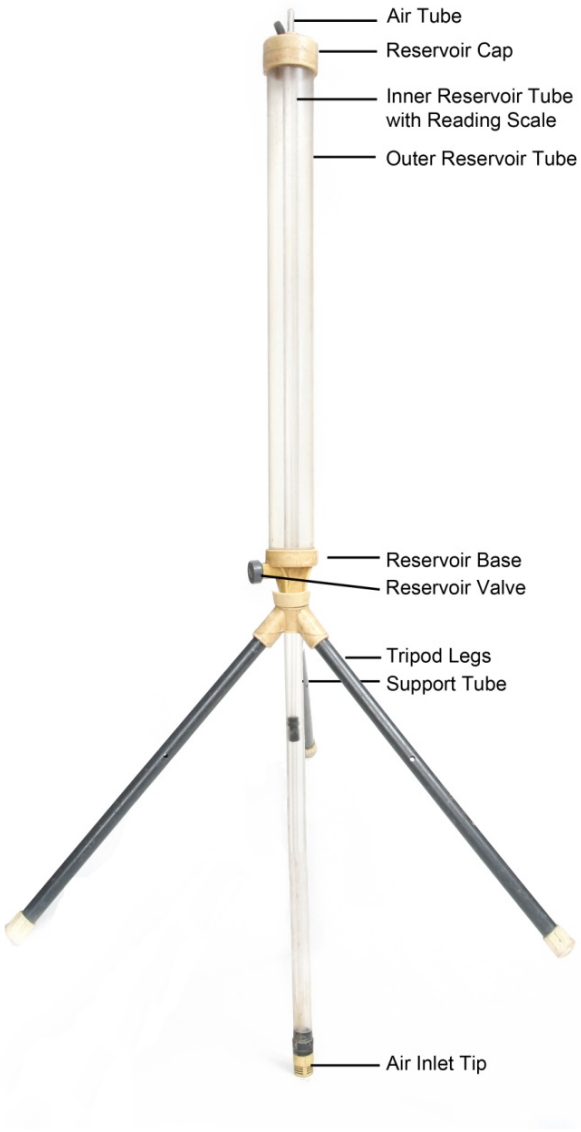

Figure 8. The Guelph Permeameter, used to calculate saturated hydraulic conductivity at selected field sites.

2.5.2.2 Tension Infiltrometer(TI)

The Tension Infiltrometer (20 cm version) was purchased from Hoskin Scientific. Prior to use, the soil needs to be prepared before placing the tension disk on it. A flat location is scouted and a ring that is slightly larger than the circumference of the tension disk (20 cm diameter) is placed on the soil to determine the area that needs to be cleared. Any leaves, debris, roots, and small vegetation are removed leaving only the bare soil. Areas with extruding roots are avoided as they will significantly alter the infiltration rates. Scissors are used to cut vegetation or roots at the surface of the soil to avoid macropores that can be created if they are pulled out. A carpenter's level is used to ensure the area where the tower and baseplate will be placed are level. Local loose soil or coarse sand is added to any crevasses at the surface within the ring perimeter so to make the soil surface completely flat. This ensures maximum contact between the disc and the soil surface. The ring is removed before setting the baseplate on the prepared soil.

A pan is filled with tap water in which the baseplate with the membrane attached is fully submerged. The tube is attached to the baseplate and the valve is left in the open position to allow air out of the disc, tube and membrane while allowing water to fill. A stopper is placed at the bottom outlet of the water reservoir. Clamp B is opened, clamp C is closed, clamp A is opened, the top of the water reservoir is removed and water is filled until 5 cm from the top. The top is replaced and Clamp A is closed. The top of the bubble tower is removed and filled until 7cm from the top. The top is replaced with the air entry tube pushed in to the resting position. The tensions are set in order of highest (-10 cm) to lowest (-2.5 cm). To set a tension of -10 cm, the parker fitting is loosened and air entry tube is pulled up until the bottom of the tube is 10+4 cm below the water surface. The 4 cm is the calibration factor. Once the tension is set, clamp B is closed, the stopper on the water tower is removed and attached to the tubing from the baseplate while keeping the disc submerged. The valve is opened and the tower is rocked back and forth to let any air bubbles from the baseplate to go into the water tower. The prepared soil surface is lightly sprayed with water using an atomizer if the soil is particularly dry; this will prevent air from entering the baseplate when placed on the soil. While keeping the valve in the open position, the baseplate is transferred on to the prepared surface. Simultaneously, the tower is also placed on the soil. The tube attaching the baseplate and tower is kept straight and a carpenter's level is placed extending from the leveling block to the top of the baseplate. The tower is raised (adding something underneath the base) or lowered (burrowing the soil on which it is placed) until it's completely level with the baseplate. This is to ensure that the tension at the membrane will be equivalent to what is set with the air entry tube. Clamp B and clamp C are opened. Bubbles rising from both the bubble and water tower indicate infiltration is occurring and that the setup is correct. The water level drop from the water reservoir is recorded every 2 minutes until steady state infiltration is achieved (a consistent rate of drop for 3 or more consecutive time intervals). To set the next tension, the shut–off valve and clamp B are closed. If needed, the water reservoir is refilled at this time. The parker fitting is loosened to adjust the air entry

tube to the new tension and tightened once set. Measurements for the new tension is started by opening the shut–off valve, clamp B and clamp C. In total, measurements are made with three different tensions: -2.5 cm, -5 cm, and -10 cm tensions (Kodešová et al. 2010).

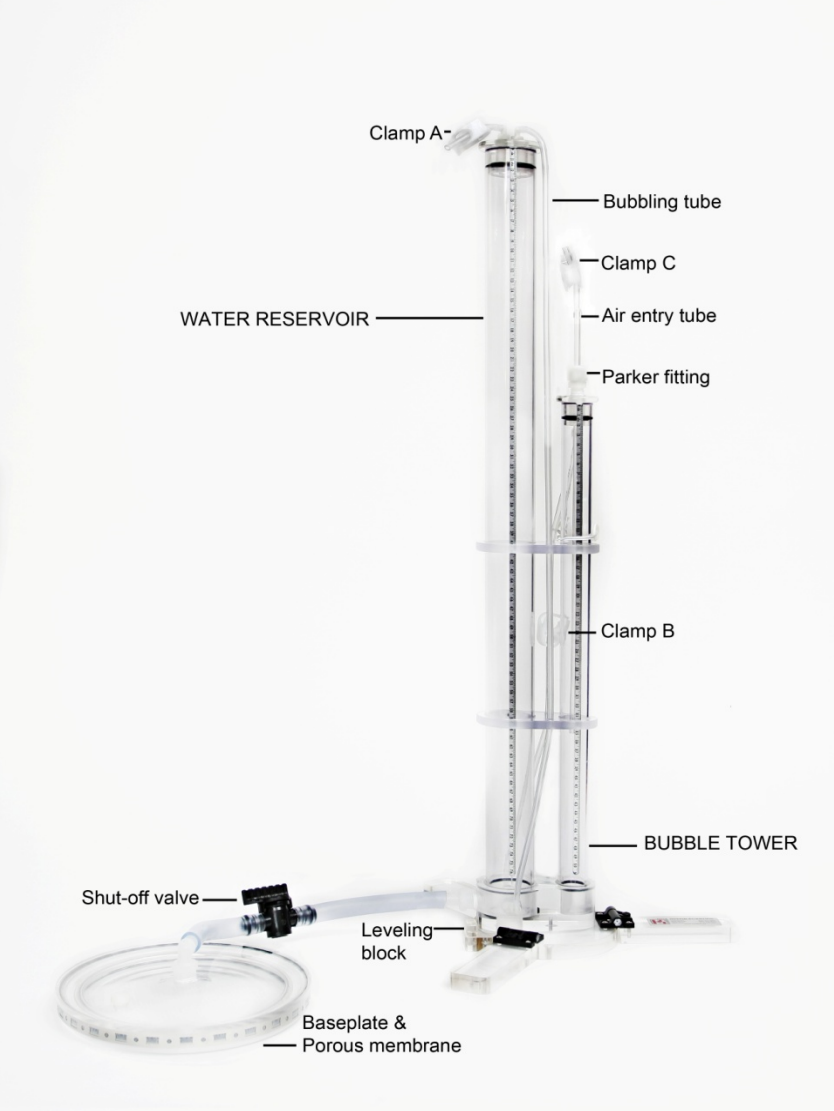

Figure 9. The Tension Infiltrometer, used to calculate saturated hydraulic conductivity at selected field sites.

Measurements taken by the TI can be used to estimate both saturated and unsaturated hydraulic conductivity, but as proposed by (Gardner 1958), unsaturated hydraulic conductivity will vary with matric

potential. Since SWAT only supports a single value of saturated hydraulic conductivity, only this is calculated from the following expressions:

$$Q(h_1) = \pi r^2 K_{sat} \exp(\alpha h_1) \left[1 + \frac{4}{\pi r \alpha}\right] \quad (37)$$

$$Q(h_2) = \pi r^2 K_{sat} \exp(\alpha h_2) \left[1 + \frac{4}{\pi r \alpha}\right] \quad (38)$$

where Q is the volume of water entering the soil per unit time (cm^3h^{-1}) for the respective tension head, r is the radius of the circular base (10cm), K_{sat} is the saturated hydraulic conductivity, α is a constant, and h is the negative tension head that is set (i.e.,-2.5, -5, -10). Dividing Eq. (38) by Eq. (37), allows you to solve for the α constant:

$$\alpha = \frac{ln[Q(h_2)/Q(h_1)]}{h_2 - h_1} \quad (39)$$

Q (cm^3/hr) for a certain tension can be calculated by multiplying the inside circumference of supply tube by the water level drop rate in the supply tube at steady state. Knowing Q for two tension heads (h_1 and h_2), α can be solved. Q and α can be used in Eq. (37) or (38) for the respective tension to solve for K_{sat}. Our study measures water level drop at 3 tensions, and the α level can be different based on the two tensions used to calculate it (e.g., -2.5 and -5, or -5 and -10). As a result, we calculate α with tensions -2.5 and -5 and again with tensions -5 and -10. The two α values are averaged and is used to calculate K_{sat}.

2.5.3 Ancillary Data

The soil moisture is measured before and after each infiltration measurement using the Theta Probe ML2x (Delta-T devices 1999) combined with the HH2 Moisture Meter from Delta-T Devices (Delta-T devices 2005). Soil moisture readings prior to infiltration measurements were not taken directly on the sampling area but in very close proximity, in order to avoid the Theta probe tongs from disturbing the soil surface. Soil moisture readings taken following the infiltration measurements weare done directly on the area sampled. An infrared thermometer (DeltaTRAK'sThermotrace 15030) is used to record temperature of the water used and the temperature of the soil before and after the infiltration measurements. Local weather data (average wind speed, air temperature, wind chill, humidity, and heat stress index) was measured at each HRU sampling location with a handheld weather station (Kestrel 3000) at the beginning and end of infiltration measurements to ensure consistent environmental conditions throughout the infiltration measurements.

2.5.4 Leaf Area Index

Many environmental models require the quantification of leaf area as it is essential to assessing the radiation regime for the surface below and affects the mass/energy exchange between plants and the surrounding atmosphere (Neumann et al. 1989). In the hydrological model used in this study, leaf area is used as a parameter to quantify potential growth of plants and evaporation of plants in bodies of water. If the Penman–Monteith method is chosen to calculate potential evapotranspiration, leaf area will be used to calculate canopy resistance and transpiration from plants. Leaf area of the canopy is also used to calculate interception of precipitation (canopy storage) if the GA runoff equation is used over the CN method (Neitsch et al. 2011). With the exception of canopy storage, which can be altered at the HRU level, all other values pertaining to LAI can only be changed at the plant type level. The leaf area of vegetation is commonly interpreted through the leaf area index (LAI) (Neumann et al. 1989), defined by Watson (1947) as the dimensionless one sided green leaf area per unit ground surface. Sampling for direct measurement of leaf area can be grouped into two broad categories: the dispersed individual plant method (DIP) and the stratified-clip method (Norman and Campbell 1989). For the later, a wire frame is placed denoting an area to be clipped usually in a stratified manner at different heights in the canopy. Consequently, LAI is measured for a group of plants; a practical method for plants with smaller leaves such as grasses and crops (Norman and Campbell 1989). The DIP method samples only one plant at a time and thus it is used for studies requiring detailed canopy structure information (Norman and Campbell 1989). Once sampled, there are three widely used techniques for attaining the area of the leaves collected: automatic planimeters, leaf area to weight ratios and area from leaf dimensions. The interested reader is directed to Ross (1981) for extensive discussion on these methods. As direct methods of measuring LAI are impractical for sampling an expansive area, indirect methods were considered for this study and is discussed in detail below.

2.5.4.1 Canopy Radiation Models

Indirect optical methods for measuring LAI, such as tracing radiation and architecture of canopies (TRAC), LAI-2000, and hemispherical photographs are preferred for fast measurement times and their non–destructive nature (Zhang et al. 2005). All indirect methods solve for LAI using an inverse solution of a canopy radiation/ light penetration model (Norman and Campbell 1989). Canopy radiation models link LAI and canopy architecture to the quantity of solar radiation penetrating the canopy, under the assumption of random spatial distribution of leaves (Monsi and Saeki 2005). Canopy architecture or structure can be termed as the organization and amount of aboveground plant tissue (Norman and Campbell 1989). While the canopy structure plays an intricate role in plant-environment interactions, the level of complexity and spatiotemporal variability makes it difficult to quantify (Bréda 2003). However, owing to the close coupling of canopy structure and canopy radiation, canopy features can be inferred from applying above and below canopy radiation measurements to inversed radiative transfer models (Norman and Campbell 1989). These models essentially calculate the probability of solar radiation being

intercepted by the canopy and the probability of penetration through the canopy (Neumann et al. 1989). Two methods (LAI-2000 and hemispherical photographs) of measuring this probability is used in this study and will be discussed below.

2.5.4.2 LAI- 2000 LI-COR

The LAI–2000 has been used in many studies pertaining to different vegetation types including agricultural crops (Hicks and Lascano 1995), coniferous stands (Gower and Norman 1991; Deblonde et al. 1994) and deciduous stands (Dufrene and Breda 1995; Cutini et al. 1998). LAI-2000 works on a principle of knowing the ratio between the above and below canopy radiation. This can be achieved through a number of setups. One way is to have two different sensors connected to the same data logger, with each being designated to either above or below canopy measurements. Alternatively, one sensor can be used by alternating between above and below canopy measurements. With both methods, above canopy measurements can be problematic if the canopy is particularly high. In such circumstances, a reading of a nearby clear open area can be used to simulate above canopy radiation if the view of the sensor is free from obstruction. Theoretically, the opening diameter (within the vegetation) has to be at least seven times the canopy height to ensure there are no trees protruding into the field of view of the sensor. A semi–circle view cap is placed on top of the sensor's field of view (Figure 11) to null any shadows cast by the person holding the LAI–2000 arm from the calculations. Despite this aid, a lack of clear openings within the study site limited the use of this instrument to agricultural crops (corn) and grasses. For these sites, one reading above (Figure 10a) the canopy and 3 readings below (Figure 10b) the canopy (at various positions) were taken (LI-COR 1992). LAI for tall closed canopy vegetation was estimated through digital hemispherical photographs (DHP). Readings from LAI–2000 and DHP were taken approximately 45 minutes before sunrise or on uniform cloudy days.

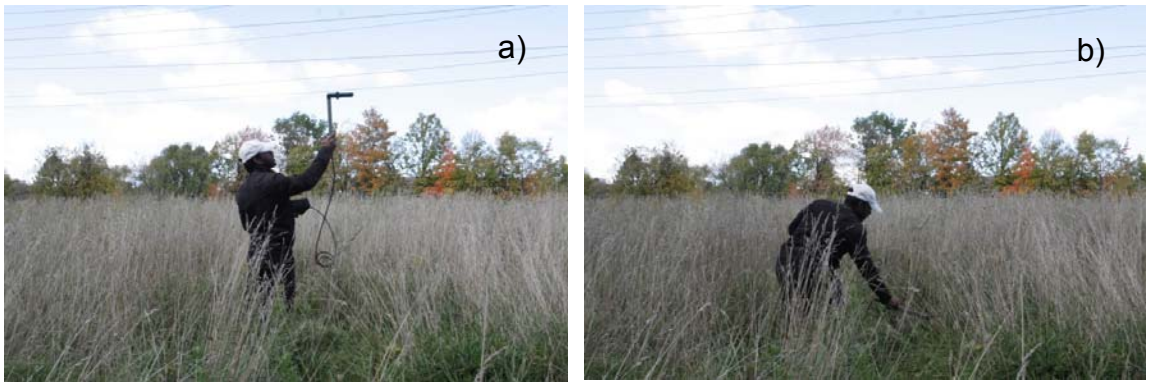

Figure 10. Using the LAI-2000 to measure radiation above (a) and below (b) canopy to indirectly measure LAI.

Figure 11. LAI-2000 arm with the semi-circle view cap to exclude user's shadow to affect readings.

2.5.4.3 Hemispherical Photograph

Photographs have been used to study the obstruction of irradiation at a site as early as 1892 (Anderson 1964). Although architects had a strong influence in developing the theory behind calculating the effect of obstruction on irradiance (Anderson 1964), it has been adapted to meteorology and biology to study sky conditions and plant canopy cover/ canopy radiation regimes respectively (Chen et al. 1991). The ability to view the entire hemisphere of the sky over the study site is a particular advantage of the hemispherical photographs (Figure 12). Taking such a photograph under a canopy allows for analysis of gaps and obstructed light by the canopy foliage. Using the DHP-TracWin software (Leblanc 2008), the gap fraction of the image can be identified and used to calculate plant area index (PAI), which includes both green and non–green canopy elements. Inserting the needle–to–shoot ratio and the woody–to–total area ratio into the program converts PAI into LAI. Table 6 shows ratios found in literature that were used for our study based on the tree species type.

Table 6. Needle to shoot ratio and woody to total area ratios used in DHP–TracWin software to convert PAI into LAI.

Species	Needle : Shoot (γ_E)	Woody : Total Area (α)
Balsam Fir 1980[a]	1.71	0.15
Intermediate Balsam Fir IBF [a]	1.71	0.2
Young Balsam Fir YBF [a]	1.71	0.2
Red Pine[b]	2.08	0.07
Broad leaf[d]	1	0.1-0.3 (used 0.2)
Conifers[c]	1.57	0.15

([a] Chen et al. 2006; [b] Gower et al. 1999; [c] Chen et al. 2006; [d] Dufrene and Breda 1995)

To take hemispherical photographs, a tripod is used with the Nikon Coolpix 4500 camera and the Nikon fisheye converter FC-E8 attachment (Figure 13). Using the spot metering exposure setting, the camera is zoomed into one of the canopy gaps (such that only the clear gap is visible) to expose correctly for the sky (foliage should be underexposed in the image by correctly exposing for the sky). All pictures are taken with an aperture setting of 5.3. Using the camera's manual option, the shutter speed is set to reflect the spot metering exposure. The lens is zoomed back out when the picture is ready to be taken. This is a modified method of Zhang et al. (2005), where an additional telephoto lens is used to get the correct exposure of the sky through a canopy gap. Pictures are taken at 5 locations (one in the middle and one for each cardinal direction approximately 10 feet from the centre) and the 55-60° zenith angles (see Figure 12) are analyzed using the DHP–TracWin software (Leblanc 2008). At each location, the picture is taken 3 times, one at the correct exposure, one at a stop higher and one at a stop lower (by increasing or decreasing shutter speed). Upon reviewing the pictures on the computer, the most correctly exposed image is chosen for analysis.

LAI could not be readily altered for each HRU within SWAT, however, CANMX which describes the maximum storage of a canopy to hold intercepted precipitation can be altered at the HRU level and be derived from LAI. The von Hoyningen-Huene method is used to convert LAI to CANMX based on Kozak et al. (2007) suggestion:

$$CANMX = 0.935 + (0.498 \cdot LAI) - 0.00575 \cdot (LAI)^2 \quad (40)$$

where $CANMX$ is the maximum canopy storage (mm), and LAI is the leaf area index. Where applicable, both DHP and LAI–2000 were used at the same site to compare measurements.

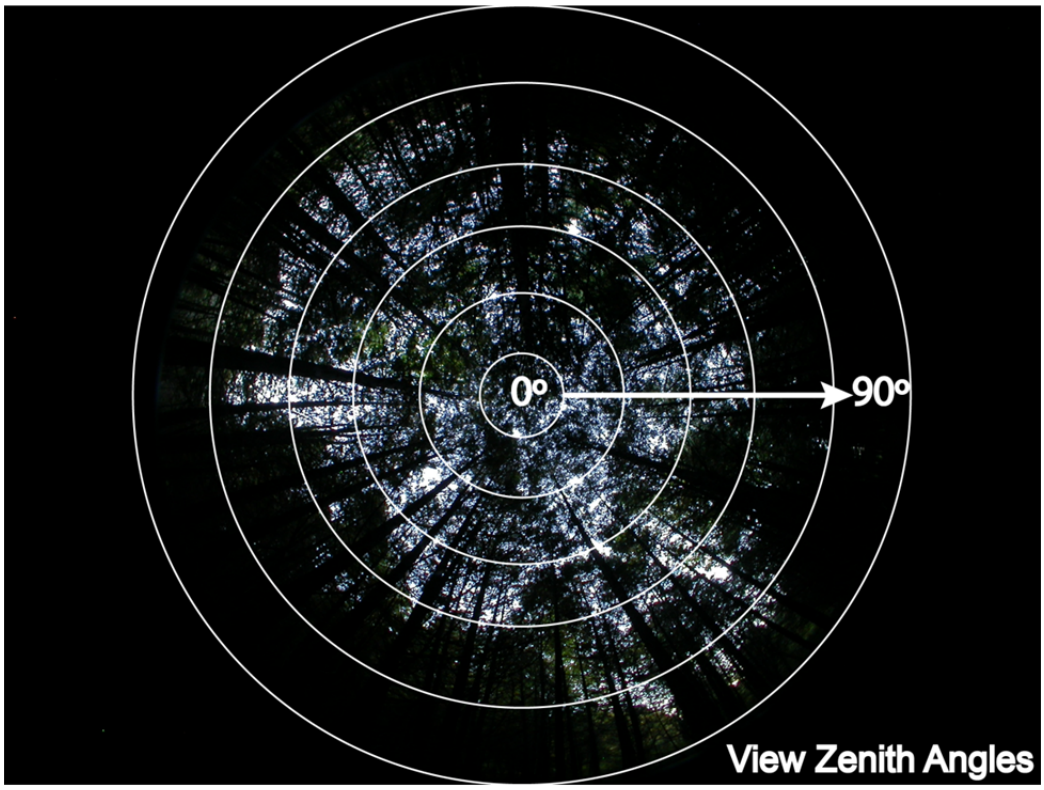

Figure 12. Hemispherical photograph with zenith angle rings; 55°-60° ring is used for gap fraction analysis (Adapted from Leblanc 2008).

Figure 13. a) Digital Nikon Coolpix 4500 camera and fish eye hemispherical lens used to estimate LAI for tall dense canopies (b)

2.6 ArcSWAT

Using the 10 m resolution DEM, watershed delineation is carried out with a threshold factor of 4100 cells. During an iterative process, this threshold was found to be the one that best satisfies most of the streams published in the National Hydro Network. Locations where measured streamflow data exists are marked during the delineation process. A lookup table (text file) is created to match the soil and LCLU types from the GIS layer to the SWAT database based on SWAT codes. This lookup file is uploaded into ArcSWAT, so that the raw soil and LCLU layers are converted to contain SWAT codes. Once HRU definition is finished, the user defines which HRUs are kept. All HRUs other than those representing less than 5% of the soil, slope, or LCLU combination within the subbasin are kept in this study. These small HRUs, although not having an impact on the flow out, increase the computational time and storage space requirement. The weather generator and climate data inputs are loaded into ArcSWAT in the format specified by ArcSWAT user manual (Arnold et al. 2011). With daily precipitation input, the CN method is the default runoff equation. If GA method is to be run, sub–daily precipitation needs to be loaded and the "Rainfall-Runoff Method" in the "General Watershed Parameters" needs to be edited. The years of the simulation are selected (2005-2010) which includes the warm up year of 2005, the calibration years of 2006–2008, and the validation year of 2010. The year 2009 is omitted as a result of no stream gauge data for that period. The "NYSKIP" parameter is given a value of 1 in the run tab to indicate that the first year of the simulation period (2005) is to be treated as the warm up year. The 64–bit debug version of the executable file was used to run the simulations.

2.7 SWAT–CUP

SWAT–CUP (Calibration and Uncertainty Programs) is a computer program developed by Dr. Karim C. Abbaspour for calibration of SWAT models (Abbaspour 2012). It contains multiple techniques including SUFI–2 (Sequential Uncertainty Fitting), PSO (particle swarm optimization), GLUE (Generalized Likelihood Uncertainty Equation), ParaSol (Parameter Solution), and MCMC (Markov Chain Monte Carlo) which allow for sensitivity analysis, calibration, validation, and uncertainty analysis of SWAT models. This study uses the 2012 version of the program and the SUFI–2 algorithm for calibration and validation.

2.7.1 Calibration

SUFI–2 is used as an optimization algorithm with the Nash–Sutcliffe Efficiency (NSE) as the objective function (Yang et al. 2008). Physically meaningful absolute minimum and maximum ranges for parameters are selected based on SWAT manual (Neitsch et al. 2011) and placed in the "Absolute_SWAT_Values.txt" tab. A sensitivity analysis was carried out in ArcSWAT with all the parameters that affect the flow out. Based on the sensitivity analysis and guidelines given by SWAT–user community (online "SWAT–user" google groups), 17 parameters were chosen for calibration process (Table 7).

Table 7. Parameters used for calibration based on sensitivity analysis and SWAT–user experience, their description and the level at which they are altered during calibration.

Parameter	Description	Level
CN2	Moisture condition II curve number	LCLU
SOL_AWC	Available water capacity	Soil + Top 2 Layers
ESCO	Soil evaporation compensation coefficient	Soil
GW_REVAP	Reevaporation coefficient	LCLU
REVAPMN	Threshold water level in shallow aquifer for revap	Soil
GWQMN	Threshold water level in shallow aquifer for base flow	Basin
OV_N	Manning's n value for overland flow	LCLU
SLSUBBSN	Average slope length	Basin
CH_K1	Effective hydraulic conductivity of tributary channel	Basin
ALPHA_BF	Baseflow recession constant	Basin
SMFMX	Melt factor on June 21	Basin
SMFMN	Melt factor on December 21	Basin
CH_K2	Effective hydraulic conductivity of the main channel	Basin
GW_DELAY	Delay time for aquifer recharge	Basin
CH_N1	Manning's n value for tributary channels	Basin
CH_N2	Manning's n value for the main channel	Basin
EPCO	Plant uptake compensation factor	Basin

The parameters to be calibrated are specified by the user in the "Par_inf.txt" tab. A range of values (max and min) are given for each parameter within which the SUFI–2 algorithm will randomly sample for each simulation. This is carried out for each selected parameter, and essentially a vector of values for the parameters is created for each iteration. However, the range of specified values affect the original value of the parameter differently based on the 3 notations used with parameters to express how values should change during calibration: r , a, and v. Specifying "r" denotes that the original value of the parameter will be multiplied by the user entered percentage range, while "a" denotes that a value between the specified range will be added or subtracted from the original value. Typically, r and a are used for spatially variable parameters, so that the variability of the original value is preserved. The "v" prefix is used to denote that the original value should be replaced by the specified value. This notation is used for a parameter that has the same value basin wide or for assigning a specific value. In our study, the "v" prefix was only used with SMFMX and SMFMN. It was also used to parameterize the model with the field collected data (bulk density, hydraulic conductivity and CANMX). Since the exact value is known for these three parameters, both their min and max values will be the same as the field collected value. All other parameters were used with the "r" notation.

SWAT–CUP allows parameters to be calibrated based on the hydro group of the soil, the soil texture, LCLU, subbasin number, slope, and layers/columns (where applicable) or any combination of these categories that the parameter supports. However, there was one problem in specifying the field

collected data to the HRU it was collected in. HRUs are created based on combinations of LCLU, slope, and soil type not texture. A number of soil types can potentially have the same soil texture. Unfortunately, the soil type cannot be specified in SWAT–CUP. As a work around to change parameters at the HRU level, since the soil texture attribute is not used in any model calculations, for each soil type, its texture was given a unique arbitrary code (a-z in our study) in SWAT's user soil database. In this way, the newly added unique codes for soil texture will reflect the differences in soil types allowing parameters to be applied and calibrated at the HRU level. For example, in our study, the arbitrarily assigned soil texture code "b" reflects the soil type "Bottomland" and therefore to specify the saturated hydraulic conductivity (Sol_K) at the third soil layer for the HRU combination soil type: Bottomland/ LCLU: FRSE/ slope: 2-10 within subbasin 138 the following notation is used: "v__SOL_K(3).sol____b__FRSE__138__2-10".

The starting and ending simulation number (or the # of simulations) is usually set to 150 simulations in the "SUFI2_swEdit.def" tab. The "File.Cio" tab contains general simulation information that is derived from the ArcSWAT simulation run. Some of the details need to be changed depending on whether the calibration simulation period or validation period is set to run. For the calibration period, we change the number of years simulated (NBYR) from 6 (2005-2010) to 4 (2005–2008). Attention needs to be given to the ending Julian day as changing the simulation period could change the value from 365 to 366 if the last year of simulation is now a leap year or vice versa. Since 2008 is a leap year, this value is changed to 366 for the calibration period.

The number of observed variables used for calibration and the values of those variables are placed in the "Observed_rch.txt" and "Observed.txt" tab. Only one observed variable (stream flow out) is used in this study, the values for which are obtained from the stream gauge "East Duffins at Claremont". The format for observed data is detailed in Abbaspour (2012). In the "SUFI2_extract_rch.def" the beginning and the end year of simulation (without the warm up period) and the subbasin to which the gauged data belongs to is specified.

Once the calibration is started, a Latin Hypercube (McKay et al. 2000) sampling is carried out, which provides *n* parameter combinations, where *n* is the specified number of simulations. We generally used 150 simulations per iteration. The number of iterations depends on the change in the objective function value. As the objective function (NSE) stops increasing with each successive iterations, calibration was stopped. After each successive iteration, the simulation with the highest NSE was regarded to have the best parameter ranges. Using these ranges, the calibration is run again in order to decrease the uncertainty in parameter values (essentially narrowing parameter value range). Calibration was carried out using the measured flow data for the stream gauge at the outlet of the study subbasin. In addition to calibration and validation of the model, the effectiveness of using field collected parameter values during calibration/validation is tested. These calibrated/validated models with field data are compared to runs parameterized by field data alone without calibration/validation. Additionally, we compared the spatial extent of field data implementation. We compared results of applying the field

collected data at the location where it is collected/within the same subbasin to applying them to all applicable HRUs within all upstream subbasins. Furthermore we compared the influence of applying different combinations of field collected data on the model response (bulk density (BD) and saturated hydraulic conductivity (Sol_K) alone vs. all three variables) (Figure 14).

It is important to note that SWAT–CUP does not reset the value of the parameters that were changed during each iteration. For a new iteration, changes are added to adjusted parameters from the previous iteration. This is required so that the calibration process is continuous from one iteration to the next. However, if the user is testing different methodologies of calibration as this study does (i.e., adding different field data), then the parameters must be reset prior to beginning of a new methodology. This can be done by copying and pasting the original "textinout" files from the "backup" folder that can be found in the project directory.

The calibration procedure was done twice once with the full modeled output and once with only the model outputs for days with measured precipitation input. The default models differ based on which group of models they belong to (Figure 14). For the calibration and validation group the default models are calibrated and validated respectively but without any field data. The default for the group of models with no calibration or validation are outputs from ArcSWAT before any calibration or validation.

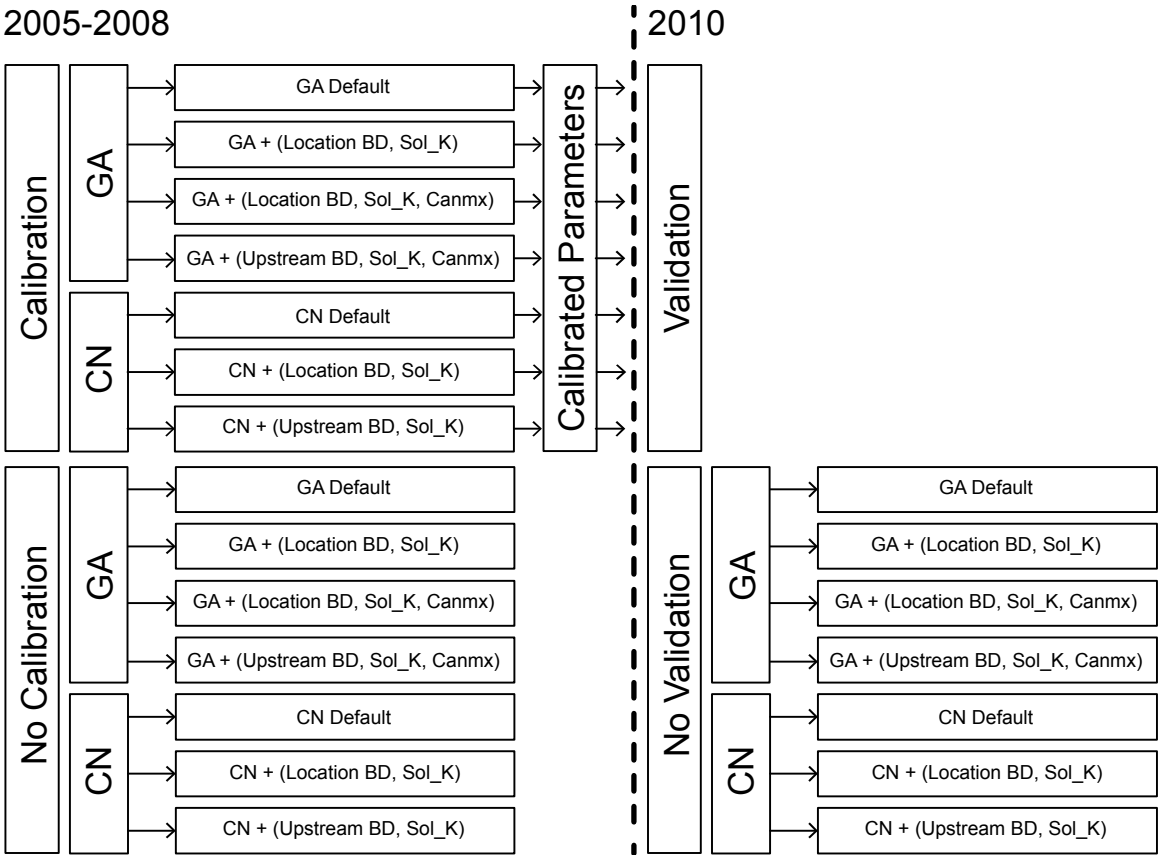

Figure 14. SWAT CUP runs with different runoff equations (CN: Curve Number, GA: Green & Ampt), calibration and validation process, with and without field data (BD: bulk density, Sol_K: saturated hydraulic conductivity, CANMX: maximum canopy storage), and with field data alone at different scales of field data implementation (Location: at the location where it is collected/within the same subbasin, Upstream: applying it to applicable HRUs within all upstream subbasins) for calibration and validation years.

2.7.2 Validation

In this study, based on the availability of stream gauge data, there is only one year of validation (2010). Validation is also carried out in SWAT–CUP and requires a few changes to the setup used for the calibration in "File.cio". The number of years of simulation is changed from 4 to 1 and the beginning year of simulation is changed from 2005 to 2010. The ending Julian day is changed from 365 to 366 as the year 2010 is not a leap year. The number of years to skip is changed from 1 to 0 since there is only one validation year. The observed data pertaining to the validation year is placed in the "Observed.txt" and "Observed.rch" files. The beginning and end year of simulation is also changed in the "SUFI2_extract_rch.def" file. The best parameter ranges produced in the last iteration of calibration is used for the validation run with the same amount of iterations.

2.8 Statistics

2.8.1 RMSE

RMSE was calculated using a bootstrap method programmed in the R statistical package. For the calibration years, 1000 iterations were carried out, and in each 250 randomly sampled observed and its matching modeled flow out data is compared to calculate the RMSE value. For the validation year of 2010, since there are fewer number of measured values (only 1 year as opposed to the 3 for calibration), each iteration contained only 50 sampled data. A box plot is drawn to depict the distribution of all the calculated RMSE values between each model run and the observed flow data.

2.8.2 ANOVA

An ANOVA is carried out for the 4 groups of model runs depicted in Figure 14 (calibration, validation, no calibration and no validation) to determine if there is any significant difference between the model outputs. If there is significant difference amongst the models, a post-hoc Tukey test is run in the R statistical program to establish which models are significantly different from each other through pair-wise comparisons.

3. Results

3.1 Soil, Slope and LCLU

Using the acquired soil, slope, and LCLU GIS layers, watershed analysis was carried out within the ArcSWAT interface following the delineation of the Duffins Creek watershed. Among the 23 soil categories, the prominent types within the Duffins watershed are: Woburn Loam (30.98%), Millikan Loam (14.88%), Pontypool Sand (10.83%), Bondhead (10.43%), Bottomland (8.66%), Peel Clay (8.49%), and Brighton Sandy Loam (6.1%) (Figure 15). Table 8 illustrates the hydrologic group (A–D) and the saturated hydraulic conductivity of each layer for these soils which were derived from accompanying tables of the GIS soil layer. The runoff potential of soils increases from hydrologic group A to D. The prominent soil classes in the Duffins watershed are in groups A and B and have moderate to high saturated hydraulic conductivities with the exception of Peel Clay.

Bottom Land, Woburn Loam and Bondhead are the three soil types that occur within the Claremont Conservation Area study site. Woburn Loam and Bondhead are both slightly stony, well drained, with no limitations for agriculture, and can support moderate infiltration when fully saturated (Land Information Ontario 2013). Bottom Land is a soil type that develops on flood lands along stream courses and as a result are prone to frequent flooding; its surface texture varies considerably depending on the type of alluvial deposits it receives (Olding et al. 1956). Milliken Loam is the second most abundant soil type in the Duffins Creek watershed. It is slightly stony, and considered to have no significant limitations for agriculture, but it is noted to be imperfectly drained (Land Information Ontario 2013). Bondhead, Woburn Loam, and Milliken Loam are medium textured soils (Hoffman et al. 1964).

Bondhead and Woburn Loam belong to the Brunisolic Grey–Brown Podzolic subgroup, while Milliken Loam is part of the Gleyed Brunisolic Grey–Brown Podzolic subgroup (Olding et al. 1956). Typical soil profiles of Woburn Loam, Bondhead, and Milliken soil types are included in Appendix C.

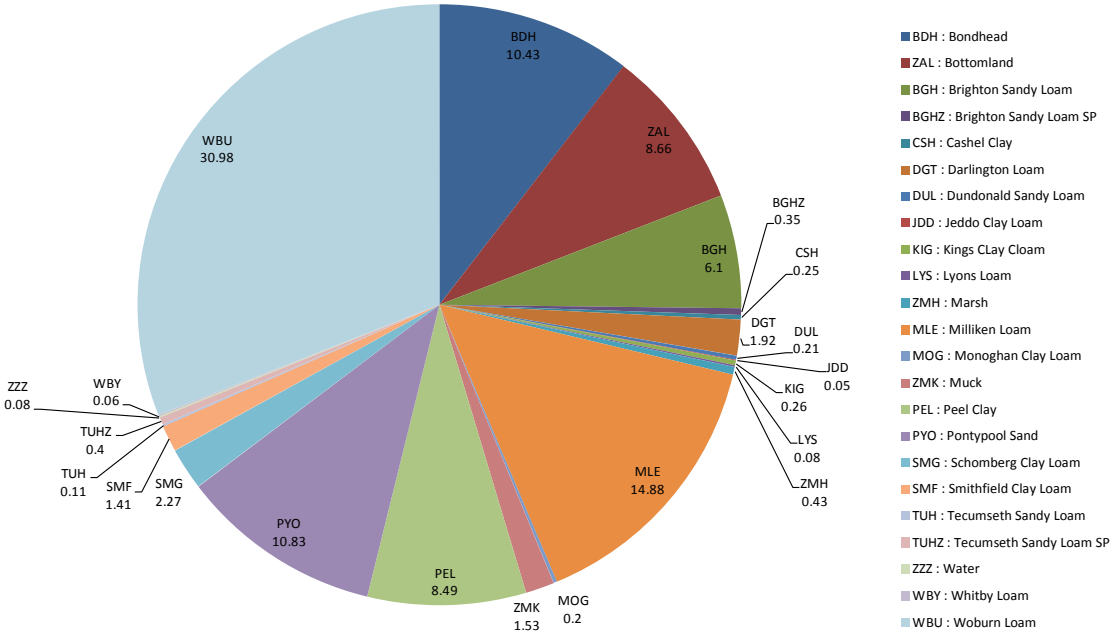

Figure 15.Percent soil type cover in Duffins Creek watershed based on GIS soil layer retrieved from the National Soil Database.

Table 8. Hydrologic soil groups and saturated hydraulic conductivities for prominent soil classes in the Duffins watershed derived from The National Soil Database.

Soil	Hydrologic Group	Sol_K Layer 1 (mm/hr)	Sol_K Layer 2 (mm/hr)	Sol_K Layer 3 (mm/hr)	Sol_K Layer 4 (mm/hr)
Woburn Loam	B	13.07	21.01	33.76	13.05
Millikan Loam	B	4.34	3.03	3.23	NA
Pontypool Sand	A	60.09	93.51	36.03	68.06
Bondhead	B	51	11.58	3.39	36.97
Bottomland	B	4.94	3.11	3.91	2.18
Peel Clay	C	5.19	2.66	2.62	1.36
Brighton Sandy Loam	A	68.51	64.99	28.38	78.55

Slopes were calculated based on DEM analysis within the ArcSWAT interface. A substantial proportion of the watershed (64%) has slopes between 10-30%. Roughly 35% of the watershed has slopes of 10% or less and only 0.21% of the watershed contains percent slope gradients greater than 30. However, as discussed previously, the empirical CN method that correlates rainfall to runoff works on the premise that the percent slope of the watershed is 5% (Neitsch et al. 2011). Although Williams (1995) describes a method to adjust CN based on the slope outside of SWAT, they were not modified in this study in order to compare CN performance with other studies.

The LCLU distribution based on datasets used in this study published in 2002 show that only 12% of the watershed is urbanized (UTRN and URHD) (Figure 17). This is in accordance with the 10% urbanized and 19% urbanizing statistic reported in the 2013 Duffins watershed report card published by the TRCA (2013). Among the remaining categories, the forest categories (FRST, FRSE, and FRSD) cover 26.31% while agricultural land (AGRR) and pasture (PAST) cover the majority of the watershed at 52.73%.

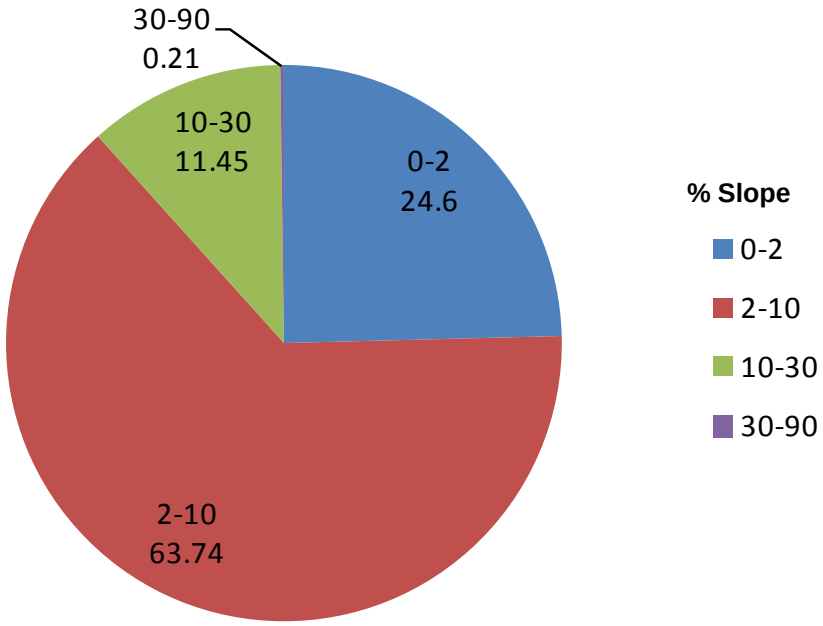

Figure 16. Percent slope coverage in the Duffins Creek watershed based on DEM retrieved from TRCA. The percent slope range is defined as greater than the lower limit and less or equal to the upper limit.

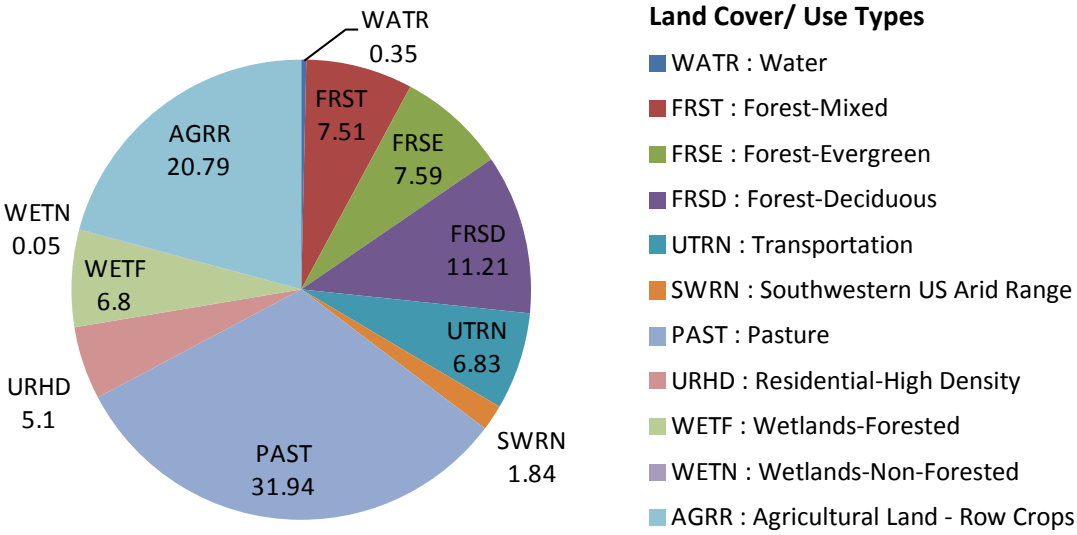

Figure 17. Percent land cover/ use types in the Duffins Creek watershed based on GIS LCLU layer retrieved from TRCA.

3.2 Field versus Database Values

Saturated hydraulic conductivities are found to be variable within the same soil type even when located within the same subbasin (Figure 18 – 19). Qualitatively, there seems to be no obvious pattern of cluster of low or high values based on soil type. Generally, saturated hydraulic conductivities for the first soil layer measured by the Tension Infiltrometer (Figure 18) are lower than those collected by the Guelph Permeameter for the second soil layer (Figure 19). Furthermore, the first layer of each soil typically has lower variability in saturated hydraulic conductivity than the second layer (Figure 20). Between soil types, the variability and medians of field measured hydraulic conductivities are more differentiated for the second soil layer than the first. With the exception of the first layer of Bondhead (BDL1), the database values fall within or very close to the range of the measured hydraulic conductivities and even at the median value for some soil layers. However, database values are not capable of representing the variability of field collected hydraulic conductivities. Additionally, for the first soil layer, database values are higher than the full range of field collected values. For the second layer, the database value is lower than the median of the field collected values for BDL2 and BTL2, but for WLL2 it remains higher.

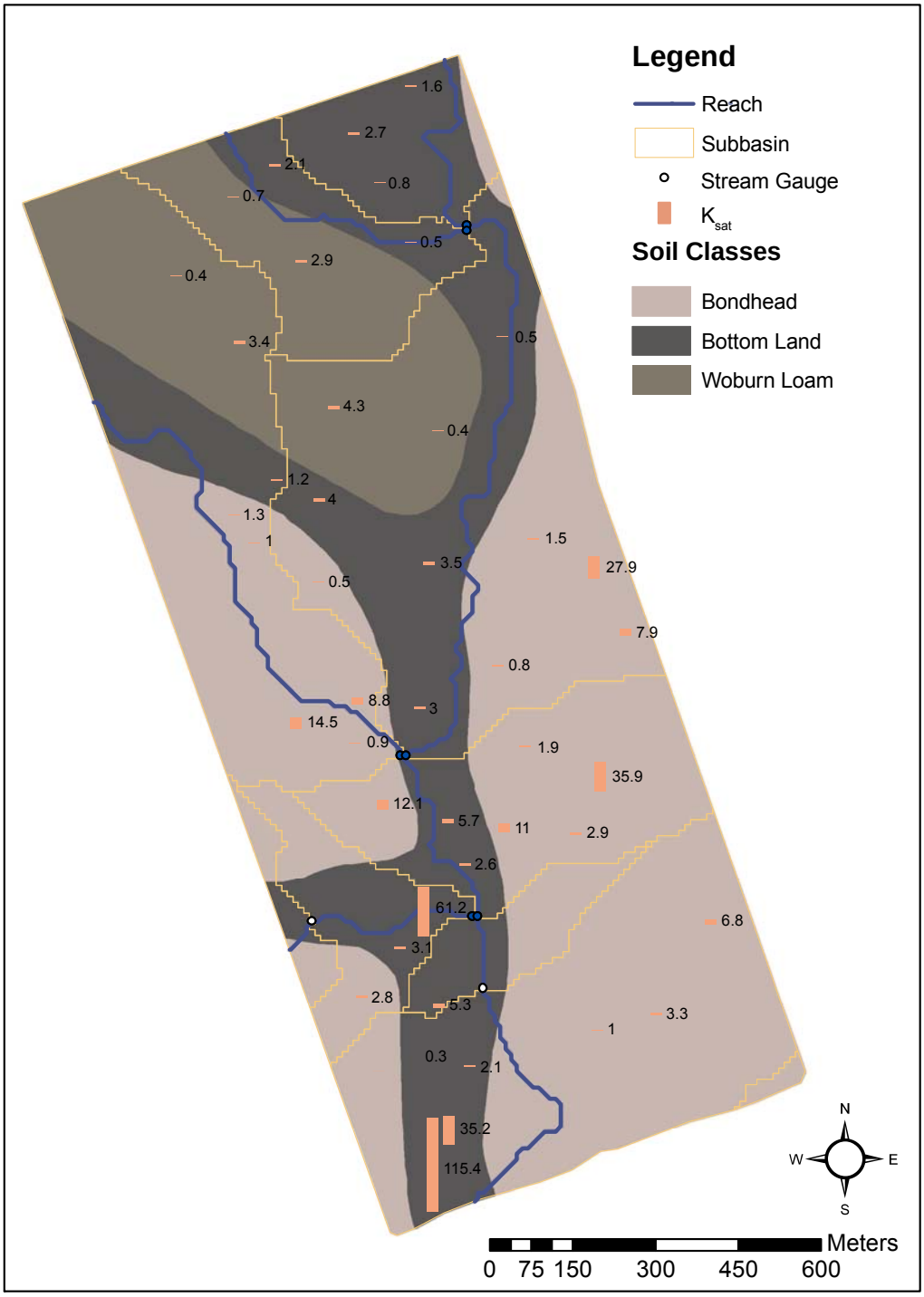

Figure 18. Spatial distribution of saturated hydraulic conductivity (K_{sat}) (mm/hr) calculated from Tension Infiltrometer measurements at Claremont study site.

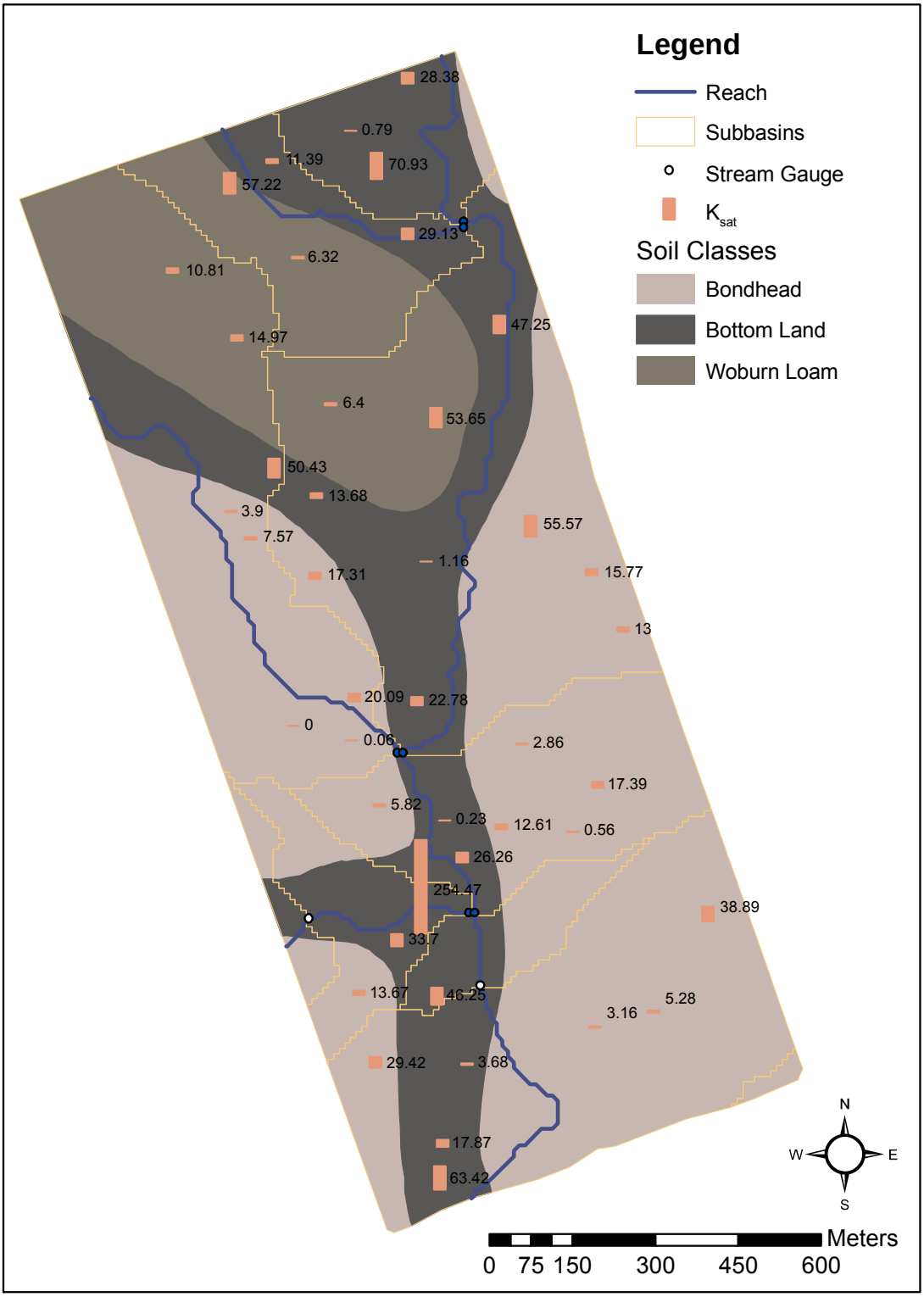

Figure 19. Spatial distribution of saturated hydraulic conductivity (K_{sat}) (mm/hr) calculated from Guelph Permeameter measurements at Claremont study site.

Database values of bulk density usually fall within or very close to the range of the field collected values with the exception of BDL4 and BTL4. However, field data show a range of variability that cannot be represented in the model if the single database value is used. Excluding BDL1, the database values fall towards the higher end of the field data range. Bulk density is seen to generally increase with depth for each soil type (Figure 21).

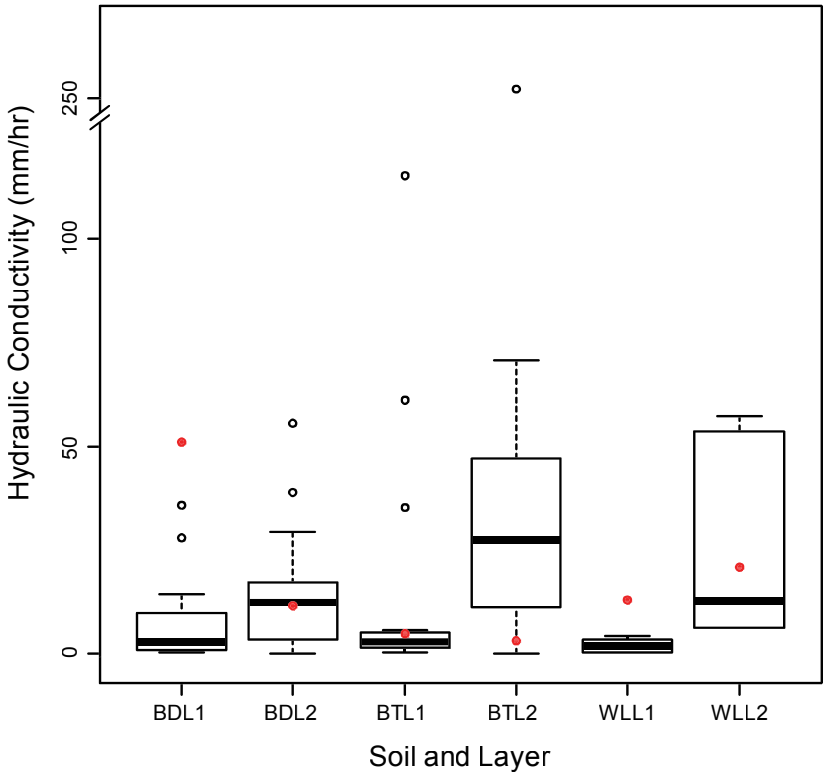

Figure 20. Distribution of field collected soil hydraulic conductivities for the first (L1) and second layer (L2) of the soil types Bondhead (BDL1, BDL2), Bottomland (BT1, BT2), and Woburn Loam (WLL1, WLL2). The single value recorded in the database for each soil layer is represented by the filled circle.

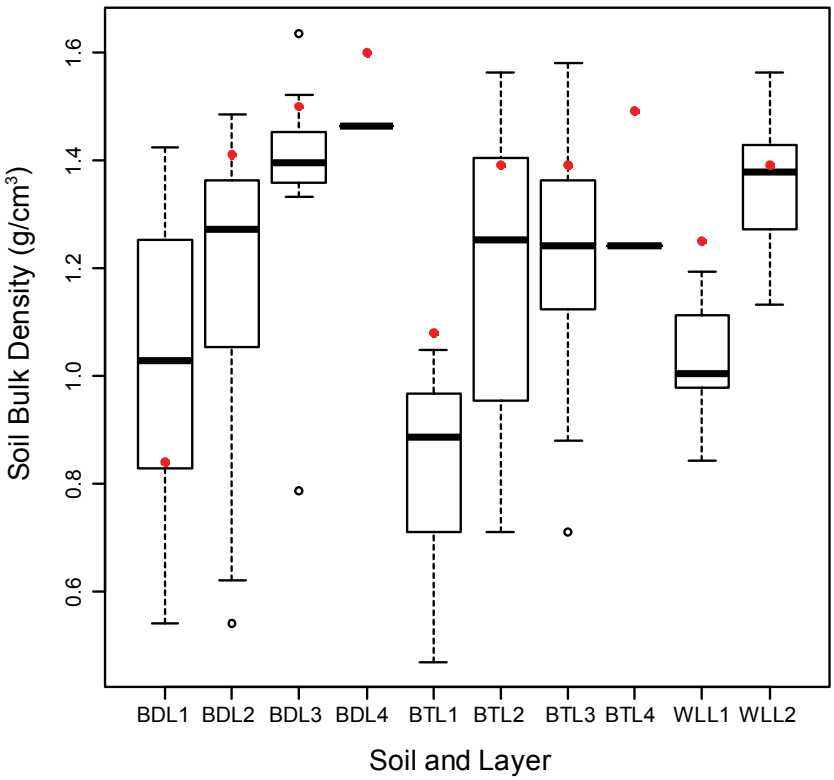

Figure 21. Distribution of field collected soil bulk density for the first four layers (L1–L4) of Bondhead (BD) and Bottomland (BT) and first two layers (L1–L2) for Woburn Loam (WL). The filled circles specify the single value recorded in the database for each soil layer.

Overall, CANMX values calculated from field measured LAI ranged from approximately 1 to 3.5. Variability in CANMX values is evident in both between and within LCLU types (Figure 22). For LCLU types FRSE, FRST, and WETF, the medians of CANMX ranges are comparable between the different instruments used (LAI–2000 vs. DHP). When comparing CANMX values for the 11 sites where both LAI–2000 and DHP were used, there is an indication of a strong positive correlation (Figure 23). A Pearson's correlation coefficient of 0.77 between the two data sets was calculated using Microsoft Excel's "CORREL" function. Agricultural land cover (AGRR) measured by the LAI–2000 and mixed forest land cover measured by the DHP have the greatest variability. It is important to note that PAST_H, PAST_L, and WETF_L have very low variability due to a limited number of samples taken. Database values were not included in along with field data as CANMX has a value of zero for every HRU.

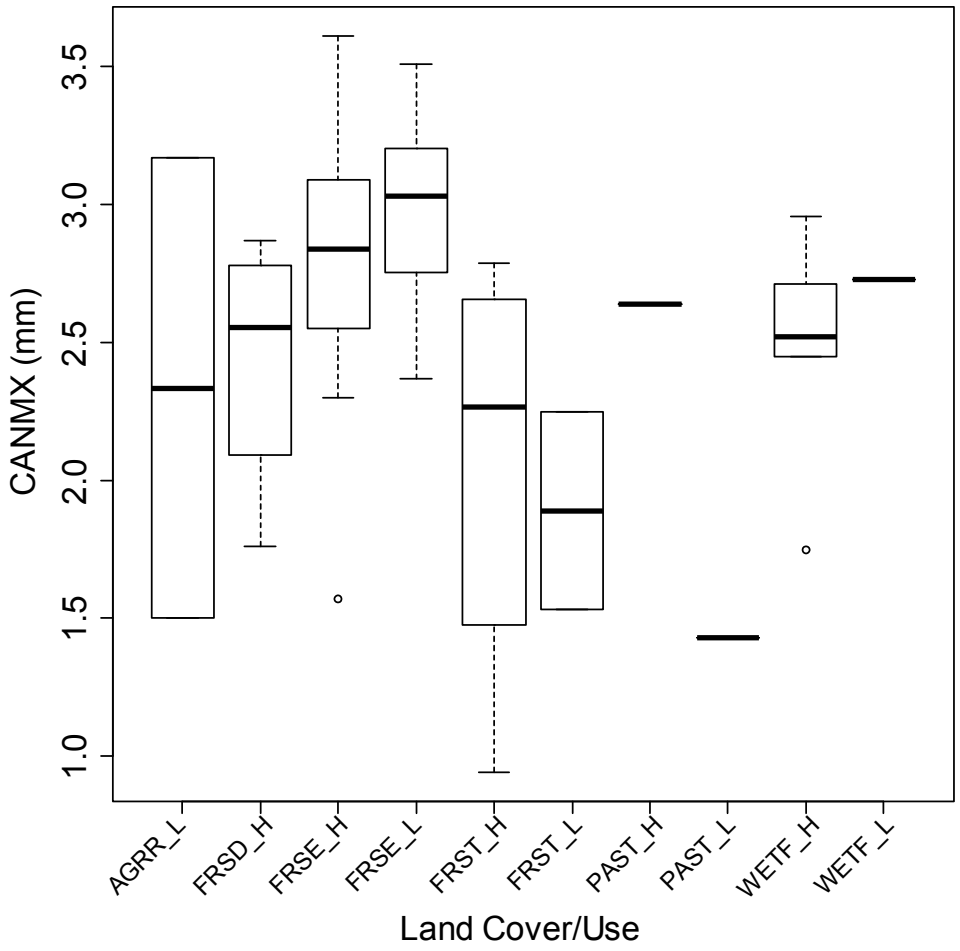

Figure 22. Distribution of maximum canopy storage (CANMX) for different land cover/ uses (AGRR: agriculture, FRSD: deciduous forest, FRSE: evergreen forest, FRST: mixed forest, PAST: pasture, WETF: forested wetland) calculated from field measured LAI using LAI–2000 (_L) and digital hemispherical photographs (_H).

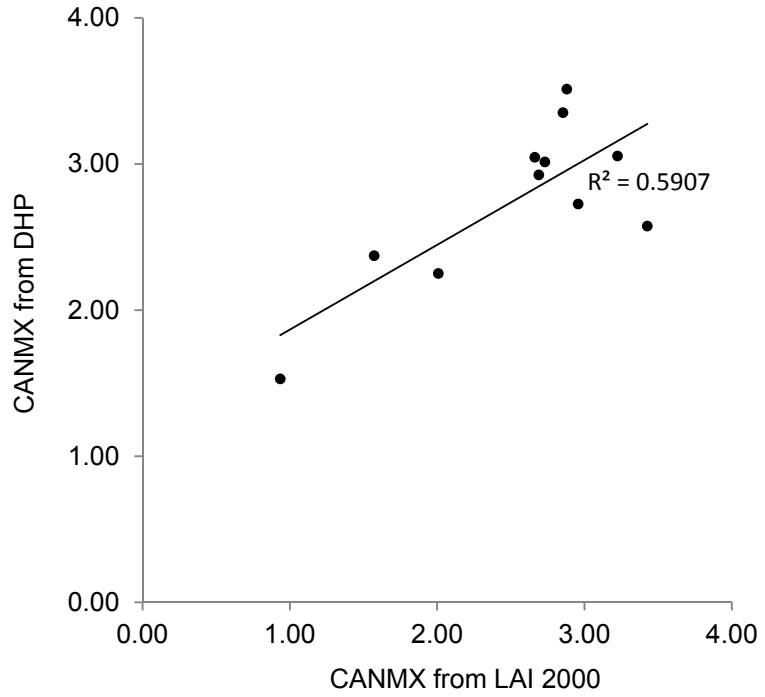

Figure 23. Scatter plot comparing CANMX values calculated from LAI measurements made by LAI–2000 and DHP shows a strong positive correlation. The Pearson's correlation coefficient between the two data set is 0.77.

3.3 Effect of Field Data on Calibration and Validation Processes

The effectiveness of field data on calibration and validation processes was firstly assessed based on bootstrapped RMSE calculations between the model and the measured stream flow. ANOVAs were used to check if the distribution of bootstrapped RMSE values were significantly different between model runs. RMSE was calculated 1000 times for each model run (Figure 24a-e). For each iteration a number of (250 for the calibration years 2006-2008 and 50 for the validation year 2010) random pairs of modeled and measured stream flow values are selected and evaluated for the RMSE. Selected pairs are returned into the full pool of paired values from which a random selection is drawn again; this process is continued 1000 times.

The first group of calibration models (Figure 24a) did not show the effectiveness of the field data in either calibration or validation processes. RMSE was evaluated for the full calibration period of 2006 and 2008 including days with flow out based on estimated as opposed to measured precipitation. Statistically, models 1–3 (CN models) are significantly different from models 4–7 (GA models) ($p<0.05$). However, there is no significant difference between models 1–3 or 4–7 based on whether field data is used or not (Table 10,Table 11). Between CN and GA runs, adding field data to locations where they were measured or applying it all upstream HRU combinations did not change the RMSE distribution from

the default calibrated model. Therefore, adding field data to either the CN or GA model did not affect the model response.

If only model outputs produced from measured precipitation records are used in the calibration and validation process and subsequently for the RMSE evaluation, a larger variation between the distribution of RMSE values is realized between and within the CN and GA models (Figure 24 b–e). From here on in, all other model comparisons are carried out with the exclusion of flow out records that were produced with estimated precipitation as opposed to measured precipitation. The RMSE was re-evaluated for the calibration group with this modification (Figure 24b). The median of RMSE distribution is slightly increased when field data is applied to CN runs. Calibration of GA model without any field data yielded RMSE values significantly greater than any of the CN model runs. However, the addition of field collected bulk density and soil hydraulic conductivity to the GA method, decreased the distribution of RMSE values to be significantly lower than all the CN model runs (Table 12 and 13). Performance of both CN and GA models did not benefit from application of field parameters to all upstream HRU combinations nor did GA model benefit from inclusion of CANMX values.

Adding field data to the validation process did not reduce RMSE values for CN or GA models (Figure 24c). In fact, validation with field data significantly increased the RMSE values for the CN model. There is a lack of differentiation between the default GA validated model and those with field data (Table 15). Nevertheless, all GA models have significantly lower RMSE values than the CN models (Table 15).

Without any calibration, GA method with field data has lower RMSE values than the CN models (with or without field data) (Figure 24d). However, GA models including CANMX (model 6) and applying all three parameters to all upstream HRU combinations (model 7) did not significantly differ from only applying Sol_K and BD where they were measured and to alike combinations within the subbasin (model 5) (Table 17). Interestingly, without field data, the uncalibrated GA model did not have a significantly different RMSE value from uncalibrated CN model (Table 17).

For the year 2010, when the models are not validated, adding field collected BD and Sol_K decreased RMSE values for both CN and GA models, with GA model medians lower than the CN (Figure 24e). Adding CANMX to the GA model in addition to Sol_K and BD did not significantly alter the RMSE distribution (Table 19). Applying the field collected parameters to all upstream HRU combinations resulted in the lowest RMSE value for GA method but did not cause any significant change to the CN model (Table 19).

For the calibration years (2006–2008) the uncalibrated models (Figure 24d) outperformed calibrated models (Figure 24b). However, uncalibrated models show a larger variability in RMSE values. For the validation year 2010, the comparison between models with and without validation slightly varies for CN and GA models. For CN method, the validated model without field data outperform all other 2010 CN models. However, while addition of field data with validation increased RMSE, adding field data without validation decreased RMSE values. These relationships hold true for GA method as well, but with

the exception that integrating field data to the validation processes did not increase RMSE values, but nor did it decrease them.

It appears that generally, the CN method has the potential to benefit from field data when no calibration or validation is carried out while GA method can benefit from field data in either circumstance. Both CN and GA exhibit lower RMSE values during validation year in comparison to the calibration years.

Table 9. Descriptions of the different model runs for calibration, validation, no calibration, and no validation scenarios.

Model Number	Description
1	Default Curve Number (CN) model
2	CN model with field collected bulk density (BD) and saturated soil hydraulic conductivity (Sol_K) applied to where they were measured
3	CN model with field collected bulk density (BD) and saturated soil hydraulic conductivity (Sol_K) applied to where they were measured and to all matching upstream HRU combinations
4	Default Green & Ampt (GA) model
5	GA model with field collected bulk density (BD) and saturated soil hydraulic conductivity (Sol_K) applied to where they were measured
6	GA model with field collected bulk density (BD), saturated soil hydraulic conductivity (Sol_K), and, maximum canopy storage (CANMX) applied to where they were measured
7	GA model with field collected bulk density (BD), saturated soil hydraulic conductivity (Sol_K), and, maximum canopy storage (CANMX) applied to where they were measured and to all matching upstream HRU combinations

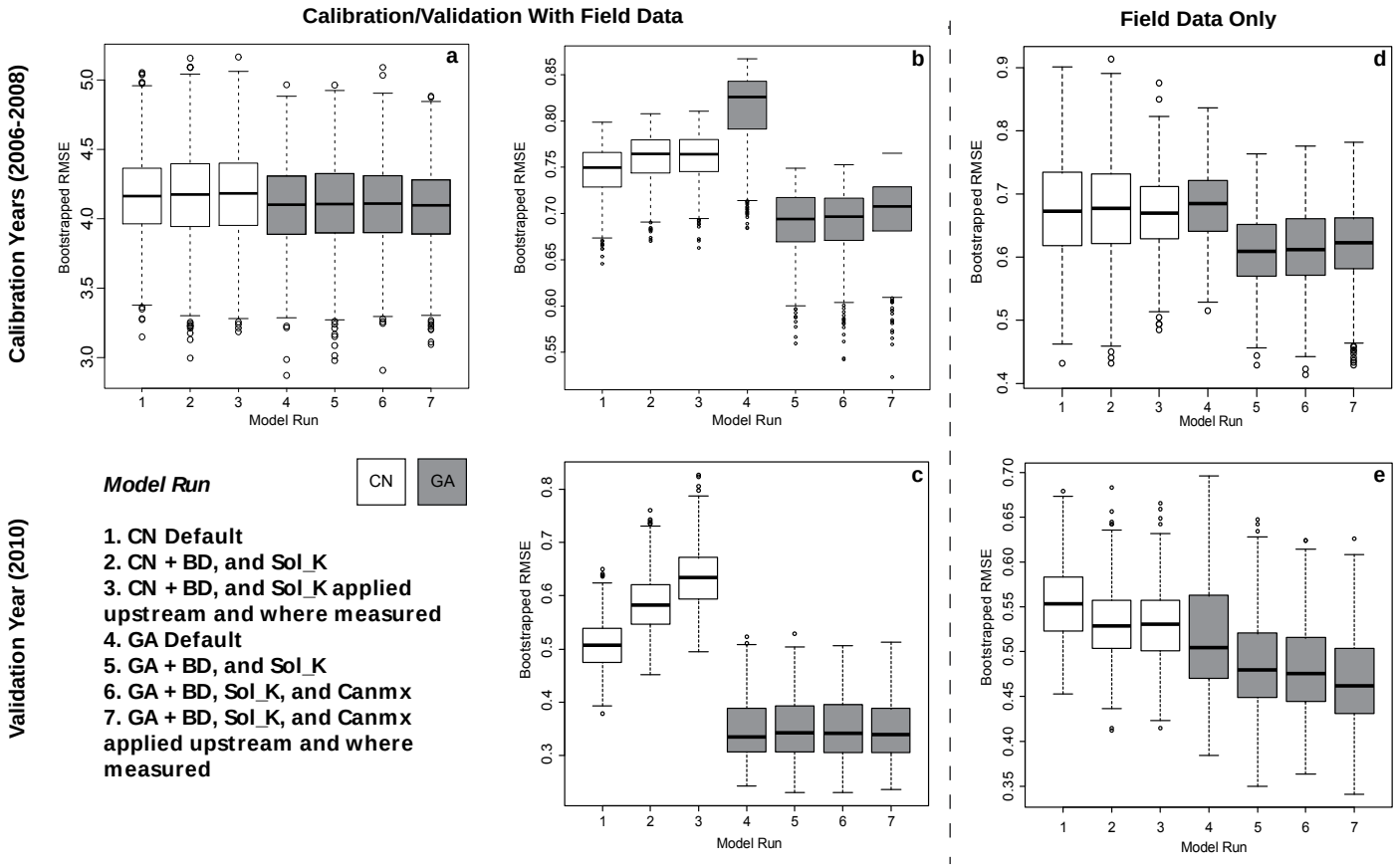

Figure 24. Bootstrapped RMSE for CN (runs 1–3) and GA (runs 4–7) a) calibrated models with field data, using the full record of modeled output; b) calibrated models with field data, using only modeled output records calculated from measured precipitation ; c) validated models with calibrated parameter values and field data, using only modeled output records calculated from measured precipitation; d) uncalibrated models, with and without field data for calibration years of 2006–2008, using only modeled output records calculated from measured precipitation; e) uncalibrated models, with and without field data for validation year of 2010, using only modeled output records calculated from measured precipitation .

Table 10. One–way ANOVA results for calibrated models (1-7) with all output records inclusive.

Source of Variation	*SS*	*df*	*MS*	*F*	*P-value*
Between Groups	7.9	6	1.3129	13.33	4.47E-15
Within Groups	683.9	6993	0.0985		

Table 11. Matrix of *p*–values from Post–Hoc Tukey multiple comparisons of means for calibrated models (1-7) with all output records inclusive. Bold values are significant at $p < 0.05$.

Model	1	2	3	4	5	6
1						
2	0.9986					
3	0.9878	1.0000				
4	**0.0007**	**0.0001**	**0.0000**			
5	**0.0004**	**0.0000**	**0.0000**	1.0000		
6	**0.0038**	**0.0005**	**0.0001**	0.9995	0.9981	
7	**0.0000**	**0.0000**	**0.0000**	0.9585	0.9781	0.7975

Table 12. One–way ANOVA results for calibrated models (1-7) excluding output records for days without measured rainfall data.

Source of Variation	*SS*	*df*	*MS*	*F*	*P-value*
Between Groups	12.737	6	2.123	2232	<2e-16
Within Groups	6.651	6993	0.001		

Table 13. Matrix of *p*–values from Post–Hoc Tukey multiple comparisons of means for calibrated models (1-7) excluding output records for days without measured rainfall data. Bold values are significant at $p < 0.05$.

Model	1	2	3	4	5	6
1						
2	**0.0000**					
3	**0.0000**	0.5690				
4	**0.0000**	**0.0000**	**0.0000**			
5	**0.0000**	**0.0000**	**0.0000**	**0.0000**		
6	**0.0000**	**0.0000**	**0.0000**	**0.0000**	0.9890	
7	**0.0000**	**0.0000**	**0.0000**	**0.0000**	**0.0000**	**0.0000**

Table 14. One–way ANOVA results for validated models (1-7) excluding output records for days without measured rainfall data.

Source of Variation	*SS*	*df*	*MS*	*F*	*P-value*
Between Groups	97.4	6	16.234	5865	<2e-16
Within Groups	19.36	6993	0.003		

Table 15. Matrix of *p*-values from Post–Hoc Tukey multiple comparisons of means for validated models (1-7) excluding output records for days without measured rainfall data. Bold values are significant at $p<0.05$.

Model	1	2	3	4	5	6
1						
2	**0.0000**					
3	**0.0000**	**0.0000**				
4	**0.0000**	**0.0000**	**0.0000**			
5	**0.0000**	**0.0000**	**0.0000**	0.5241		
6	**0.0000**	**0.0000**	**0.0000**	1.0000	0.5487	
7	**0.0000**	**0.0000**	**0.0000**	1.0000	0.6467	1.0000

Table 16. One–way ANOVA results for models 1-7 with field data only and no calibration for years 2006-2008.

Source of Variation	*SS*	*df*	*MS*	*F*	*P-value*
Between Groups	6.58	6	1.0975	242.1	<2e-16
Within Groups	31.69	6993	0.0045		

Table 17. Matrix of *p*-values from Post–Hoc Tukey multiple comparisons of means for models 1-7 with field data only and no calibration for years 2006-2008. Bold values are significant at $p<0.05$.

Model	1	2	3	4	5	6
1						
2	**0.0024**					
3	**0.0066**	1.0000				
4	0.9999	**0.0072**	**0.0184**			
5	**0.0000**	**0.0000**	**0.0000**	**0.0000**		
6	**0.0000**	**0.0000**	**0.0000**	**0.0000**	0.9586	
7	**0.0000**	**0.0000**	**0.0000**	**0.0000**	0.2773	**0.0224**

Table 18. One–way ANOVA results for models 1-7 with field data only and no validation, for the year 2010.

Source of Variation	*SS*	*df*	*MS*	*F*	*P-value*
Between Groups	5.68	6	0.9467	401.4	<2e-16
Within Groups	16.5	6993	0.0024		

Table 19. Matrix of *p*–values from Post–Hoc Tukey multiple comparisons of means for models 1-7 with field data only and no validation, for the year 2010. Bold values are significant at $p<0.05$.

Model	1	2	3	4	5	6
1						
2	**0.0000**					
3	**0.0000**	0.2417				
4	**0.0000**	**0.0000**	**0.0002**			
5	**0.0000**	**0.0000**	**0.0000**	**0.0000**		
6	**0.0000**	**0.0000**	**0.0000**	**0.0000**	0.3024	
7	**0.0000**	**0.0000**	**0.0000**	**0.0000**	**0.0000**	**0.0000**

3.4 Nash–Sutcliffe Efficiency versus Root Mean Square Error

The two statistics, NSE calculated in SWAT–CUP and RMSE median values calculated in R, used to compare model stream flow outputs to measured stream flow generally indicate the same relative order of model performances (Table 20). The exception are the calibration models (2006–2008) with stream flow records omitted for days without measured precipitation data. According to the NSE values, the CN models outperform all the GA models. However based on RMSE medians, the GA models with field data perform better than all CN models. Furthermore, NSE values for GA models suggest that there is a lack of influence of field data on model output. However, RMSE medians suggest that there is a notable difference between GA models with field data which works to improve performance. Regardless of the commonality between the relative ranking of model performance, NSE and RMSE values suggest different outcomes regarding modeling success. NSE values should be greater than 0 to establish that the calibrated/validated model is a better predictor of the hydrological response than the mean of the measured stream flow data (Krause et al. 2005). In our study, all of the models from the calibration procedure (with omitted results for days without measured precipitation) satisfy this standard. However, for the validation process only the GA models meet this standard while all other models have negative NSE values. RMSE values range from 0 to ∞ (0 being a perfect fit) and all of our models have RMSE medians of less than 5. Moreover, with the exception of the group of models calibrated with the full record of stream flow outputs, all other models have RMSE medians of less than 1.

Table 20. Nash–Sutcliffe Efficiency (NSE) and bootstrapped Root Mean Square Error (RMSE) median values for comparing daily modeled and measured stream flow for years 2006-2008 and 2010 with and without calibration/validation and field data.

	2006-2008						2010			
Model	Calibration and Field Data[a]		Calibration and Field Data[b]		Field Data Only[b]		Validation (Excluding Rainfall No Data Days)[b]		Field Data Only[b]	
	NSE	RMSE Median	NSE	RMSE Median	NSE	RMSE Median	NSE	RMSE Median	NSE	RMSE Median
1	-0.441	4.164	0.37	0.748	-0.29	0.684	-0.91	0.507	-1.25	0.55
2	-0.441	4.174	0.35	0.762	-0.26	0.672	-1.55	0.588	-1.08	0.533
3	-0.442	4.183	0.3	0.766	-0.24	0.673	-1.99	0.633	-1.07	0.525
4	-0.394	4.1	0.26	0.826	-0.29	0.681	0.08	0.341	-0.98	0.505
5	-0.396	4.105	0.26	0.695	-0.04	0.614	0.08	0.338	-0.73	0.48
6	-0.395	4.111	0.26	0.694	-0.04	0.611	0.08	0.34	-0.73	0.477
7	-0.393	4.098	0.25	0.707	-0.07	0.621	0.08	0.341	-0.63	0.465

[a] Full flow out record is used

[b] Days with "No Data" for precipitation are omitted

3.5 Graphical Comparisons of Model Responses

A few selected modeled responses were graphed with precipitation and measured stream flow to inquire if they compliment the statistical evaluations (Figure 25–27). PCP2031 and PCP2015 are rainfall data from their respective gauges. SWAT assigns each subbasin the closest rain gauge for precipitation input. PCP2015 and PCP2031 are assigned to 238 and 116 subbasins respectively. The subbasins within our Claremont study site are assigned PCP2015. For the year 2006, PCP2015 is indicated to have very long durations of "No Data" (Figure 25). As a result much of the precipitation falling on our study subbasins for the year 2006 is estimated based on the weather generator. Since the calibration process affects the entire watershed and not just the study subbasins, the decision was made to exclude records from calibration only if values were missing for both precipitation gauges. Calibrating the year 2006 despite the missing values from PCP2015 shows the effect of the weather generator and calibration on model output. There is a degree of agreement between the modeled storm flows (spikes) and the measured data, but there are still evidences of misalignment for days such as 2006/07/16, 2006/04/21, and 2006/06/01(Figure 25). Furthermore a number of storm flows are missed by the calibrated models between 2006/08/27–2006/09/24 (Figure 25). In comparison, modeled responses for years 2008 (Figure 26) and 2010 (Figure 27) which have measured precipitation for both rain gauges show a closer alignment with measured flow data.

For the calibration year of 2006 depicted in Figure 25, models 1 (calibrated CN without field data) and 4 (calibrated GA without field data) have very similar flow regimes. Although models 1 and 4 are evaluated to be significantly different by the post–hoc Tukey test (Table 13), the RMSE statistic included all 3 years of calibration (2006–2008) where as the graphs are depicting 1 year at a time; there is evidence of greater variability in flow amount between models 1 and 4 in 2008 (Figure 26). However, it is evident that model 5 (calibrated GA with field data) is better aligned with the measured flow data than both model 1 and 4 in years 2006 (Figure 25) and 2008 (Figure 26). In Figure 27, models 1 and 4 from group c (2010 validated CN and GA model without field data), and model 1 from group e (2010 default CN model without validation or field data) are presented. Comparing model 1 from both groups, one can gauge the effectiveness of validation on CN method for the year 2010. Even though improvement of model performance is small, there is certainly a decrease in the difference between modeled and measured data. However, it is evident that model 4 in group c (validated GA model with field data) is markedly better aligned with the measured data than the calibrated or uncalibrated CN method. However, in all three hydrographs (Figure 25-27), the onset of the models (immediately following winter months) do not have the baseflow aligned with the measured data.

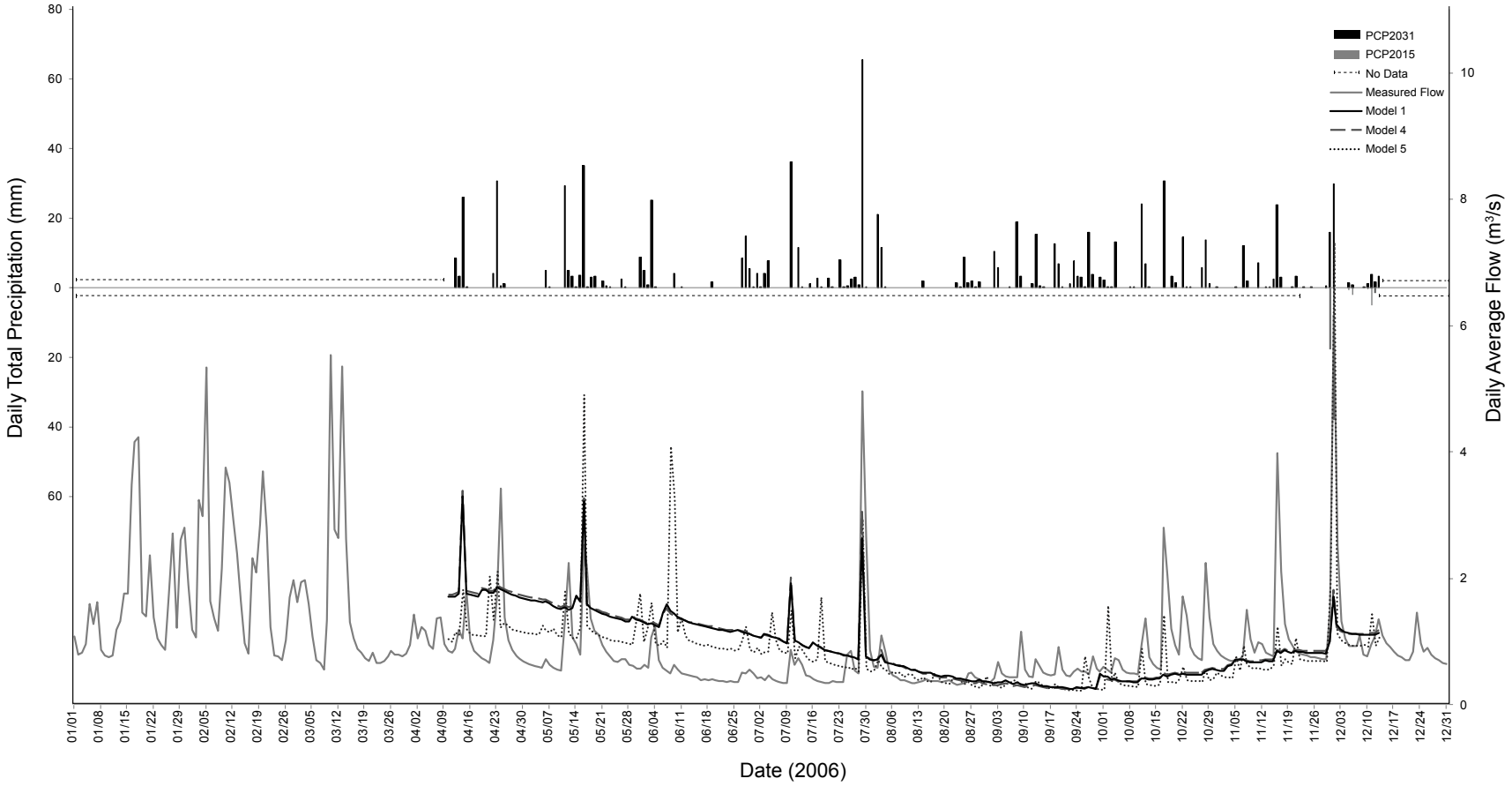

Figure 25. Precipitation, measured and calibrated model (1, 4, 5) flow out for the year 2006 with deleted records for days without measured precipitation (from both gauges).

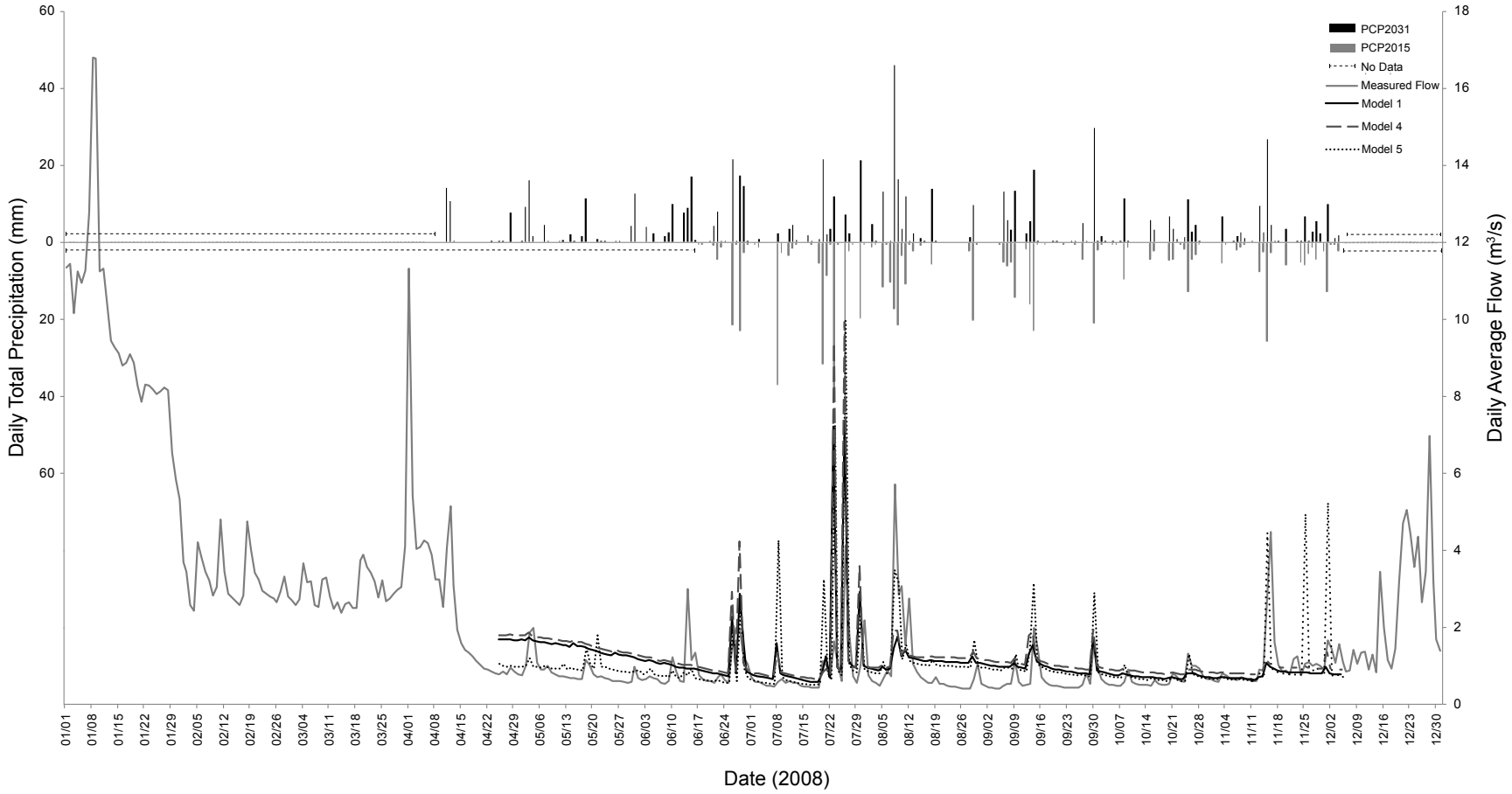

Figure 26. Precipitation, measured and calibrated model (1, 4, 5) flow out for the year 2008.

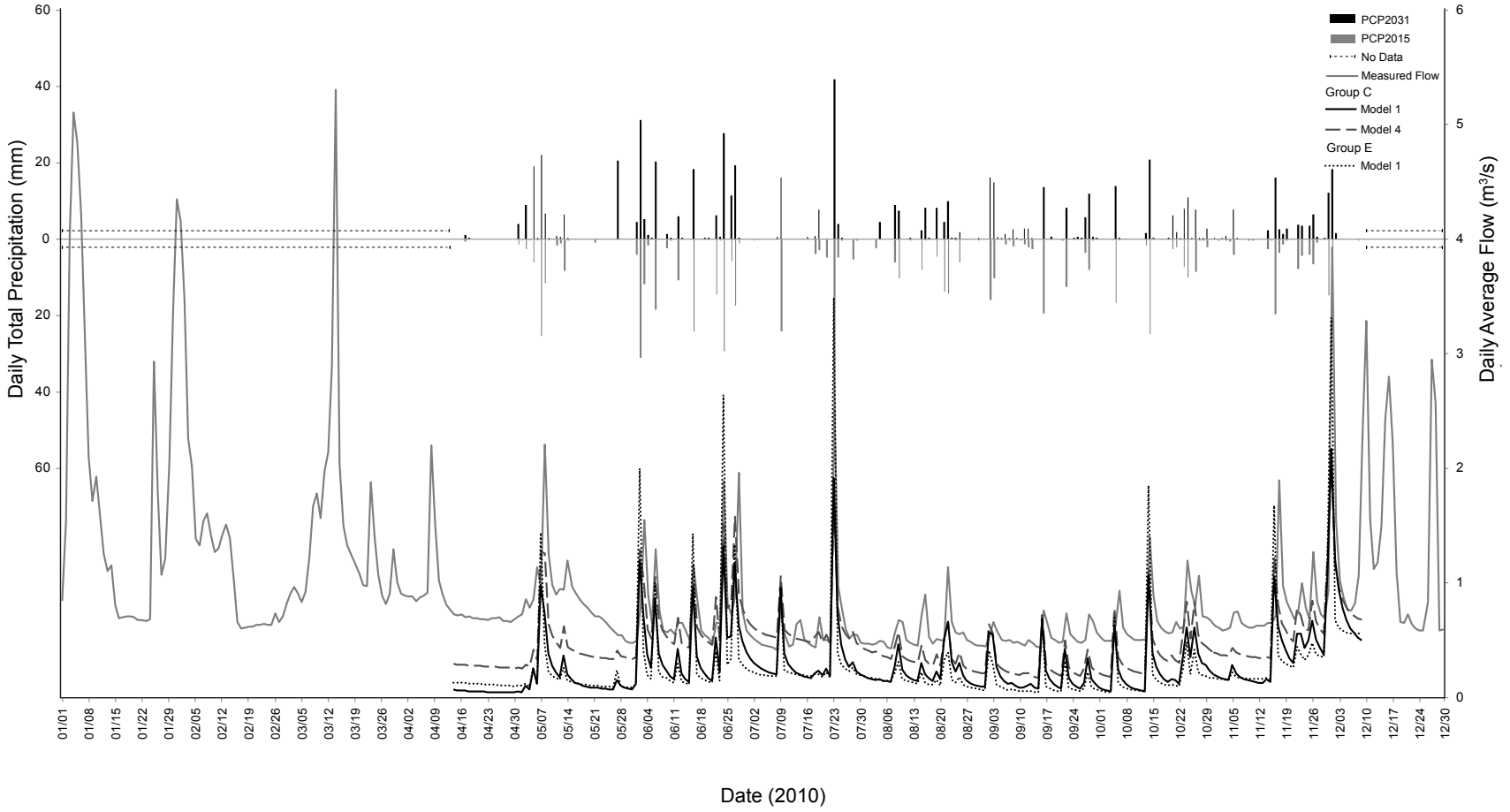

Figure 27. Precipitation, measured and model (Group C: Model 1 and Model 4, Group E: Model 1) flow out for the year 2010.

4. Discussion

4.1 Soil, Slope and LCLU

The empirical CN runoff method which correlates runoff to precipitation is based on the premise that the watershed has a slope of 5%. In Figure 17, it is evident that a large proportion of the Duffins watershed does not satisfy this premise. As infiltration and runoff are affected by the slope of the landscape, the empirical relationship does not hold true to the original experimental design from which the CN values are based on (Ebrahimian et al. 2012). This discrepancy may be a factor involved in poor model performance when using the CN method.

Generally, % slopes between 0–2 (~ 0–1.1°) are considered to be flat or nearly level, % slopes between 2–10 (~1.1–5°) are considered to be very gentle to gentle slopes, and % slopes between 10–30 (~5–16.5°) are moderate to strong slopes with anything greater to be very strong or steep slopes (Canada Agriculture and Agri-Food 1978). Therefore, slightly less than 2/3 of the Duffins Creek watershed (64%) can be described as having moderate to strong slopes, 1/4 of the watershed to be level or nearly level, and 12% of the watershed having gentle slopes. Huang et al. (2013) found that a slope gradient of 17% was optimal for infiltration and soil moisture storage. Following rainfall events, Huang et al. (2013) found the greatest soil moisture increase for 17% slope gradient followed by the 9% gradient, both which had twice as much soil moisture increase as the 27% and 36% gradients. The 17% gradient ranked optimal for infiltration as gentler slopes allow depositional soil crusts preventing infiltration while steeper slopes cause water to runoff faster (Huang et al. 2013). However, there have been contradicting conclusions on the influence of slope on infiltration (Fox et al. 1997), attributable to the local differences of soil type, texture and presence of aggregates. While there is a general expectation for infiltration to decrease as slope increases, the formation of rills on slopes can cause the reverse (Fox et al. 1997). As a result, this study is unable to establish the effect of topography on infiltration in the Duffins Creek watershed. However, the prominent soil classes found in Duffins watershed reduce runoff potential as the majority belong to hydrological soils groups A and B which have low runoff potential (Table 8). Furthermore, as only 12% of the watershed has been urbanized (Figure 15), this highly natural watershed can be expected to have substantial baseflow in its channels as a result of soil water recharge through infiltration and relatively high saturated hydraulic conductivities. The storm water response can also be expected to be dampened by that natural state of the watershed.

4.2 Setting Up the SWAT Model for Canadian Watersheds

Setting up the SWAT model for a Canadian watershed is certainly possible but requires custom built soil databases, weather generator, and hydrometeorological input and output data that are temporally aligned. The parameters required by the soil database listed in Table 5 is available through the Canadian Soil Information Service website with the exception of soil albedo and USLE soil erodibility

factor. The data to satisfy the SWAT model for GTA watersheds at a fine spatial resolution (DEM: 10 m, LCLU: 20 m, Soil: 25 m) and temporal resolution (hourly) is available but may need to be accessed through the appropriate conservation authority. Although it is available to the public at no cost, it is not always published online. Climate input and model output (i.e., flow, nutrients, sedimentation) are essential for proper model calibration and currently limits where models can be applied with confidence.

4.3 Importance of Precipitation Data

The importance of the integrity, density, and continuity of precipitation data to achieve satisfactional model output is unquestionable. There is much agreement that hydrological model output errors are associated especially with the lack of spatial variability of rainfall (Santhi et al. 2001). Although the Duffins watershed was chosen based on availability of hydro–meterological data, it was still not sufficient. There is a need for an increased density of this dataset within the GTA watersheds, including precipitation measurements during winter months. A lack of winter precipitation limits analysis of the spring melt process and disrupts the continuous soil moisture accounting scheme. As a result, the modeled baseflow at the onset of spring does not match the measured flow without calibration (Figure 25**,** Figure 27). Calibrating further with this misalignment of baseflow can lead to the over exaggeration of some other parameters leading to an overall poor fit between the observed and measured stream flow.

The weather generator functions on the basis of a mix of stochastic and statistical process that maybe sufficient for a single day of missing precipitation data but can be very misleading when used for months of continuous missing records as in the case of the year 2006 in our study (Figure 25). Any agreement between modeled and measured data can be likely attributed to the measured precipitation of PCP2031 gauge falling on roughly 33% of the watershed that it is assigned to and perhaps to the calibration process. However, the calibration process can be undermined by such long periods of estimated precipitation. Estimated precipitation from 2006 for the PCP2015 gauge can produce a flow regime much different from that of the measured record. During calibration, there is an attempt to match these two different regimes through the alteration of parameter values that may not reflect the physical basis of the watershed. Although a better fit might be achieved for the year 2006, the calibrated parameters may negatively affect the model response for the subsequent years. This is evident in Figure 23 b and d, as uncalibrated models outperformed calibrated models for both CN and GA methods. In addition, the stochastic nature of precipitation generation may produce very different precipitation values each time the model is run (i.e., running the model with different land use change scenarios) concealing the effect of the independent variable of interest (e.g., land use change). Thus, if SWAT is used for future predictions, a precipitation record should be created by the user instead of relying on the weather generator.

4.4 HRU Discretization

Although the HRU discretization is somewhat limiting compared to a fully distributed model, it is an acceptable compromise between discretization detail and model processing and calibration time. With more finer discretization, storage space to save outputs and time for model processes will increase (Arnold et al. 2010). Currently, even though HRUs do not have a spatial location, their effect on the hydrology can be viewed in terms of percentages of the subbasin with certain hydrologic properties attributed to the specific soil/LCLU/slope combination. Property developers in the GTA are asked to submit a stormwater management report for before and after development (City of Toronto 2010). It is evident that consultants hired to do such evaluations are using models such as Visual Otthymo (R.V. Anderson Associates Ltd. 2011) which is a single event hydrological model and is based on the SCS CN method (Clarifica 2009). It also addresses variability in the landscape hydrology as percentages of the landscape (i.e., percentage of pervious vs. impervious areas). SWAT has been discounted for some engineering applications due to the inability to model single events. Although calibrating a single event model is much easier, it can be misleading as shown in our results pertaining to the difference in calibration success based on the wetness or the dryness of the year. The difference can be attributed to the complexity of continuous soil moisture accounting scheme, which is not considered in a single event model. Such models then predict peak flows based on the theoretical CN at antecedent moisture condition I (dry), II (not wet and not dry), or III (wet) and neglects the continuous influence of previous precipitation events and/or antecedent soil moisture conditions affecting the storage capacity of the watershed area in question. This can lead to unrealistic estimation of storm water management requirements. Using the SWAT model on a continuous time scale incorporating hypothetical rainfall patterns (i.e., 100 year storms) can circumvent this problem. SWAT's responsiveness to LCLU change even at the subwatershed scale (Hernandez et al. 2000) makes it a useful model for predicting impact of future developments projected for the Durham region (growth to 1 million by 2021) (TRCA 2002b).

4.5 Field Data

Physically based distributed hydrological models can be instrumental in understanding the dynamic continuous hydrological response of a watershed. Although hydrological models have advanced to account for the spatial variability of a number of parameters, they are limited by the collection and/or the availability of such parameters as inputs (Dahlke et al. 2009). Spatial distribution of many parameters are dependent on province wide surveys of LCLU and soils. In such cases, the variability of parameters within a LCLU or soil type is unaccounted for. Changes in LCLU for purposes of development occur at a smaller scale where knowing the variability within the soil type or LCLU can render the model to become more representative of the study area.

Infiltration values from the field work show that not only does hydraulic conductivity vary within a soil type, but even from one layer to another (Figure 20). The lower infiltration rates/hydraulic conductivity measured for the surface layer can be attributed to soil crusts and/or compaction, both working to

constrain the amount of pathways for infiltrating water (Shen et al. 2009; Kodešová et al. 2010). The higher variability of hydraulic conductivity for the second soil layer is likely a result of more variability in soil structure and pore space (preferential pathways) (Carrick et al. 2010) (Figure 20). This variability is absent in the model if only database values from provincial soil surveys are used. In accordance with many other studies (Carvallo et al. 1976; Russo et al. 1997; Gupta et al. 2006), qualitatively, a correlation between hydraulic conductivity and soil type or watershed position could not be established; it remains as a parameter that is very much locally influenced (Figure 18-19). Physically based models utilize equations derived from homogenous systems (Beven 1989). However, our field work suggests that SWAT's default level of homogeneity (i.e., at the soil type or LCLU) for parameters such as Sol_K, bulk density and LAI is not sufficient. Although never fully satisfied, at a finer scale of an HRU, it becomes less of a gross assumption than at the soil type or LCLU level.

With the exception of BDL1 (Figure 20), most of the database values fall within or very near the distribution of field collected values. As a result, any increased performance from integration of hydraulic conductivity is not a result of using values very different from the database value, but the accounting of this spatial variability at soil type and possibly soil layer level. Unless modeling a fully saturated watershed (no more infiltration), Brath and Montanari (2000) advise that neglecting spatial variability of infiltration rates can accumulate significant error in the model response. Furthermore, this variability range from the field data can be used to set up calibration ranges for similar soil type/HRUs outside of the study subbasins. The discrepancy in hydraulic conductivity values for BDL1 could be the result of instrumentation used (systematic error) or differences in soil surface crusting/conditions (random error).

Similarly, systematic and random errors can help explain discrepancy between field measured bulk density and database values (Figure 21). With the exception of BDL1, the database values consistently fall towards the higher end of the field value range (Figure 21). This is likely caused by a systematic error, perhaps associated with the estimation of corer volume or in differentiating soil layers. Commonality between database and field values may become apparent for BDL4 and BTL4 with additional sampling that will reduce the random error of spatial uniqueness of soil structure. The increase in bulk density with depth is expected as surface layers are expected to be less dense (Frasier and Keiser 1993).

4.5.1 Hydraulic Conductivity: TI versus GP

Similar to this study, Kodešová et al. (2010) compare saturated hydraulic conductivities (K_{sat}) from both the TI and GP to find that GP values to be more variable than the TI and an order of magnitude higher. This order of magnitude difference can be seen in Bottomland and Woburn Loam soils in this study (Figure 20). However, Kodešová et al. (2010) attribute this disparity to the different instruments used while our study suggests the difference is also affected by the depth at which the instruments were used. They controlled for the influence of soil depth by taking measurements with the TI and GP at depths of 5 and 10 cm respectively (Kodešová et al. 2010). The TI measurements are not affected by the

soil crust and their field observation suggested that their soil is relatively homogenous from below the soil crust to a depth of 25 cm. Nevertheless, their conclusion of instrumental differences cannot be applied readily to our study as they only used one tension (-2 cm) for the TI and one pressure head (5 cm) for the GP to calculate the K_{sat}, which varies from our methods of calculation (3 tensions and 2 heads). In fact, using different theories or methods to evaluate raw data for hydraulic properties has been found to cause variability as large as those induced by scale, spatial and temporal variability (Fodor et al. 2011).

The TI is regarded to measure the K_{sat} of the soil matrix (excluding the macropores), where the GP allows preferential flow through macropores (Kodešová et al. 2010; Rienzner and Gandolfi 2014). The negative tension applied by the TI restricts flow through the large pores in the soil. As a result it has been reported that TI does not measure the true K_{sat} of the soil layer (Rienzner and Gandolfi 2014). Using mini tensiometers in conjunction with TI, Vandervaere et al. (1997) was able to evaluate saturated hydraulic conductivities for both the soil crust and the soil underlying it separately. They conclude that K_{sat} for the soil crust was three to six times lower than the soil underneath and that the pore size was significantly lower for the crust (reduced macropores). Since the TI was used for both depths, this eliminates the effect of the instrument and method used to evaluate K_{sat} and thereby supports our explanation of soil depths (particularly on the soil crust versus 30 cm below) to explain disparity in K_{sat} measurements between GP and TI. Furthermore, this outlines the importance of including the K_{sat} of the top layer of the soil (with the soil crust) in hydrological models as it will affect the initial infiltration rate (Carrick et al. 2010). In accordance with this study, Vandervaere et al. (1997) found improvement in model (Soil Vegetation Atmosphere Transfer model) hydrologic predictions when including K_{sat} evaluated by TI measurements of the soil surface. The TI remains to be a valuable instrument for this purpose and should be used in conjunction with the GP. Furthermore, since the TI restricts water flow through macropores, measurements for surface infiltration rates by the TI may offer more representative values for modeling purposes, which would otherwise be influenced by localized macropore structure. For future directions, TI and GP measurements should be compared controlling for soil depth as outlined in Kodešová et al. (2010) but by calculating saturated hydraulic conductivity as outlined in this study. Differences acknowledged in a large sample group can be implemented as calibrating range about the actual field measured value within SWAT–CUP parameterization scheme.

4.5.2 Leaf Area Index: DHP versus LAI-2000

The largest variability in CANMX was noted for agricultural row crops (AGRR–which is corn in our study) and mixed forest (deciduous and coniferous) (Figure 22). Since only the LAI–2000 was used for the AGRR land cover type, it is not certain if the variability is caused by the type of instrument used. One source of variability can be the different densities of planted crops or the leaf orientation at each site. A number of studies have looked at maximizing the productivity of corn by altering their leaf orientation and densities, and therefore a natural significant variation of this property can be expected between stands (Russell 1972; Vidovic 1974). It is conceivable that the mixed forest (deciduous and coniferous) land

cover type will have a larger range of values for CANMX from both instruments as each site will have a different proportion of deciduous and coniferous trees (Figure 22). Values from the DHP and LAI–2000 for the sites in common show good correlation along the 1:1 line (r = 0.77) (Figure 23). Due to the requirement of an open sky free from obstructions, it is difficult to use the LAI–2000 when amidst a dense tall canopy, but it functions well for open sky conditions available over grass fields, crops and sparse trees. Conversely, while the DHP can function under tall dense tree canopies, it requires that the vegetation not be too close to the lens of the camera such that it over predicts the canopy cover (i.e., a small leaf, close enough to the lens can shade a significant portion of it). When comparing measurements for FRSE and FRST land cover types, there is no consistent bias of over or under prediction by either instrument (Figure 22). Differences are likely due to random errors such as the slightly different position within the site where measurements were taken. Since a good correlation exists between these two instruments, they can be used together for their respective purposes. Chen et al. (1997) reported similar results of agreement between LAI values from hemispherical photographs (film as opposed to digital) and LAI-2000. Comparison at the point level showed some differences between the two instruments, which was attributed to the differences in placement of the two instruments under the canopy or the camera angle; these errors were balanced when comparing at the plot level (Chen et al. 1997). Nevertheless, measurements should be made with both instruments at sites where both instruments can be used (likely a site with access to open sky) to ensure a good correlation.

4.6 Calibration/Validation

In our study, flow records were omitted from calibration process only if precipitation data was missing for both gauges on that day. In retrospect, if sufficient number of records can be retained for the calibration and validation process, records should be omitted based on the data availability for the gauge associated with the subbasin of interest and those upstream of the study flow gauge. The precipitation gauge PCP2015 (input for the study subbasin and most of the upstream contributing subbasins) was missing data for most of the year 2006. This can be responsible for the slightly higher RMSE value for the 2006–2008 calibration year in comparison to the 2010 validation year (Figure 24).

The first group of calibration models (Figure 24a), for which the full 3 year record was used for calibration (including days with stream output response from weather generator's estimated precipitation) showed no effect of field data on the hydrological response. The significant difference between CN (models 1–3) and GA (models 4–7) models can be attributed to the inherent differences between the CN and GA methods of calculating runoff. Since excluding days without measured precipitation revealed the influence of field data thereafter (Figure 24b–e), it can be speculated that the error accumulated from long periods of estimated precipitation can outweigh the effect of field data. This may be the result of both the importance of precipitation in the model (Santhi et al. 2001) and the scale at which the two affect the model; spatially measured field data is only affecting 10 out of the 78 upstream subbasins that precipitation influences.

Validation RMSE values were lower than RMSE values for the calibration period. The calibration year however has three years of data while the validation year has only one. More years of simulation increases the opportunity for more errors between simulated and measured data (i.e., likely more occurrences of missed local precipitation events). Furthermore, the one year of validation (2010) has a better measured precipitation record in comparison to the year 2006 which is included in the calibration period (Figure 25). This also explains why the uncalibrated models (2006–2008) perform better than the calibrated models. That is, forcing a stream flow regime largely influenced by estimated precipitation (for most of 2006) to calibrate with the measured stream flow will exaggerate parameters beyond the bounds of representing the physical basis of the watershed and reduces the overall performance of the model. Inversely, if adequate data for calibration is present, calibration and validation process shows improvement in model performance; validated model for the year 2010 (Figure 24c) has lower RMSE value than the 2010 model that is not validated (Figure 24d).

In actuality, for reasons such as missing input or calibration data, there is a demand for models that can help predict the impact of land use change without calibration and validation (1985). This study demonstrates that when there is a lack of important input data like precipitation or if there is no measured historical data for calibration (i.e., stream flow), it is better not to calibrate the model. However, a study testing 28 surface hydrology models received less than satisfactory results when using models without calibration (1985). As an alternative, our study shows that adding field data such as hydraulic conductivity and bulk density to a model that is not calibrated can increase its performance at the sub–watershed level (Figure 24d). In such circumstances, we found the physically based GA method to benefit more and perform better with field data than the empirically based CN method (Figure 24d, e).

4.7 Effect of Field Data on Models

The benefits gained by either the GA or CN method from field measured BD and Sol_K can be linked to how these parameters are implemented within the model equations. Bulk density is used to estimate the porosity of the soil (Eq. (23)), which is required to calculate the change in volumetric moisture content across the wetting front (Eq. (21)), which is necessary for the total cumulative infiltration calculation at the end of each time step (Eq. (19)). However, these equations are only used in the GA method. The CN method lumps infiltration as part of the initial abstraction term I_a estimated to be 20% of the retention parameter S in the CN equation (Eq. (9), (11)). Bulk density is also used to calculate the wilting point of plants as a fraction of the total soil volume, which when added to the available water capacity (AWC), can determine the field capacity. The field capacity parameter is utilized in the above mentioned Eq. (21) to calculate the change in volumetric moisture content across the wetting front. Within the CN method, field capacity is used to calculate the shape factors w_1 (Eq. (13)) and w_2 (Eq.(14)) involved in solving for the retention parameter S. In both methods, field capacity defines the threshold of soil layer saturation, and when exceeded, triggers lateral flow of soil water. The field collected parameter K_{sat} (Sol_K) is used to calculate effective hydraulic conductivity (Eq. (20)), instantaneous (Eq. (17)) and

cumulative infiltration (Eq.(19)) when the GA method is used. For both CN and GA method it affects the redistribution of water laterally within the soil (i.e., net lateral flow discharge at the outlet), and the groundwater flow from storage to the channel as baseflow. Evidentially, both BD and Sol_K intrinsically affect the GA method more than the CN.

Even though the lateral movement of soil water is influenced by field parameters in the CN method, the actual partitioning of precipitation input into surface and subsurface water is affected by the collected field parameters only in the GA method. Since both CN and GA methods receive identical amounts of precipitation input, any difference in the hydrological response is a reflection of the partitioning of the precipitation input into the various components of the hydrological cycle (e.g., runoff vs. infiltration). As a result the spatially variable field parameters Sol_K and BD benefits the GA method more than the CN. Using field measured values for the CN model that controls the lateral movement of water (BD and Sol_K) without calibrating the partitioning of input precipitation may cause a hydrologic imbalance for the sub–watersheds. This imbalance could possibly explain the underperformance of the CN models when calibrated with field data (Figure 24b, c).

However, Figure 24e shows the potential benefit of field data on the CN model. Adding field data to the CN model for the year 2010 without validation is the only instance where field data increases the CN model performance. This suggests that for the CN model, the field data is causing an imbalance in the validation or calibration process. Since the field data plays different roles in the two methods, it can be possible that the imbalance is caused more so in the CN method and not for the GA. Perhaps if calibrated parameter ranges are reviewed and adjusted manually such that there is no interference between calibrated and field collected parameters, CN model can also see the benefits of field collected parameters.

The CANMX parameter calculated from field collected LAI values does not cause any significant change to the GA model response (Table 11,13,15,17,19). The parameter is used by SWAT to calculate the daily maximum precipitation that can be trapped in the canopy or the "maximum canopy storage" (Neitsch et al. 2011). Soil water is evaporated only once stored canopy water has been depleted (Neitsch et al. 2011). However, within SWAT, all HRUs by default have a value of zero for this parameter. It is unexpected that adding field collected values did not alter the model response in any way and is suspected that there may be an underlying issue of malfunctioning program code.

Implementation of field data into models has been rare due to either the inability to integrate field data, a lack of a clear framework, or the cost and labour involved. While the HRU discretization framework was effective in implementing field data in the SWAT model, cost and labour efficient methods need to be developed in order for modelers to adopt field data implementation, at least for the most influential parameters.

4.8 Measured Versus Simulated Hydrographs

There is evidence of misalignment in Figure 25 of storm flows as a result of missing precipitation in 2006. In other years with measured precipitation data, although the amplitudes for storm flows may differ between observed and modeled responses, the occurrences of storm flows match between the two. The difference in amplitude can be the result of inaccuracies of the amount of precipitation or improperly calibrated parameters. Sieck et al. (2007) reported 2-10% undercatch by rain gauges that are above ground in comparison to buried rain gauges at the ground surface. They advise that multiple rain gauges should be installed at a site to account for random errors of wind effect on rainfall catch (Sieck et al. 2007). We do see increased storm flow amplitudes with the addition of field collected BD and Sol_K (Figure 25-26), but this can be expected as field collected hydraulic conductivities for the first soil layer are generally lower than database values (Figure 20). As a result, less water is expected to infiltrate and more surface runoff will be generated, causing increased amplitudes in the hydrographs for storm flows (i.e., more storm water reaches the river quickly as opposed to slower infiltrated soil water pathway).

Graphically we see that for 2006 (Figure 25) and 2008 (Figure 26), calibrated GA and CN models without field data have similar hydrological response. However, for the 2010 (Figure 27), GA model has a very different response that better matches the measured stream flow regime. The difference seen between the CN and GA validated model is suspected to be in relation to the different baseflow levels proceeding the winter months; the GA model has baseflow starting much closer to the measured stream flow values, and from there matches the rest of measured flow regime much closer than the CN model. This stresses the importance of calibrating for both the baseflow and storm flow components of the hydrographs (Neitsch et al. 2002). It also shows that there are inherent difference between the CN and GA models but may only be brought out depending on the precipitation input regime. For future studies, when dealing with a lack of precipitation data, a two step calibration process can be followed manually to some extent. Calibrations should be run with the appropriate parameters to match base flows first and then subsequently be calibrated to match the storm runoffs (peaks).

4.9 Calibration Statistics: RMSE versus NSE

Generally, the efficiency criteria is based on the difference between the observed and simulated variable normalized by the variability in the observations (Krause et al. 2005). As a result, the efficiency parameter is predominantly influenced by larger differences that incur from high streamflow events. Attempts to minimize this difference in calibration results in better fitting of high flow events while lower flow events may be neglected (Krause et al. 2005). The NSE is reported to produce higher values (indicates better model performance) for catchments with higher dynamic flow (more peak flows), while an equivalent NSE value for a lower dynamic catchment will require a better fit (Krause et al. 2005). This disadvantage is caused by the squaring of the difference between the observed and predicted value. The use of RMSE as an objective function has also been reported to result in over fitting of the peaks, which miscalculates the soil moisture storage (Boyle et al. 2000). Objective functions that are sensitive towards

the dynamics of the hydrograph (i.e., RMSE and NSE) are less sensitive to systematic model over– or under–prediction (Krause et al. 2005). A systematic over– and under–prediction can be seen in 2008 (Figure 26) and 2010 (Figure 27) respectively. Model 1 from group E (un–calibrated CN model without field data) depicted in the 2010 hydrograph (Figure 27) shows that there was systematic under–prediction by the default CN model prior to calibration and model 1 from group C (calibrated CN model without field data) (Figure 27) shows that calibration was insensitive to this under–prediction. Nevertheless, the method and the parameters chosen for calibration is believed to also play a role in systematic adjustments.

Krause et al. (2005) tested a number of model evaluation criteria with different observed and predicted calibration scenarios. This includes both graphical and quantitative statistics, which was divided into three main categories: standard regression, dimensionless techniques, and error indices (Krause et al. 2005). There was found to be very little correlation between the various evaluation criteria, affirming the idea that different evaluation criteria were sensitive to different parts of the hydrograph. Some proved to be more sensitive to peak flows while others towards low flows (Krause et al. 2005). Criteria that seemed to be more global or in between, presented average values, never achieving desirable values.

Desirable values for the RMSE and NSE at the daily level has not been standardized. At the monthly time scale, NSE values greater than 0.5 are desirable, but suggestions for daily flow values have not been presented (Moriasi et al. 2007). It is likely that since the daily time scale has much more data points being compared, the evaluation criteria can be much more easily swayed by extreme values and not represent the overall goodness of fit. Although RMSE and NSE values for the models in our study have similar relative ranks, their values depict slightly different conclusion regarding model validity (Table 20). NSE values fall near zero and even below, suggesting that the average of the measured flow values serve as a better predictor of stream flow than the modeled response. The corresponding RMSE medians are less than 0.5 mm. In studies such as Singh et al. (2004) such RMSE values had corresponding NSE values that were greater than 0.8. Graphically we can see that at times, the average of the measured values would be preferred over the modeled response only because of the systematic over– and under–prediction, not because of the models ability to portray the dynamics of the system. As a result it is wise to follow advice of Legates and McCabe (1999) and include graphical, dimensionless statics (i.e., NSE), and error indices (i.e., RMSE) to evaluate the calibrated model. For this study it is believed that calibration needs to be carried out further, perhaps including phases of manual parameter changes to correct for systematic error.

Finally, there is an assumption that all error is within the predicted set but it is not necessarily always the case; stream gauges can malfunction causing error in measured data. In addition, although we eliminated days without measured rainfall from the calibration process so that the modeled output for that day is not matched with the measured, soil moisture will still be affected by the estimated rainfall input from those days and will influence hydrologic routing on subsequent days. In addition, the

importance of reliable and dense precipitation/ flow gauge data cannot be undermined by the calibration process. Furthermore, the need for field data should not be neglected by good evaluation criteria values. It must be noted that calibration can yield the same objective function values for a number of different parameter values. Therefore, parameter values assigned through calibration (i.e., hydraulic conductivity) may not reflect that locale, but can be offset by other errors in other locations. The problem arises when the model is used for location based analysis such as for impacts of land use change, where modeling of local parameters such as the hydraulic conductivity are fundamental for modeling real world scenario.

4.10 Extending Field Data to Other Subbasins

Field data sampling scheme should correspond with the structure and scale of the model (Beven and O'Connell 1982). This approach is carried out in our study by using the HRU discretization to choose sampling sites. This method provides a framework for applying measured values from representative sites to other areas of the watershed as suggested by Bathurst (1986) for cost and labour efficiency. In our study, when applying measured field data to the model, values were applied to the HRU where it was measured and to any identical HRU combination within the same subbasin. Separately, when also applied to matching HRUs existing outside of the subbasin (to all upstream occurrences) where the parameter was measured, the modeled response was mixed between neutral, increased and decreased performance (Figure 24). For the calibration years a neutral or decreased performance is evidenced, while a neutral or increased performance is witnessed in the validation year. An increased performance is evidenced only for the GA model without validation for the year 2010. The error involved with the lack of measured precipitation in the year 2006 may be obscuring the result for the calibration years. Local heterogeneities even among identical HRU combinations can also explain these neutral to decreased performances. In future studies, the extension of field measurements at representative sites to outside subbasins can be carried out by allowing a small window of calibration range (i.e., +/- 20%) about the measured values. HRUs where actual measurements were taken can be given that exact value without calibration.

5. Conclusions

1.) The SWAT hydrological model was primarily developed for watersheds in the United States. It contains databases for attributing model parameters based on soils, crops, and land cover/use (LCLU). Climate normal data already exists within accompanying databases with all the weather stations found in the US (used for predicting climate data for missing input values). However, SWAT allows users to add new entries to any of the databases provided all required parameters are satisfied. This allows SWAT to be implemented internationally. Crops and LCLU databases are generally inclusive of all the varieties found internationally. The soils layer provided by STATSGO at a spatial resolution of 1:250,000 is implemented into SWAT, but no other layers at finer resolutions. Using SWAT internationally, including in

Canada, requires users to build climate normal database for each weather station, hydro–climate data, and soils database if the soil layer is required to be at a finer resolution than 1:250,000.

2.) Using HRU discretization to pick sampling areas worked effectively to correspond field data spatially into the model. Furthermore, sampled data at a HRU can be extended to the same HRU combinations that occur within the subbasin. Therefore, to address issues of cost and time of field work, if only a limited number of samples can be taken, they should be taken at HRU combinations that cover the larger percentages of the subbasin. It is recommended that HRUs spanning large extents or occurring at multiple regions of the subbasin be sampled at more than one instance to account for localized variability. The effect of applying field collected values to HRUs outside of the subbasin it was collected in is inconclusive.

3.) A number of studies have compared in–situ saturated hydraulic conductivity from the TI and GP, but in practical application, this study finds such a comparison to be misguided. TI estimates saturated hydraulic conductivity for the top soil layer, and GP does not account for water movement through this top layer (used 30cm below the surface in a borehole). TI measurements showed less variability than GP, and generally, saturated hydraulic conductivity values of the top layer measured by the TI are smaller than those measured with GP for lower layers (2nd). However, the results cannot be distinguished as being the effect of instrumental precision or soil layer properties. In this study, the saturated hydraulic conductivity measured by TI and GP are successfully used in tandem, for the first and second layer respectively.

The various LAI measurement methods have their limitations. LAI–2000 requires a sampling of a clear view of the sky (for over–canopy measurements) that must stay consistent when taking the under–canopy readings. It is difficult to get over–canopy readings deep within a closed canopy forest or wooded lots. Digital hemispherical photographs can be utilized in these circumstances but cannot be used with short canopies, where LAI–2000 can be utilized effectively. To justify the complementation of the two methods, this study tested and found agreeable measures of LAI from both instruments for common sites (Pearson's correlation coefficient (r) of 0.77).

4.) SWAT's database is limited to representing spatial variability at the categorical level (i.e., by soil type or LCLU), but cannot account for variability within each category. With the exception of few, database values for bulk density and hydraulic conductivity fell within or near the range of field collected values, with some falling right at the median.

5.) Field collected parameters can be easily implemented into SWAT using either the ArcSWAT database editor or as in our study, through SWAT–CUP parameterization scheme. Field collected values are applied to their respective locations by specifying the subbasin and LCLU/soil/slope combinations. However, because specification by soil type is not available in SWAT-CUP (only by soil texture is possible) a work around must be implemented by assigning arbitrary unique values to soil textures for each soil type, so that parameters can be altered at the HRU level.

6.) If calibration or validation is not carried out (i.e., due to lack of truth data for calibration/validation), adding in–situ hydraulic conductivity and bulk density proved to markedly improve performance for CN method during the validation year and during the calibration and validation years for the GA method. Effect of CANMX and applying field data to all upstream combinations remain inconclusive. Field data does not improve CN method during calibration or validation, which is likely due to the lack of integration of the field collected values into the CN method. GA method is significantly improved with field data during calibration years, but not during validation years. It appears contrary to popular conclusion, that GA can outperform CN when modeling at the subbasin scale with field collected hydraulic conductivity and bulk density.

7.) This project presents two points on the spectrum of hydrological modeling endeavors: empirical (CN) vs. physically based (GA). In both cases, past historical responses to input are used to predict the future. Although, no approach is completely physically based, that is, even physically based approaches have assumptions of ideal situations and even empirically derived coefficients, this study suggests they can outperform the empirical CN based method if used correctly. If physically based models are not satisfied correctly (i.e., using a single hydraulic value for a soil type no matter where it occurs) it can lead to poor performance as many have noted in literature regarding their experience using the GA method. An attempt must be made to satisfy physically based models with physically measured parameters before they can be fairly compared to empirical methods.

Many hydrological modelers are not opting for physically based distributed models for watershed analysis due to the higher number of parameters that need to be satisfied. Furthermore, those that do use these models are only considering the heterogeneity of the parameters at a very coarse scale (i.e., at the LCLU or soil class level). The HRU discretization method of the SWAT hydrological model offers a viable framework for field collection of parameters to account for this heterogeneity at a finer scale and has shown to significantly improve validity of the model when the physically based runoff method (GA) is utilized. The framework presented in this thesis is labour intensive, but it is required to have some confidence that the parameterized model is in fact representing the physical processes at work in the watershed. Following this framework will be difficult if governing bodies of watersheds continue to depend on external consultants to provide watershed analysis. It is unrealistic to follow this framework for an entire watershed as part of a smaller study due to issues of time and expense. Ideally, the governing bodies themselves should continue to collect field data of important parameters over the years as the landscape changes and update their models. Moreover, the importance of dense and strategic gauging of precipitation and stream flow will become apparent with this undertaking by the governing body.

6. References

Abbaspour K.C. (2012) SWAT-CUP 2012: SWAT Calibration and Uncertainty Programs-A user manual. 103.

Abbaspour K.C., Johnson C.A., and van Genuchten M. (2004) Estimating Uncertain Flow and Transport Parameters Using a Sequential Uncertainty Fitting Procedure. *Vadose Zone Journal*, **3**, 1340–1352.

Abbaspour K.C., Yang J., Maximov I., Siber R., Bogner K., Mieleitner J., Zobrist J., and Srinivasan R. (2007) Modelling hydrology and water quality in the pre-alpine/alpine Thur watershed using SWAT. *Journal of Hydrology*, **333**, 413–430.

Abbott M., Bathurst J., and Cunge J. (1986) An introduction to the European Hydrological System—Systeme Hydrologique Europeen,"SHE", 1: History and philosophy of a physically-based, distributed modelling system. *Journal of Hydrology*, **87**, 45–59.

Achouri M. and Gifford G.F. (2013) Spatial and seasonal variability of field measured infiltration rates on a rangeland site in Utah. *Journal of Range Management*, **37**, 451–455.

Allen R., Jensen M., Wright J., and Burman R. (1989) Operational estimates of reference evapotranspiration. *Agronomy Journal*, **81**, 650–662.

Allen R.G. (1986) A Penman for all seasons. *Journal of Irrigation and Drainage Engineering*, **112**, 348–368.

Anderson M.C. (1964) Studies of the woodland light climate: I. The photographic computation of light conditions. *The Journal of Ecology*, **52**, 27.

Arnold J., Allen P., and Volk M. (2010) Assessment of different representations of spatial variability on SWAT model performance. *Transactions of the American Society of Agricultural and Biological Engineers*, **53**, 1433–1443.

Arnold J., Kiniry J., Srinivasan R., Williams J., Haney E., and Neitsch S. (2011) Soil and Water Assessment Tool: input/output file documentation version 2009, technical report No. 365. 662.

Arnold J., Srinivasan R., Muttiah R., and Allen P. (1999) Continental scale simulation of the hydrologic balance. *Journal of the American Water Resources Association*, **35**, 1037–1051.

Arnold J.G. and Allen P.M. (1996) Estimating hydrologic budgets for three Illinois watersheds. *Journal of Hydrology*, **176**, 57–77.

Arnold J.G., Allen P.M., and Bernhardt G. (1993) A comprehensive surface-groundwater flow model. *Journal of Hydrology*, **142**, 47–69.

Arnold J.G. and Fohrer N. (2005) SWAT2000: current capabilities and research opportunities in applied watershed modelling. *Hydrological Processes*, **19**, 563–572.

Arnold J.G., Srinivasan R., Muttiah R.S., and Williams J.R. (1998) Large area hydrological modeling and assessment. Part I: Model development. *Journal of the American Water Resources Association*, **34**, 73–89.

Bathurst J. and Cooley K. (1996) Use of the SHE hydrological modelling system to investigate basin response to snowmelt at Reynolds Creek, Idaho. *Journal of Hydrology*, **175**, 181–211.

Bathurst J.C. (1986) Physically-based distributed modelling of an upland catchment using the Systeme Hydrologique Europeen. *Journal of Hydrology*, **87**, 79–102.

Beven K. (1989) Changing ideas in hydrology—the case of physically-based models. *Journal of Hydrology*, **105**, 157–172.

Beven K. (1993) Prophecy, reality and uncertainty in distributed hydrological modelling. *Advances in Water Resources*, **16**, 41–51.

Beven K. and Binley A. (1992) The future of distributed models: model calibration and uncertainty prediction. *Hydrological Processes*, **6**, 279–298.

Beven K. and Freer J. (2001) Equifinality, data assimilation, and uncertainty estimation in mechanistic modelling of complex environmental systems using the GLUE methodology. *Journal of Hydrology*, **249**, 11–29.

Beven K. and O'Connell P. (1982) On the role of physically-based distributed modelling in hydrology. 40.

Beven K.J. (1985) Distributed models. *Hydrological forecasting* (ed. by M. Anderson and T. Burt), pp. 604. Wiley, New York.

Beven K.J. (2000) *Rainfall-runoff modelling : the primer.* J. Wiley, New York.

Bicknell B., Imhoff J., Jr. Kittle J., Jr. Donigian A., and Johanson R. (1997) Hydrological Simulation Program-Fortran: user's manual for version 11: U.S. Environmental Protection Agency. 755.

Blackie J. and Eeles C. (1985) Lumped catchment models. *Hydrological forecasting* (ed. by M. Anderson and T. Burt), pp. 311–345. John Wiley and Sons, Chichester.

Bosch D.D., Sheridan J.M., Batten H.L., and Arnold J.G. (2004) Evaluation of the SWAT model on a coastal plain agricultural watershed. *Transactions of the American Society of Agricultural and Biological Engineers*, **47**, 1493–1506.

Bouraoui F., Galbiati L., and Bidoglio G. (2002) Climate change impacts on nutrient loads in the Yorkshire Ouse catchment (UK). *Hydrology and Earth System Sciences*, **6**, 197–209.

Bouwer H. (1969) Infiltration of water into nonuniform soils. *Journal Irrigation and Drainage Division*, **95**, 451–462.

Boyle D.P., Gupta H. V., and Sorooshian S. (2000) Toward improved calibration of hydrologic models: Combining the strengths of manual and automatic methods. *Water Resources Research*, **36**, 3663–3674.

Boyle D.P., Gupta H. V., Sorooshian S., Koren V., Zhang Z., and Smith M. (2001) Toward improved streamflow forecasts: value of semidistributed modeling. *Water Resources Research*, **37**, 2749–2759.

Brath A. and Montanari A. (2000) The effects of the spatial variability of soil infiltration capacity in distributed flood modelling. *Hydrological Processes*, **14**, 2779–2794.

Bréda N.J.J. (2003) Ground-based measurements of leaf area index: a review of methods, instruments and current controversies. *Journal of Experimental Botany*, **54**, 2403–17.

Canada Agriculture and Agri-Food (1978) Soil phase. *The Canadian system of soil classification* (ed. by R.. Haynes), pp. 187. National Research Council of Canada, Ottawa.

Carrick S., Almond P., Buchan G., and Smith N. (2010) In situ characterization of hydraulic conductivities of individual soil profile layers during infiltration over long time periods. *European Journal of Soil Science*, **61**, 1056–1069.

Carvallo H., Cassel D., Hammond J., and Bauer A. (1976) Spatial variability of in situ unsaturated hydraulic conductivity of Maddock sandy loam. *Soil Science*, **121**, 1–8.

Chaplot V. (2005) Impact of DEM mesh size and soil map scale on SWAT runoff, sediment, and NO3–N loads predictions. *Journal of Hydrology*, **312**, 207–222.

Chaplot V., Saleh A., and Jaynes D. (2005) Effect of the accuracy of spatial rainfall information on the modeling of water, sediment, and NO3–N loads at the watershed level. *Journal of Hydrology*, **312**, 223–234.

Chapman L. and Putnam D. (1984) *The physiography of Southern Ontario.* Ontario Ministry of Natural Resources, Toronto.

Chen E. and Mackay D.S. (2004) Effects of distribution-based parameter aggregation on a spatially distributed agricultural nonpoint source pollution model. *Journal of Hydrology*, **295**, 211–224.

Chen J.M., Black T.A., and Adams R.S. (1991) Evaluation of hemispherical photography for determining plant area index and geometry of a forest stand. *Agricultural and Forest Meteorology*, **56**, 129–143.

Chen J.M., Govind A., Sonnentag O., Zhang Y., Barr A., and Amiro B. (2006) Leaf area index measurements at Fluxnet-Canada forest sites. *Agricultural and Forest Meteorology*, **140**, 257–268.

Chen J.M., Rich P.M., Gower S.T., Norman J.M., and Plummer S. (1997) Leaf area index of boreal forests: Theory, techniques, and measurements. *Journal of Geophysical Research*, **102**, 29429–29443.

CHESS (2001) Climate, Hydrochemistry and Economics of Surface-water Systems. *nwl.ac.uk*, 1–32.

Cho J., Barone V.A., and Mostaghimi S. (2009) Simulation of land use impacts on groundwater levels and streamflow in a Virginia watershed. *Agricultural Water Management*, **96**, 1–11.

Chow V. Te (1964) *Handbook of applied hydrology : a compendium of water- resources technology.* McGraw-Hill, New York.

City of Toronto (2010) Stormwater management report: terms of reference. 6.

Clarifica (2009) Visual OTTHYMO user's guide. 111.

Conan C., Bouraoui F., Turpin N., De Marsily G., and Bidoglio G. (2003) Modeling flow and nitrate fate at catchment scale in Brittany (France). *Journal of Environmental Quality*, **32**, 2026–2032.

Cotter A., Chaubey I., Costello T., Soerens T., and Nelson M. (2003) Water quality model output uncertainty as affected by spatial resolution of input data. *Journal of the American Water Resources Association*, **39**, 977–986.

Crawford N. and Linsley R. (1966) Digital simulation in hydrology: Stanford Watershed Model IV, technical report 39. 187.

Cutini A., Matteuci G., and Mugnozza G. (1998) Estimating of leaf area index with the Li-Cor LAI 2000 in deciduous forests. *Forest Ecology and Management*, **105**, 55–65.

Dahlke H., Behrens T., Seibert J., and Anderson L. (2009) Test of statistical means for the extrapolation of soil depth point information using overlays of spatial environmental data and bootstrapping techniques. *Hydrological Processes*, **23**, 3017–3029.

Davie T. (2008) *Fundamentals of hydrology.* Routledge, New York.

Deblonde G., Penner M., and Royer A. (1994) Measuring leaf area index with Li-Cor LAI-2000 in pine stand. *Ecology*, **75**, 1507–1511.

Delta-T devices (1999) Theta Probe soil moisture sensor, version ML2x-UM-1.21: user manual. 22.

Delta-T devices (2005) User manual for the HH2 moisture meter version 4. 117.

Dingman L. (2002) *Physical hydrology.* Prentice Hall, Upper Saddle River.

Dufrene E. and Breda N. (1995) Estimation of deciduous forest leaf area index using direct and indirect methods. *Oecologia*, **104**, 156–162.

Ebrahimian M., Nuruddin A., Mohd Soom M., Mohd Sood A., and Neng L. (2012) Runoff estimation in steep slope watershed with standard and slope-adjusted curve number methods. *Polish Journal of Environmental Studies*, **21**, 1191–1202.

Efron B. (1981) Nonparametric estimates of standard error: the jackknife, the bootstrap and other methods. *Biometrika*, **68**, 589.

Fairfield J. and Leymarie P. (1991) Drainage networks from grid digital elevation models. *Water Resources Research*, **27**, 709–717.

Flanagan D., Gilley J., and Franti T. (2007) The USDA water erosion prediction project (WEPP): development history, model capabilities, and future enhancements. *Transactions of the American Society of Agricultural and Biological Engineers*, **50**, 1603–1612.

Fodor N., Sándor R., Orfanus T., Lichner L., and Rajkai K. (2011) Evaluation method dependency of measured saturated hydraulic conductivity. *Geoderma*, **165**, 60–68.

Fox D., Bryan R., and Price A. (1997) The influence of slope angle on final infiltration rate for interrill conditions. *Geoderma*, **80**, 181–194.

Frasier G.W. and Keiser J. (1993) Thin layer measurement of soil bulk density. *Journal of Range Management*, **46**, 91–93.

Freeze R. (1980) A stochastic-conceptual analysis of rainfall-runoff processes on a hillslope. *Water Resources Research*, **16**, 391–408.

Freeze R. and Harlan R. (1969) Blueprint for a physically-based, digitally-simulated hydrologic response model. *Journal of Hydrology*, **9**, 237–258.

Gardner W. (1958) Some steady-state solutions of the unsaturated moisture flow equation with application to evaporation from a water table. *Soil Science*, **85**, 228–232.

Gassman P., Osei E., Saleh A., and Hauck L. (2002) Application of an environmental and economic modeling system for waterhsed assessments. *Journal of the American Water Resources Association*, **38**, 423–438.

Gassman P., Reyes M., Green C., and Arnold J. (2007) The soil and water assessment tool: historical development, applications, and future research directions. *Transactions of the American Society of Agricultural and Biological Engineers*, **50**, 1211–1250.

Gosain A., Rao S., and Basuray D. (2006) Climate change impact assessment on hydrology of Indian river basins. *Current Science*, **90**, 346–353.

Gower S. and Norman J. (1991) Rapid estimation of leaf area index in conifer and broad leaf plantations. *Ecology*, **72**, 1896–1900.

Gower S.T., Kucharik C.J., and Norman J.M. (1999) Direct and indirect estimation of leaf area index , f APAR , and net primary production of terrestrial ecosystems. *Remot Sensing of Environment*, **70**, 29–51.

Grayson R.B., Moore I.D., and McMahon T.A. (1992) Physically based hydrologic modeling: 1. A terrain-based model for investigative purposes. *Water Resources Research*, **28**, 2639–2658.

Green W. and Ampt G. (1911) Studies on soil physics Part I - The flow of air and water through soils. *Journal of Agricultural Science*, **4**, 1–24.

Grizzetti B., Bouraoui F., and De Marsily G. (2005) Modelling nitrogen pressure in river basins: A comparison between a statistical approach and the physically-based SWAT model. *Physics and Chemistry of the Earth, Parts A/B/C*, **30**, 508–517.

Gupta N., Rudra R., and Parkin G. (2006) Analysis of spatial variability of hydraulic conductivity at field scale. *Canadian Biosystems Engineering*, **48**, 55–62.

Gupta V. and Waymire E. (1983) On the formulation of an analytical approach to hydrologic response and similarity at the basin scale. *Journal of Hydrology*, **65**, 95–123.

Hargreaves G., Hargreaves G., and Riley J. (1985) Agricultural benefits for Senegal river basin. *Journal of Irrigation and Drainage Engineering*, **111**, 113–124.

Harmel R.D., Cooper R.J., Slade R.M., Haney R.L., and Arnold J.G. (2006) Cumulative uncertainty in measured streamflow and water quality data for small watersheds. *Transactions of the American Society of Agricultural and Biological Engineers*, **49**, 689–701.

Hasumi H. (2002) Modeling the global thermohaline circulation. *Journal of Oceanography*, **58**, 25 – 33.

Haverkamp S., Srinivasan R., Frede H.G., and Santhi C. (2002) Subwatershed spatial analysis tool: discretization of a distributed hydrologic model by statistical critieria. *Journal of the American Water Resources Association*, **38**, 1723–1733.

Hendriks M.R. (2010) *Introduction to physical hydrology.* Oxford University Press, New York.

Hernandez M., Miller S., and Goodrich D. (2000) Modeling runoff response to land cover and rainfall spatial variability in semi-arid watersheds. *Environmental Monitoring and Assessment*, **64**, 285–298.

Hershfield D. (1961) Rainfall frequency atlas of the United States for durations from 30 minutes to 24 hours and return periods from 1 to 100 years. 66.

Heuvelmans G., Muys B., and Feyen J. (2004) Analysis of the spatial variation in the parameters of th SWAT model with application in Flanders, Northern Belgium. *Hydrology and Earth System Sciences*, **8**, 931–939.

Hicks S. and Lascano R. (1995) Estimation of leaf-area index for cotton canopies using the LI-COR LAI-2000 plant canopy analyzer. *Agronomy Journal*, **87**, 458–464.

Hoffman D.W., Matthews B.C., and Wicklund R.E. (1964) Soil associations of Southern Ontario. 21.

Hornberger G.M., Beven K.J., Cosby B.J., and Sappington D.E. (1985) Shenandoah watershed study: Calibration of a topography-based, variable contributing area hydrological model to a small forested catchment. *Water Resources Research*, **21**, 1841–1850.

Horton R. (1933) The role of infiltration in the hydrologic cycle. *Transactions-American Geophysical Union*, **14**, 446–460.

Hsieh P.-H., Kuo J.-T., Wu E.M.-Y., Ciou S.-K., and Liu W.-C. (2010) Optimal best management practice placement strategies for nonpoint source pollution management in the Fei-Tsui reservoir watershed. *Environmental Engineering Science*, **27**, 441–449.

Huang J., Wu P., and Zhao X. (2013) Effects of rainfall intensity, underlying surface and slope gradient on soil infiltration under simulated rainfall experiments. *CATENA*, **104**, 93–102.

Jakeman A. and Hornberger G. (1993) How much complexity is warranted in a rainfall-runoff model? *Water Resources Research*, **29**, 2637–2649.

Jha M., Pan Z., Takle E., and Gu R. (2004) Impacts of climate change on streamflow in the Upper Mississippi River Basin: A regional climate model perspective. *Journal of Geophysical Research*, **109**, 1–12.

Joel A. and Messing I. (2001) Arid land research and management infiltration rate and hydraulic conductivity measured with rain simulator and disc permeameter on sloping arid land. *Arid Land Research and Management*, **15**, 371–384.

Kalin L. and Hantush M.M. (2006) Hydrologic modeling of an Eastern Pennsylvania watershed with NEXRAD and rain gauge data. *Journal of Hydrologic Engineering*, **11**, 555–570.

Kannan N., White S., Worrall F., and Whelan M. (2007) Sensitivity analysis and identification of the best evapotranspiration and runoff options for hydrological modelling in SWAT-2000. *Journal of Hydrology*, **332**, 456–466.

Kasenow M. (1997) *Applied ground-water hydrology and well hydraulics.* Water Resources Publications, Highlands Ranch, CO.

Khakbaz B., Imam B., Hsu K., and Sorooshian S. (2012) From lumped to distributed via semi-distributed: Calibration strategies for semi-distributed hydrologic models. *Journal of Hydrology*, **418-419**, 61–77.

King K., Arnold J., and Bingner R. (1999) Comparison of Green-Ampt and curve number methods on Goodwin Creek watershed using SWAT. *Transactions of the American Society of Agricultural and Biological Engineers*, **42**, 919–925.

Klemeš V. (1983) Conceptualization and scale in hydrology. *Journal of Hydrology*, **65**, 1–23.

Kodešová R., Šimůnek J., Nikodem A., and Jirků V. (2010) Estimation of the dual-permeability model parameters using tension disk infiltrometer and guelph permeameter. *Vadose Zone Journal*, **9**, 213.

Kozak J.A., Ahuja L.R., Green T.R., and Ma L. (2007) Modelling crop canopy and residue rainfall interception effects on soil hydrological components for semi-arid. *Hydrological Processes*, **241**, 229–241.

Krause P., Boyle D., and Bäse F. (2005) Comparison of different efficiency criteria for hydrological model assessment. *Advances in Geosciences*, **5**, 89–97.

Land Information Ontario (2013) Land information Ontario data description: soil survey complex v.4. 16.

Larson L. and Peck E. (1974) Accuracy of precipitation measurements for hydrologic modeling. *Water Resources Research*, **10**, 857–863.

Leblanc S. (2008) DHP-TRACwin Manual. *Canada Centre for Remote Sensing, Québec, Canada*, 1–29.

Lee K.S. and Chung E.-S. (2007) Development of integrated watershed management schemes for an intensively urbanized region in Korea. *Journal of Hydro-Environment Research*, **1**, 95–109.

Legates D. and McCabe G. (1999) Evaluating the use of “goodness-of-fit” measures in hydrologic and hydroclimatic model validation. *Water Resources Research*, **35**, 233–241.

LI-COR (1992) LAI-2000 plant canopy analyzer: operating manual. 175.

Linsley R., Kohler M., and Paulhus J. (1982) *Hydrology for engineers.* McGraw-Hill, New York.

Di Luzio M., Arnold J., and Srinivasan R. (2005) Effect of GIS data quality on small watershed stream flow and sediment simulations. *Hydrological Processes*, **19**, 629–650.

Manguerra H. and Engel B. (1998) Hydrologic parameterization of watersheds for runoff prediction using SWAT. *Journal of the American Water Resources Association*, **34**, 1149–1162.

Masih I., Maskey S., Uhlenbrook S., and Smakhtin V. (2011) Assessing the impact of areal precipitation input on streamflow simulations using the SWAT model. *JAWRA Journal of the American Water Resources Association*, **47**, 179–195.

McKay M., Beckman R., and Conover W. (2000) A comparison of three methods for selecting values of input variables in the analysis of output from a computer code. *Technometrics*, **21**, 239–245.

Mein R. and Larson C. (1973) Modeling infiltration during a steady rain. *Water Resources Research*, **9**, 384–394.

Mishra S.K. and Singh V.P. (2004) Validity and extension of the SCS-CN method for computing infiltration and rainfall-excess rates. *Hydrological Processes*, **18**, 3323–3345.

Monsi M. and Saeki T. (2005) On the factor light in plant communities and its importance for matter production. *Annals of Botany*, **95**, 549–67.

Monteith J. (1965) Evaporation and the environment. *The state and movement of water in living organisms* pp. 205–234. Cambridge University Press, Swansea.

Montgomery D., Grant G., and Sullivan K. (1995) Watershed analysis as a framework for implementing ecosystem management. *Water Resources Bulletin*, **31**, 369–386.

Moradkhani H. and Sorooshian S. (2008) General review of rainfall-runoff modeling: model calibration, data assimilation, and uncertainty analysis. *Hydrological Modelling and the Water Cycle* (ed. by S. Sorooshian), pp. 1–24. Springer, New York.

Moriasi D., Arnold J., Van Liew M., Bingner R., Harmel R., and Veith T. (2007) Model evaluation guidelines for systematic quantification of accuracy in watershed simulations. *Transactions of the American Society of Agricultural and Biological Engineers*, **50**, 885–900.

Muleta M.K. and Nicklow J.W. (2005) Sensitivity and uncertainty analysis coupled with automatic calibration for a distributed watershed model. *Journal of Hydrology*, **306**, 127–145.

Murray F. (1967) On the computation of saturation vapor pressure. *Journal of Applied Meteorology*, **6**, 203–204.

Muttiah R.S. and Wurbs R. a. (2002) Modeling the impacts of climate change on water supply reliabilities. *Water International*, **27**, 407–419.

Nash J. and Sutcliffe J. (1970) River flow forecasting through conceptual models part I. A discussion of principles. *Journal of Hydrology*, **10**, 282–290.

Natural Resources Conservation Service (1986) Urban hydrology for small watersheds : technical release 55. 49.

Nearing M., Liu B., Risse L., and Zhang X. (1996) Curve number and Green-Ampt effective hydraulic conductivities. *Water Resources Bulletin*, **32**, 125–136.

Neitsch S., Arnold J., Kiniry J., Srinivasan R., and Williams J. (2002) The Soil and Water Assessment Tool user's manual. *Temple, TX*, 472.

Neitsch S., Arnold J., Kiniry J., and Williams J. (2011) Soil and Water Assessment Tool: theoretical documentation, version 2009. *Texas, …*, 647.

Neumann H.H., Den Hartog G., and Shaw R.H. (1989) Leaf area measurements based on hemispheric photographs and leaf-litter collection in a deciduous forest during autumn leaf-fall. *Agricultural and Forest Meteorology*, **45**, 325–345.

Norman J. and Campbell G. (1989) Canopy structure. *Plant physiological ecology: field methods and instrumentation.* (ed. by R. Pearcy, J. Ehleringer, H. Mooney, and P. Rundel), pp. 301–325. Chapman and Hall, London; New York.

Nunes J.P., Seixas J., and Pacheco N.R. (2008) Vulnerability of water resources, vegetation productivity and soil erosion to climate change in Mediterranean watersheds. *Hydrological Processes*, **22**, 3115–3134.

Olding A.., Wicklund R.., and Richards N.. (1956) Soil survey of Ontario county. 60.

Osunbitan J. a., Oyedele D.J., and Adekalu K.O. (2005) Tillage effects on bulk density, hydraulic conductivity and strength of a loamy sand soil in southwestern Nigeria. *Soil and Tillage Research*, **82**, 57–64.

Peck A.J., Luxmoore R.J., and Stolzy J. (1977) Effects of spatial variability of soil hydraulic properties in water budget modeling. *Water Resources Research*, **13**, 348–354.

Penman H. (1956) Evaporation: an introductory survey. *Netherlands Journal of Agricultural Sciences*, **1**, 9–29.

Penman H.L. (1948) Natural evaporation from open water, bare soil and grass. *Proceedings of the Royal Society A: Mathematical, Physical and Engineering Sciences*, **193**, 120–145.

Philip J. (1954) An infiltration equation with physical significance. *Soil Science*, **77**, 153–158.

Philip J. (1969) Theory of infiltration. *Advances in Hydroscience*, **5**, 215–296.

Pitt R. and Clark S.E. (2008) Integrated Storm-Water Management for Watershed Sustainability. *Journal of Irrigation and Drainage Engineering*, **134**, 548–555.

Priestley C. and Taylor R. (1972) On the assessment of surface heat flux and evaporation using large-scale parameters. *Monthly Weather Review*, **100**, 81–92.

R.V. Anderson Associates Ltd. (2011) Toronto Community Housing - West Don Lands Block 1: site stormwater management report. 86.

Rathjens H. and Oppelt N. (2012a) SWATgrid: An interface for setting up SWAT in a grid-based discretization scheme. *Computers and Geosciences*, **45**, 161–167.

Rathjens H. and Oppelt N. (2012b) SWAT model calibration of a grid-based setup. *Advances in Geosciences*, **32**, 55–61.

Rawls W. and Brakensiek D. (1985) Prediction of soil water properties for hydrologic modeling. *Watershed management in the 80's* (ed. by E. Jones and T. Ward), pp. 293–299. American Society of Civil Engineers, New York, N.Y.

Refsgaard J. (1996) Terminology, modelling protocol and classification of hydrological model codes. *Distributed hydrological modelling* (ed. by M. Abbott and J. Refsgaard), pp. 17–26. Kluwer Academic, Dordrecht.

Renschler C. and Lee T. (2005) Spatially distributed assessment of short- and long-term impacts of multiple best management practices in agricultural watersheds. *Journal of Soil and Water Conservation*, **60**, 446–456.

Reynolds W. and Elrick D. (1986) A method for simultaneous in situ measurement in the vadose zone of field-saturated hydraulic conductivity, sorptivity and the conductivity-pressure head relationship. *Ground Water Monitoring and Remediation*, **6**, 84–95.

Richards L., Gardner W., and Ogata G. (1956) Physical processes determining water loss from soil. *Soil Science Society of America Proceedings*, **20**, 310 – 314.

Richardson C. (1981) Stochastic simulation of daily precipitation, temperature, and solar radiation. *Water Resources Research*, **17**, 182–190.

Rienzner M. and Gandolfi C. (2014) Investigation of spatial and temporal variability of saturated soil hydraulic conductivity at the field-scale. *Soil and Tillage Research*, **135**, 28–40.

Ritchie J. (1972) Model for predicting evaporation from a row crop with incomplete cover. *Water Resources Research*, **8**, 1204–1213.

Ross J. (1981) *The radiation regime and architecture of plant stands.* Springer Netherlands, Dordrecht.

Russell W. (1972) Effect of leaf angle on hybrid performance in maize (zea-mays L). *Crop Science*, **12**, 90–92.

Russo D., Russo I., and Laufer A. (1997) On the spatial variability of parameters of the unsaturated hydraulic conductivity. *Water Resources Research*, **33**, 947–956.

Sahrawat K.L., Wani S.P., Pathak P., and Rego T.J. (2010) Managing natural resources of watersheds in the semi-arid tropics for improved soil and water quality: a review. *Agricultural Water Management*, **97**, 375–381.

Sahu R.K., Mishra S., and Eldho T. (2010) An improved AMC-coupled runoff curve number model. *Hydrological Processes*, **24**, 2834–2839.

Santhi C., Arnold J., Williams D., Srinivasan R., and Hauck L. (2001) Validation of the SWAT model on a large river basin with point and nonpoint sources. *Journal of the American Water Resources Association*, **37**, 1169–1188.

Sharda V. and Ojasvi P. (2005) Water harvesting through watershed management in different agro-ecological regions of India. *Indian Journal of Agricultural Sciences*, **75**, 771–780.

Sharma M., Gander G., and Hunt C. (1980) Spatial variability of infiltration in a watershed. *Journal of Hydrology*, **45**, 101–122.

Sharpley A. and Williams J. (1990) EPIC-erosion/productivity impact calculator: 1. Model documentation. *Technical Bulletin-United States Department of Agriculture*, 235.

Shen Z.Y., Gong Y.W., Li Y.H., Hong Q., Xu L., and Liu R.M. (2009) A comparison of WEPP and SWAT for modeling soil erosion of the Zhangjiachong Watershed in the Three Gorges Reservoir Area. *Agricultural Water Management*, **96**, 1435–1442.

Shih D.-S., Li M.-H., and Wu R.-S. (2007) Distributed flood simulations with coupling gauge observations and radar-rainfall estimates. *Water Resources Management*, **22**, 843–859.

Shin D., Lee K.-K., and Kim J.-W. (1998) Spatial variability of conductivity as applied to distributed parameter infiltration models. *Journal of the American Water Resources Association*, **34**, 545–558.

Sieck L.C., Burges S.J., and Steiner M. (2007) Challenges in obtaining reliable measurements of point rainfall. *Water Resources Research*, **43**, 1–23.

Singh J., Knapp H.V., and Demissie M. (2004) Hydrologic modeling of the Iroquois River Watershed using HSPF and SWAT. 24.

Singh V., Bankar N., Salunkhe S., Bera A., and Sharma J. (2013) Hydrological stream flow modelling on Tungabhadra catchment: parameterization and uncertainty analysis using SWAT CUP. *Current Science*, **104**, 1187–1199.

Smith R., Smettem K., Broadbridge P., and Woolhiser D. (2002) *Infiltration theory for hydrologic applications.* American Geophysical Union, Washington, D.C.

Soil Conservation Society (1972) Section 4: Hydrology. *National engineering handbook* pp. 1–24. Soil Conservation Society,

Sophocleous M., Koelliker J., Govindaraju R., Birdie T., Ramireddygari S., and Perkins S. (1999) Integrated numerical modeling for basin-wide water management: The case of the Rattlesnake Creek basin in south-central Kansas. *Journal of Hydrology*, **214**, 179–196.

Sophocleous M. and Perkins S.P. (2000) Methodology and application of combined watershed and ground-water models in Kansas. *Journal of Hydrology*, **236**, 185–201.

Stone M.C., Hotchkiss R.H., Hubbard C.M., Fontaine T.A., Mearns L.O., and Arnold J.G. (2001) Impacts of climate change on Missouri river basin water yield. *Journal of the American Water Resources Association*, **37**, 1119–1129.

Takle E., Jha M., and Anderson C. (2005) Hydrological cycle in the upper Mississippi River basin: 20th century simulations by multiple GCMs. *Geophysical Research Letters*, **32**, 1–5.

Thomson A., Brown R., Rosenberg N., Srinivasan R., and Izaurralde R. (2005) Climate change impacts for the conterminous USA: an integrated assessment-part 4: water resources. *Climate Change*, **69**, 67–88.

Thornthwaite C.W. (1948) An approach toward a natural classification of climate. *Geographical Review*, **38**, 55–94.

Todini E. (1988) Rainfall-runoff modeling—Past, present and future. *Journal of Hydrology*, **100**, 341–352.

TRCA (2002a) Duffins Creek state of the watershed report: surface water quantity. 1–17.

TRCA (2002b) Duffins Creek state of the watershed report: study area. 1–6.

TRCA (2002c) Duffins Creek state of the watershed report: land use and policy frameworks. 1–23.

TRCA (2002d) Duffins Creek state of the watershed report: climate. 1–7.

TRCA (2003) A watershed plan for Duffins Creek and Carruthers Creek. 214.

TRCA (2013) Duffins Creek watershed report card 2013. 2.

Tripathi M., Raghuwanshi N., and Rao G. (2006) Effect of watershed subdivision on simulation of water balance components. *Hydrological Processes*, **20**, 1137–1156.

Vandervaere P., Peugeot C., Vauclin M., Jaramillo R., and Lebel T. (1997) Estimating hydraulic conductivity of crusted soils using disc infiltrometers and minitensiometers. *Journal of Hydrology*, **189**, 203–223.

Venetis C. (1969) A study on the recession of unconfined acquifers. *International Association of Scientific Hydrology. Bulletin*, **14**, 119–125.

Vidovic J. (1974) Effect of change of leaf angle arrangement on productivity of maize (zea-mays L) stands. *Biologia Plantarum*, **16**, 174–183.

Viessman W. and Lewis G. (1995) *Introduction to hydrology.* Harper Collins College Publishers, New York.

Wang X., Melesse A., and Yang W. (2006) Influences of potential evapotranspiration estimation methods on SWAT's hydrologic simulation in a Northwestern Minnesota watershed. *Transactions of the American Society of Agricultural and Biological Engineers*, **49**, 1755–1772.

Ward R. and Robinson M. (2000) *Principles of hydrology.* McGraw-Hill, London.

Watson D. (1947) Comparative physiological studies on the growth of field crops. I. Variation in net assimilation rate and leaf area between species and varieties, and within and between years. *Annals of Botany*, **11**, 41–76.

Weber A., Fohrer N., and Möller D. (2001) Long-term land use changes in a mesoscale watershed due to socio-economic factors — effects on landscape structures and functions. *Ecological Modelling*, **140**, 125–140.

Williams J. (1995) The EPIC model. *Computer models of watershed hydrology* (ed. by V.P. Singh), pp. 909–1000. Water Resources Publications, Highlands Ranch, CO.

Willmott C.J., Ackleson S.G., Davis R.E., Feddema J.J., Klink K.M., Legates D.R., O'Donnell J., and Rowe C.M. (1985) Statistics for the evaluation and comparison of models. *Journal of Geophysical Research*, **90**, 8995–9005.

Winchell M., Srinivasan R., Di Luzio M., and Arnold J. (2013) ArcSWAT interface for SWAT2012: User's Guide. 464.

Winter T.C. (1981) Uncertainties in estimating the water balance of lakes. *Journal of the American Water Resources Association*, **17**, 82–115.

Yang J., Reichert P., Abbaspour K.C., Xia J., and Yang H. (2008) Comparing uncertainty analysis techniques for a SWAT application to the Chaohe Basin in China. *Journal of Hydrology*, **358**, 1–23.

Zedler J.B. (2003) Wetlands at your service: reducing impacts of agriculture at the watershed scale. *Frontiers in Ecology and the Environment*, **1**, 65–72.

Zhang Y., Chen J.M., and Miller J.R. (2005) Determining digital hemispherical photograph exposure for leaf area index estimation. *Agricultural and Forest Meteorology*, **133**, 166–181.

Zhu A.X. and Scott Mackay D. (2001) Effects of spatial detail of soil information on watershed modeling. *Journal of Hydrology*, **248**, 54–77.

(1985) Evaluation of hydrologic-models used to quantify major land-use change effects. *Journal of Irrigation and Drainage Engineering*, **111**, 1–17.

Appendix A: List of Acronyms

SWAT: Soil and Water Assessment Tool
HRU: hydrologic response units
CN: curve number
GA: Green & Ampt
TI: Tension Infiltrometer
GP: Guelph Permeameter
LAI: leaf area index
DHP: digital hemispherical photograph
BD: bulk density
CANMX: maximum canopy storage
SHE: Système Hydrologique Européen (hydrological model)
TOPAZ: Topographic Parameterization (program to automatically analyze landscape topography)
SWM: Standford Watershed Model
DEM: digital elevation model
GIS: geographical information system
NSE: Nash Sutcliffe efficiency
RMSE: root mean square error
GLUE: generalized likelihood uncertainty estimation
SUFI-2: sequential uncertainty fitting– 2
NEXRAD: next–generation radar
WEPP: Water Erosion Prediction Project (erosion model)
APEX: Agricultural Policy Extender (farm watershed model)
ORM: Oak Ridges Moraine
CDCD: Canadian daily climate data
LCLU: land cover/ land use
K_{sat}, Sol_K: saturated hydraulic conductivity
GP: Guelph Permeameter

Appendix B: Sample Data Collection

Table 21. Sample infiltration data collected using the Tension Infiltrometer within the study site.

Day	Month	Year	Location	Instrument	Head (cm)	Δ t (min)	Water level in reservoir h (cm)	Δh (cm)	Rate of change Δh/Δt (cm/min)
16	8	2012	SP42	TI	-10	00:00:00	7.3	0	0
16	8	2012	SP42	TI	-10	00:02:00	7.45	0.15	0.075
16	8	2012	SP42	TI	-10	00:02:00	7.7	0.25	0.125
16	8	2012	SP42	TI	-10	00:02:00	7.85	0.15	0.075
16	8	2012	SP42	TI	-10	00:02:00	8	0.15	0.075
16	8	2012	SP42	TI	-10	00:02:00	8.2	0.2	0.1
16	8	2012	SP42	TI	-10	00:02:00	8.35	0.15	0.075
16	8	2012	SP42	TI	-10	00:02:00	8.5	0.15	0.075
16	8	2012	SP42	TI	-10	00:02:00	8.65	0.15	0.075
16	8	2012	SP42	TI	-10	00:02:00	8.8	0.15	0.075
16	8	2012	SP42	TI	-10	00:02:00	9	0.2	0.1
16	8	2012	SP42	TI	-10	00:02:00	9.1	0.1	0.05
16	8	2012	SP42	TI	-10	00:02:00	9.25	0.15	0.075
16	8	2012	SP42	TI	-10	00:02:00	9.4	0.15	0.075
16	8	2012	SP42	TI	-10	00:02:00	9.5	0.1	0.05
16	8	2012	SP42	TI	-10	00:02:00	9.7	0.2	0.1
16	8	2012	SP42	TI	-10	00:02:00	9.8	0.1	0.05
16	8	2012	SP42	TI	-10	00:02:00	9.95	0.15	0.075
16	8	2012	SP42	TI	-10	00:02:00	10.05	0.1	0.05
16	8	2012	SP42	TI	-10	00:02:00	10.15	0.1	0.05
16	8	2012	SP42	TI	-10	00:02:00	10.3	0.15	0.075
16	8	2012	SP42	TI	-10	00:02:00	10.45	0.15	0.075
16	8	2012	SP42	TI	-10	00:02:00	10.55	0.1	0.05

16	8	2012	SP42	TI	-10	00:02:00	10.65	0.1	0.05
16	8	2012	SP42	TI	-10	00:02:00	10.8	0.15	0.075
16	8	2012	SP42	TI	-10	00:02:00	10.95	0.15	0.075
16	8	2012	SP42	TI	-10	00:02:00	11.05	0.1	0.05
16	8	2012	SP42	TI	-10	00:02:00	11.15	0.1	0.05
16	8	2012	SP42	TI	-10	00:02:00	11.3	0.15	0.075
16	8	2012	SP42	TI	-10	00:02:00	11.4	0.1	0.05
16	8	2012	SP42	TI	-5	00:00:00	11.55	0	0
16	8	2012	SP42	TI	-5	00:02:00	11.9	0.35	0.175
16	8	2012	SP42	TI	-5	00:02:00	12.2	0.3	0.15
16	8	2012	SP42	TI	-5	00:02:00	12.6	0.4	0.2
16	8	2012	SP42	TI	-5	00:02:00	12.8	0.2	0.1
16	8	2012	SP42	TI	-5	00:02:00	13.1	0.3	0.15
16	8	2012	SP42	TI	-5	00:02:00	13.4	0.3	0.15
16	8	2012	SP42	TI	-5	00:02:00	13.7	0.3	0.15
16	8	2012	SP42	TI	-5	00:02:00	13.9	0.2	0.1
16	8	2012	SP42	TI	-5	00:02:00	14.2	0.3	0.15
16	8	2012	SP42	TI	-5	00:02:00	14.5	0.3	0.15
16	8	2012	SP42	TI	-5	00:02:00	14.8	0.3	0.15
16	8	2012	SP42	TI	-5	00:02:00	15	0.2	0.1
16	8	2012	SP42	TI	-2.5	00:00:00	15.2	0	0
16	8	2012	SP42	TI	-2.5	00:02:00	16	0.8	0.4
16	8	2012	SP42	TI	-2.5	00:02:00	16.8	0.8	0.4
16	8	2012	SP42	TI	-2.5	00:02:00	17.5	0.7	0.35
16	8	2012	SP42	TI	-2.5	00:02:00	18.2	0.7	0.35
16	8	2012	SP42	TI	-2.5	00:02:00	19	0.8	0.4
16	8	2012	SP42	TI	-2.5	00:02:00	19.7	0.7	0.35
16	8	2012	SP42	TI	-2.5	00:02:00	20.5	0.8	0.4
16	8	2012	SP42	TI	-2.5	00:02:00	21.3	0.8	0.4
16	8	2012	SP42	TI	-2.5	00:02:00	22.1	0.8	0.4

16	8	2012	SP42	TI	-2.5	00:02:00	22.9	0.8	0.4
16	8	2012	SP42	TI	-2.5	00:02:00	23.8	0.9	0.45
16	8	2012	SP42	TI	-2.5	00:02:00	24.6	0.8	0.4
16	8	2012	SP42	TI	-2.5	00:02:00	25.5	0.9	0.45
16	8	2012	SP42	TI	-2.5	00:02:00	26.4	0.9	0.45
16	8	2012	SP42	TI	-2.5	00:02:00	27.3	0.9	0.45
16	8	2012	SP42	TI	-2.5	00:02:00	28.2	0.9	0.45

Table 22. . Sample infiltration data collected using the Guelph Permeameter within the study site.

Day	Month	Year	Location	Instrument	Head (cm)	Δ t (min)	Water level in reservoir h (cm)	Δh (cm)	Rate of change Δh/Δt (cm/min)
21	8	2012	SP22	GP	5	00:00:00	2.4	0	0
21	8	2012	SP22	GP	5	00:02:00	2.4	0	0
21	8	2012	SP22	GP	5	00:02:00	2.4	0	0
21	8	2012	SP22	GP	5	00:02:00	2.45	0.05	0.025
21	8	2012	SP22	GP	5	00:02:00	2.65	0.2	0.1
21	8	2012	SP22	GP	5	00:02:00	2.85	0.2	0.1
21	8	2012	SP22	GP	5	00:02:00	3.05	0.2	0.1
21	8	2012	SP22	GP	5	00:02:00	3.25	0.2	0.1
21	8	2012	SP22	GP	5	00:02:00	3.45	0.2	0.1
21	8	2012	SP22	GP	5	00:02:00	3.65	0.2	0.1
21	8	2012	SP22	GP	5	00:02:00	3.85	0.2	0.1
21	8	2012	SP22	GP	5	00:02:00	4.05	0.2	0.1
21	8	2012	SP22	GP	5	00:02:00	4.25	0.2	0.1
21	8	2012	SP22	GP	5	00:02:00	4.45	0.2	0.1
21	8	2012	SP22	GP	5	00:02:00	4.6	0.15	0.075
21	8	2012	SP22	GP	5	00:02:00	4.8	0.2	0.1
21	8	2012	SP22	GP	5	00:02:00	5	0.2	0.1

21	8	2012	SP22	GP	5	00:02:00	5.2	0.2	0.1
21	8	2012	SP22	GP	5	00:02:00	5.3	0.1	0.05
21	8	2012	SP22	GP	5	00:02:00	5.5	0.2	0.1
21	8	2012	SP22	GP	5	00:02:00	5.7	0.2	0.1
21	8	2012	SP22	GP	5	00:02:00	5.9	0.2	0.1
21	8	2012	SP22	GP	5	00:02:00	6	0.1	0.05
21	8	2012	SP22	GP	5	00:02:00	6.2	0.2	0.1
21	8	2012	SP22	GP	5	00:02:00	6.4	0.2	0.1
21	8	2012	SP22	GP	5	00:02:00	6.6	0.2	0.1
21	8	2012	SP22	GP	5	00:02:00	6.7	0.1	0.05
21	8	2012	SP22	GP	10	00:00:00	9.95	0	0
21	8	2012	SP22	GP	10	00:02:00	10.2	0.25	0.125
21	8	2012	SP22	GP	10	00:02:00	10.6	0.4	0.2
21	8	2012	SP22	GP	10	00:02:00	11	0.4	0.2
21	8	2012	SP22	GP	10	00:02:00	11.4	0.4	0.2
21	8	2012	SP22	GP	10	00:02:00	11.8	0.4	0.2
21	8	2012	SP22	GP	10	00:02:00	12.2	0.4	0.2
21	8	2012	SP22	GP	10	00:02:00	12.5	0.3	0.15
21	8	2012	SP22	GP	10	00:02:00	12.9	0.4	0.2
21	8	2012	SP22	GP	10	00:02:00	13.3	0.4	0.2
21	8	2012	SP22	GP	10	00:02:00	13.7	0.4	0.2
21	8	2012	SP22	GP	10	00:02:00	14.1	0.4	0.2
21	8	2012	SP22	GP	10	00:02:00	14.5	0.4	0.2
21	8	2012	SP22	GP	10	00:02:00	14.9	0.4	0.2
21	8	2012	SP22	GP	10	00:02:00	15.3	0.4	0.2
21	8	2012	SP22	GP	10	00:02:00	15.7	0.4	0.2

Appendix C: Description of Soil Profiles

Table 23. Description of soil horizons for Bondhead soil type. Source: (Olding et al. 1956).

Soil Horizon	Description
A_0	Thin mat of partially decomposed leaves etc.
A_1	0–4 inches very dark grey (10 YR 3/1) loam; fine crumb structure; very friable consistency; few stones; pH–7.1.
A_{21}	4–10 inches yellowish brown (10 YR 5/6) sandy loam; weak platy structure; very friable consistency; few stones; pH–7.0.
A_{22}	10-16 inches pale brown (10 YR 6/3) sandy loam; weak platy structures; very friable consistency; few stones; pH–6.8.
B_2	15–22 inches dark brown (10 YR 4/3) clay loam; medium sub–angular blocky structure; friable consistency; few stones; pH–7.1.
C	Pale light brownish grey (10 YR 6/3) calcareous loam till; pH–8.0.

Table 24. Description of soil horizons for Woburn soil type. Source: (Olding et al. 1956).

Soil Horizon	Description
A_0	Thin partially decomposed leaf litter.
A_1	0–4 inches very dark brown (10 YR 2/2) loam; fine crumb structure; very friable consistency; very few stones; pH–6.8.
A_{21}	4-10 inches pale brown (10 YR 6/3) sandy loam; platy structure; very friable consistency; pH–6.6.
A_{22}	10-14 inches light brownish grey (10 YR 6/2) sandy loam; medium sub–angular blocky structure; pH–6.6.
B_2	14–20 inches dark yellowish brown (10 YR 4/4) clay loam; medium blocky structure; pH–6.8.
B_3	20–27 inches grey–brown (10 YR 5/2) clay loam; medium blocky structure; pH–7.0.
C	Light olive–brown (2.5 Y 5/4) loam till; pH–7.8.

Table 25. Description of soil horizons for Milliken soil type. Source: (Olding et al. 1956).

Soil Horizon	Description
A_e	0-8 inches very dark grey–brown (10 YR 3/2) loam; fine crumb structure; very friable consistency; few stones; pH–7.0.
A_2	8–14 inches yellowish brown (10 YR 5/4) loam; fine sub–angular blocky structure; very friable; slight mottling; pH–7.0.
B_2	14–19 inches dark yellowish brown (10 YR 4/4) clay loam; medium sub–angular blocky structure; slight mottling; pH–6.8.
C	Light olive–brown (2.5 Y 5/4) loam till; pH–7.9.